

PHOTOPRODUCTION OF POSITIVE PIONS FROM HYDROGEN
AT SMALL ANGLES AT ENERGIES 700 TO 1025 MEV

Thesis by
James Harrison Boyden

In Partial Fulfillment of the Requirements
For the Degree of
Doctor of Philosophy

California Institute of Technology
Pasadena, California

1961

ACKNOWLEDGMENTS

The guidance and encouragement of Dr. R. L. Walker during this work contributed greatly to its success. His continual interest and advice during my entire graduate residence cannot be adequately acknowledged.

The interest of Dr. R. F. Bacher is greatly appreciated. The assistance and suggestions of other members of the Synchrotron Laboratory staff have been most helpful.

The assistance of J. Chang, J. Kilner and C. Peck in accumulating data is deeply appreciated. J. Link assisted in the analysis of the results.

The Synchrotron staff and crew gave excellent support in maintaining and operating the machine and equipment. Special thanks are due E. B. Emery, who maintained the liquid hydrogen target, and A. Neubeiser and L. Luke, the machine operators.

The use of the computing facilities and the cooperation of the staff of the Western Data Processing Center, University of California at Los Angeles, have been invaluable.

The financial assistance of the Ramo-Wooldridge Corporation, the Corning Glass Foundation and the Rand Corporation during my graduate residence is sincerely appreciated.

The partial financial support of the United States Atomic Energy Commission is gratefully acknowledged.

ABSTRACT

Measurements of the cross section for photoproduction of π^+ mesons from hydrogen have been extended to angles as small as 5° in the c. m. system, using a magnetic spectrometer. At a photon energy of 1025 Mev, the cross section decreases as the angle changes from 5° to 13° , reaching a minimum before increasing again to the maximum near 40° which has been previously observed (5). Less extensive measurements at energies 700, 800, 900, and 960 Mev all show a similar rapid decrease with angle in the angular range less than 15° c. m., although below 960 Mev no actual minimum is observed. These effects at small angles arise presumably from the "retardation term", or "meson current" term and its interference with other contributions to the photoproduction amplitude. It is interesting that a minimum near 15° is characteristic of the pure Born approximation (retardation term plus "S-wave").

Values of the 0° cross section that are much more accurate than previous estimates have been obtained. An attempt has been made to extract a value of the pion-nucleon coupling constant by an extrapolation into the region $\cos \theta' > 1$. Using the best set of data, the value obtained was $f^2 = 0.12 \pm 0.03$.

TABLE OF CONTENTS

<u>Chapter</u>	<u>Title</u>	<u>Page</u>
I	INTRODUCTION	1
II	THE EXPERIMENTAL METHOD	10
	A. General	10
	B. Problems at Small Angles	10
	C. The Synchrotron Beam Geometry	13
	D. The Hydrogen Target	18
	E. The Spectrometer	19
	F. The Counter System	19
	G. Particle Selection and Electronics	23
III	DATA	29
IV	DATA REDUCTION	35
	A. Cross Section Formulas	35
	B. Calculation of K	36
	C. Counting Rate Formulas	39
V	RESULTS.	42
	A. Tabular Listing	42
	B. Graphical Display	42
VI	ANALYSIS	52
	A. General	52
	B. Moravscik Curve Fitting	53
	C. The Coupling Constant	63
	D. 0° , 180° Cross Sections	69
	E. The Total Cross Section	73
VII	CONCLUSIONS AND SUGGESTIONS	75
<u>Appendix</u>		
I	BEAM MONITORING	76
II	COUNTER EFFICIENCIES	84
III	DECAY CORRECTIONS	95
IV	ABSORPTION MEASUREMENTS	121
V	ELECTRON COUNTING RATES.	126
	REFERENCES.	132

LIST OF ILLUSTRATIONS

<u>Figure</u>	<u>Title</u>	<u>Page</u>
1	"Shaking-off" and Retardation Terms Alone	4
2	Born Approximation	7
3	Pion Momentum vs. Laboratory Angle	11
4	Angular Resolution of an Aperture of Fixed Size	14
5	The Experimental Area	16
6	The Hydrogen Target and Spectrometer	20
7	Electronics Block Diagram	26
8	Angular Distributions	46
	(a) $k = 700$ Mev.	47
	(b) $k = 800$ Mev.	48
	(c) $k = 900$ Mev.	49
	(d) $k = 960$ Mev.	50
	(e) $k = 1025$ Mev	51
9	Extrapolation to the Pole $\cos \theta^{\dagger} = 1/\beta^{\dagger}$	65
10	0° and 180° Cross Sections vs. Energy	70
A1	Bremsstrahlung Spectrum $B(k, E_0)$	81
A2	Cherenkov Counter Efficiencies $\eta_{\check{C}\pi}, \eta_{\check{C}p}$	85
A3	Electron Detector Efficiency η_{Ee}	88
A4	Electron Detector Efficiency $\eta_{E\pi}$	90
A5	Electron Detector Efficiency η_{Ep}	92
A6	Decay Correction Coordinate System	97
A7	Block Diagram of Computer Program for the Decay Corrections	99
A8	Sample Results From Monte Carlo Calculations	105
A9	Muon Counting Rate, High Energy Position with Counter A2	108
A10	Momentum Response, High Energy Position with Counter A2	110

LIST OF ILLUSTRATIONS (Continued)

<u>Figure</u>	<u>Title</u>	<u>Page</u>
A11	Muon Counting Rate, Medium Energy Position	112
A12	Momentum Response, Medium Energy Position	115
A13	Muon Counting Rate, High Energy Position with Counter Al	117
A14	Momentum Response, High Energy Position with Counter Al	119
A15	Effective Absorption Length vs. Thickness of Pb	124
A16	Counting Rates of Positive Electrons from Hydrogen . . .	130

LIST OF TABLES

<u>Table</u>	<u>Title</u>	<u>Page</u>
1	Properties of the spectrometer	22
2	Description of the Counters	24
3	List of Data Points and Kinematics.	30
4	Counting Rates	32
5	Values of κ	38
6	Results for the Cross Section	43
7	Dixon-Walker Data	44
8	Least Squares Fitting Coefficients and χ^2	56
9	Artificial Data Points.	60
10	Experimental Values of the Coupling Constant	67
11	Total Cross Section.	74
A1	Ion Chamber Calibration.	79
A2	Pion Absorption Results	122
A3	Electron Counting Rates	127

I. INTRODUCTION

A great wealth of work, both experimental and theoretical, has gone into the attempt to understand the relationship between the pi meson and the nuclear force since Yukawa first proposed the existence of such a particle in 1935 (1), and it was discovered in emulsions in 1947 (2).

The most fruitful experiments have been pion-nucleon scattering and the photoproduction of pions. The most prominent feature of the data to appear thus far is the strong resonance behavior at approximately 185 Mev pion energy in the pion scattering and at approximately 330 Mev laboratory photon energy in the photoproduction experiments. The data in this region have been analyzed and the resonant state has been found to have isotopic spin $I = 3/2$ and angular momentum $J = 3/2$ with even parity. The original static theory of Chew, improved by Chew and Low, and the more recent dispersion theory of Chew, Low, Goldberger, and Nambu (3) have been quite successful at reproducing the experimental results at energies in the vicinity of this resonance and lower. At higher energies no successful theory exists as yet.

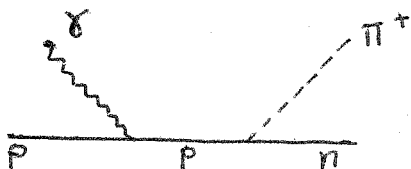
The higher energy photoproduction measurements at Cornell (4) and by Dixon and Walker of this laboratory (5) have shown a resonance behavior of the π^+ cross section in the vicinity of 700 Mev laboratory photon energy, and a possible third resonance near 1000 Mev. These resonances have also been seen in pion scattering. The fact that π^+ , p total absorption data show little evidence of the resonances that are seen in π^- , p total absorption indicates that the resonance occurs in a state with $I = 1/2$. The angular distributions near the second resonance lead

to the assignments $I = 1/2$, $J = 3/2$. Other arguments suggest an odd parity state, and thus a $D_{3/2}$ rather than a $P_{3/2}$ assignment. The third resonance assignments are somewhat less firm but are certainly $I = 1/2$ and very likely $J = 5/2$. The parity is not known.

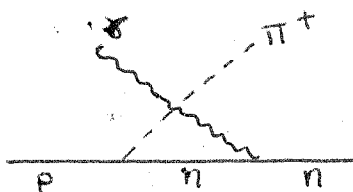
The experiment to be described here was a measurement of the differential cross section for π^+ photoproduction at the most forward angles that could be reached experimentally, in the energy range 700 to 1025 Mev. In order to demonstrate why the small angle region is of special interest, certain features of the theory will be discussed.

The lowest order Feynman diagrams which one can write are as follows:

- (1) The "shaking off" production



- (2) The crossing reaction corresponding to (1)



- (3) The "photoelectric", or meson current, production

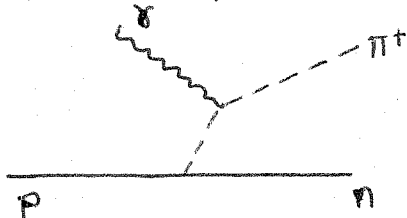


Diagram (2) will not contribute to the cross section unless the anomalous magnetic moment of the neutron is included. It is diagram (3) that is most interesting in the light of this experiment. Its effect on the

cross section can be studied by calculating the Born approximation for the above diagrams.

The low energy Born approximation amplitude for pion photo-production, for no anomalous moment, is:

$$B = \underline{\sigma} \cdot \underline{e} + \frac{\underline{\sigma} \cdot (\underline{k} - \underline{q}) \underline{q} \cdot \underline{e}}{kE_{\pi} - \underline{q} \cdot \underline{k}}$$

where $\underline{\sigma}$ is the usual spin operator, \underline{e} is the photon polarization vector, \underline{k} is the photon momentum, \underline{q} is the pion momentum and E_{π} is the total pion energy, all in the c.m. system.

The first term arises from diagram (1) and the second term from diagram (3). The first term alone leads to production of pions in S-states due to an electric dipole interaction. If relativistic corrections are made there is an additional small magnetic dipole interaction leading to p-wave states. The contribution to $\sigma(\theta')$ from this term is shown in fig. 1(a). The second term has a more complicated behavior. Averaging over spins and polarizations, we can obtain

$$\sigma(\theta') \text{ (diagram (2)) } \sim \frac{\beta'^2 \sin^2 \theta' (1 + \beta'^2 \gamma'^2 - 2\beta' \gamma' \cos \theta')}{(1 - \beta' \cos \theta')^2}$$

where

$$\beta' = \beta_{\pi} = \frac{q}{E_{\pi}}$$

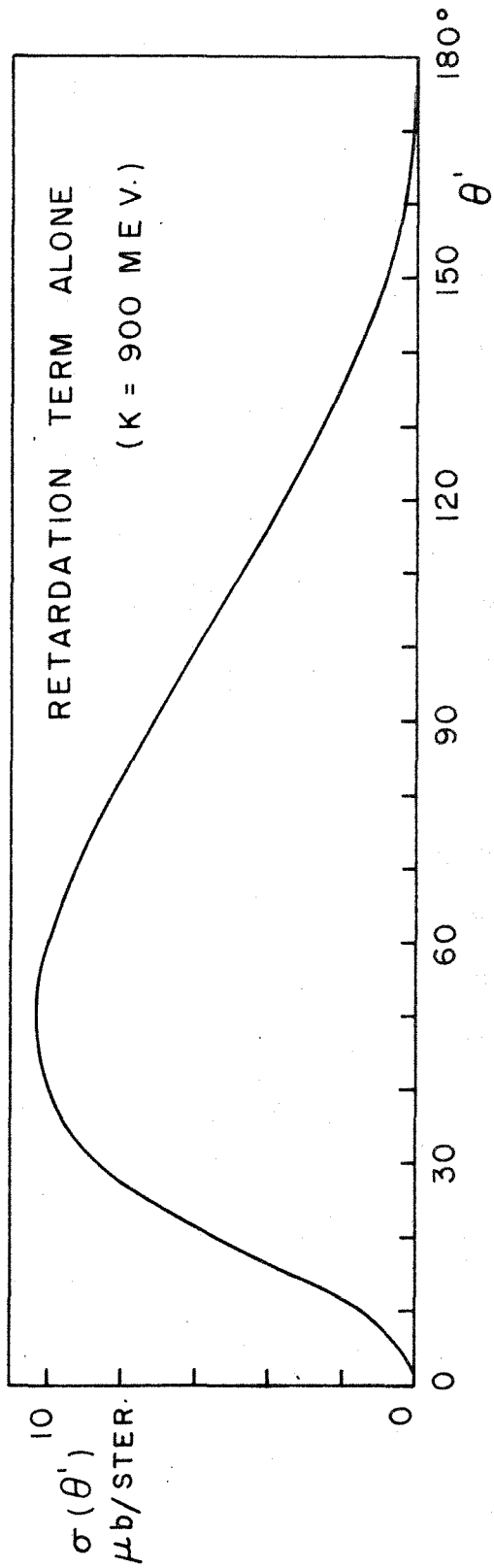
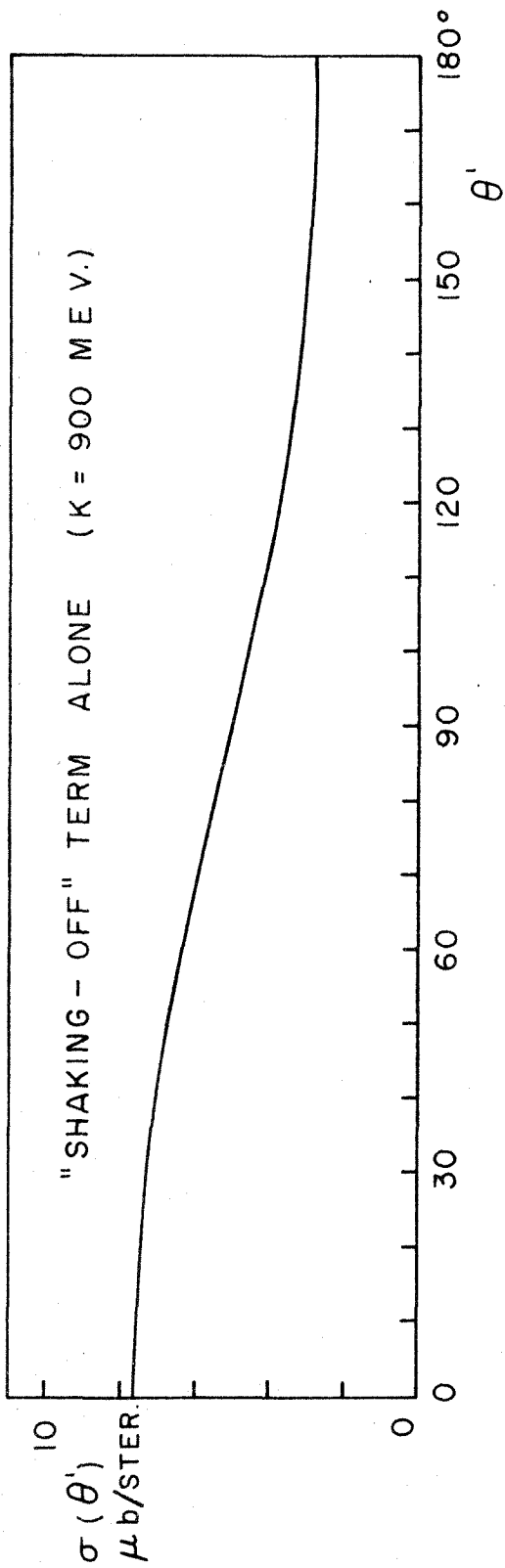
$$\gamma' = \frac{E_{\pi}}{k}$$

$$\cos \theta' = \frac{\underline{q} \cdot \underline{k}}{qk} = \cos (\text{pion angle})$$

(The primed quantities are used to agree with the c.m. notation which

Figure 1. "Shaking Off" and Retardation Terms Alone

The separate contributions from the two terms used in the calculations for fig. 1 are shown for $k = 900$ Mev.



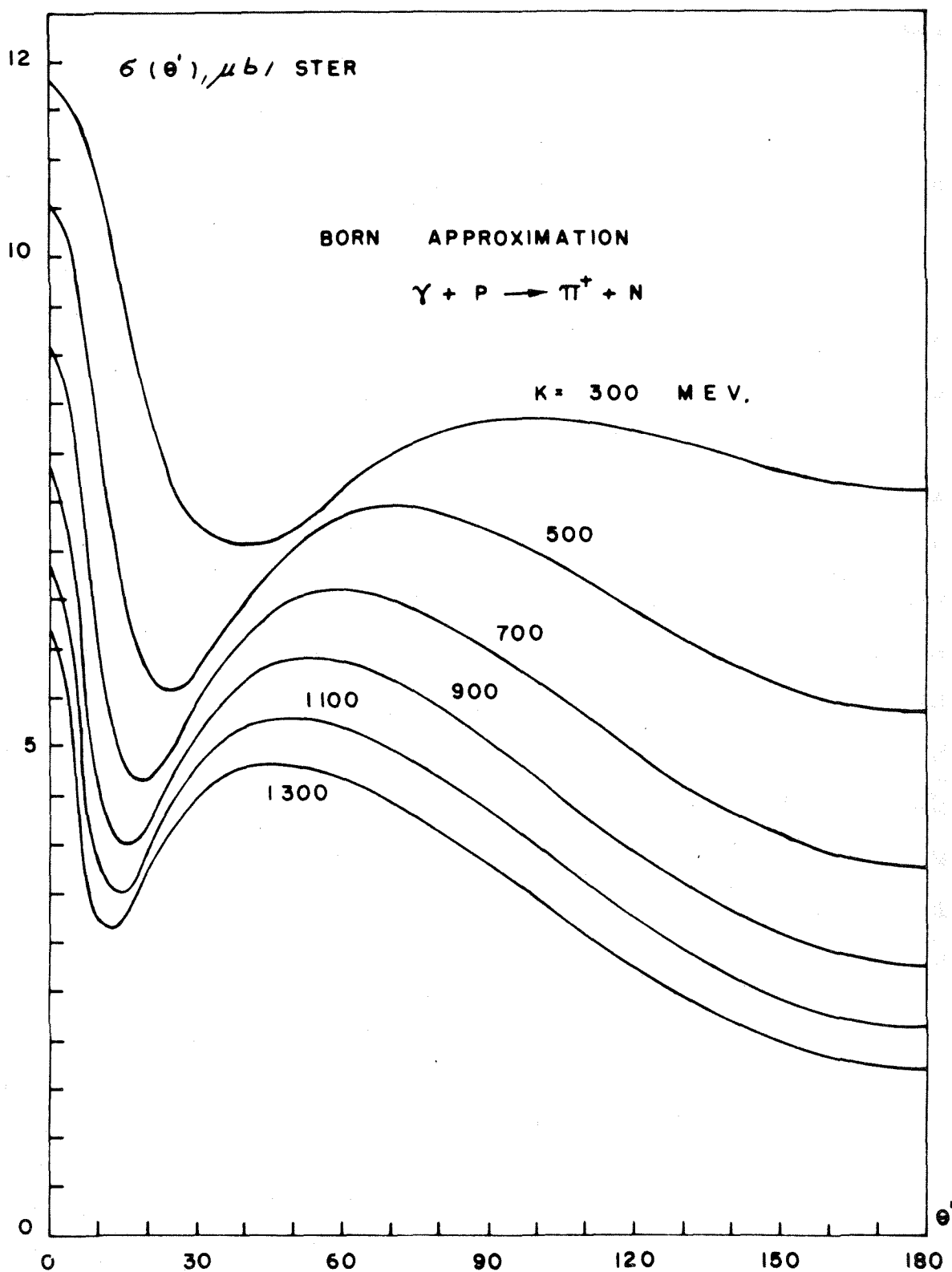
will be used later.) In fig. 1(b) is plotted the cross section due to this "retardation" term, so-called because of the characteristic denominator. The combination of these two terms, including interference, leads to results which are plotted in fig. 2, for several values of laboratory photon energy. Note that the interference between the "S-wave" part, from the "shaking off" production, and the retardation term produces a minimum in the cross section at a small angle.

It is the effect of the retardation term that makes small angle measurements of the cross section interesting, for three reasons:

- (1) The interference of the retardation term with states having high order multipoles might give information concerning these states, in particular near a resonance. In practice the interference with low order states tends to completely mask or distort the high order effects and makes interpretation difficult or impossible.
- (2) At 0° and 180° the retardation term and its interference with other terms vanish. Therefore data at these extreme angles are of value in interpreting the results without the obscuring effects of the retardation term. Because of the rapid variations in the cross section in the small angle region that can be induced by this term, it is necessary to have small angle data in order to extract an accurate value of the 0° cross section.
- (3) It is possible in principle to obtain a measurement of the pion-nucleon coupling constant by extrapolating the measured cross section into the non-physical region where $\cos \theta' > 1$, as suggested by Moravcsik (10). The details of this procedure will be given later in Section VI,

Figure 2. Born Approximation

The two diagram Born approximation results for the π^+ differential cross section, with relativistic effects included, are shown for several values of laboratory photon energy, k .



Analysis. However, it is obvious that the accuracy of the value obtained will improve as the available data points move closer to $\cos \theta' > 1$, i. e. as close to 0° as possible.

It should be pointed out that the characteristic form of the retardation term does not arise solely in the case of the Born approximation. Indeed, in any theory that can be written such a term must appear. Of course the interferences with other states will change, but it can be expected that the general behavior will be similar to that suggested by the Born approximation.

This experiment consisted of a measurement of the differential cross section for the photoproduction of positive pions from hydrogen at laboratory angles of about 3° to 15° , and laboratory photon energies of 700, 800, 900, 960, and 1025 Mev. There were additional measurements at 1025 Mev at angles up to 55° in the laboratory. The 700, 800 and 900 Mev measurements extend the Dixon-Walker data, which yielded angular distributions above 20° c.m., to c.m. angles as small as 5° . Data were taken at 1025 Mev because of the beam energy requirements of another experiment in progress and unfortunately do not tie onto other data at larger angles. The 960 Mev data was a spot check of the small angle behavior in the vicinity of the third resonance.

II. THE EXPERIMENTAL METHOD

A. GENERAL

A target containing liquid hydrogen was irradiated by the photon beam of the California Institute of Technology synchrotron. The π^+ mesons created in the reaction

$$\gamma + p \rightarrow \pi^+ + n$$

were then selected in momentum and angle by a magnetic spectrometer. The kinematics of this process are shown in fig. 3. In order to avoid counting those mesons arising from the double pion production reactions

$$\gamma + p \rightarrow \pi^+ + \begin{cases} \pi^0 + n \\ \pi^- + p \end{cases}$$

the synchrotron energy, E_0 , was chosen so that all photons were of energy below that required for producing mesons from these reactions with high enough momentum to be within the acceptance range of the spectrometer.

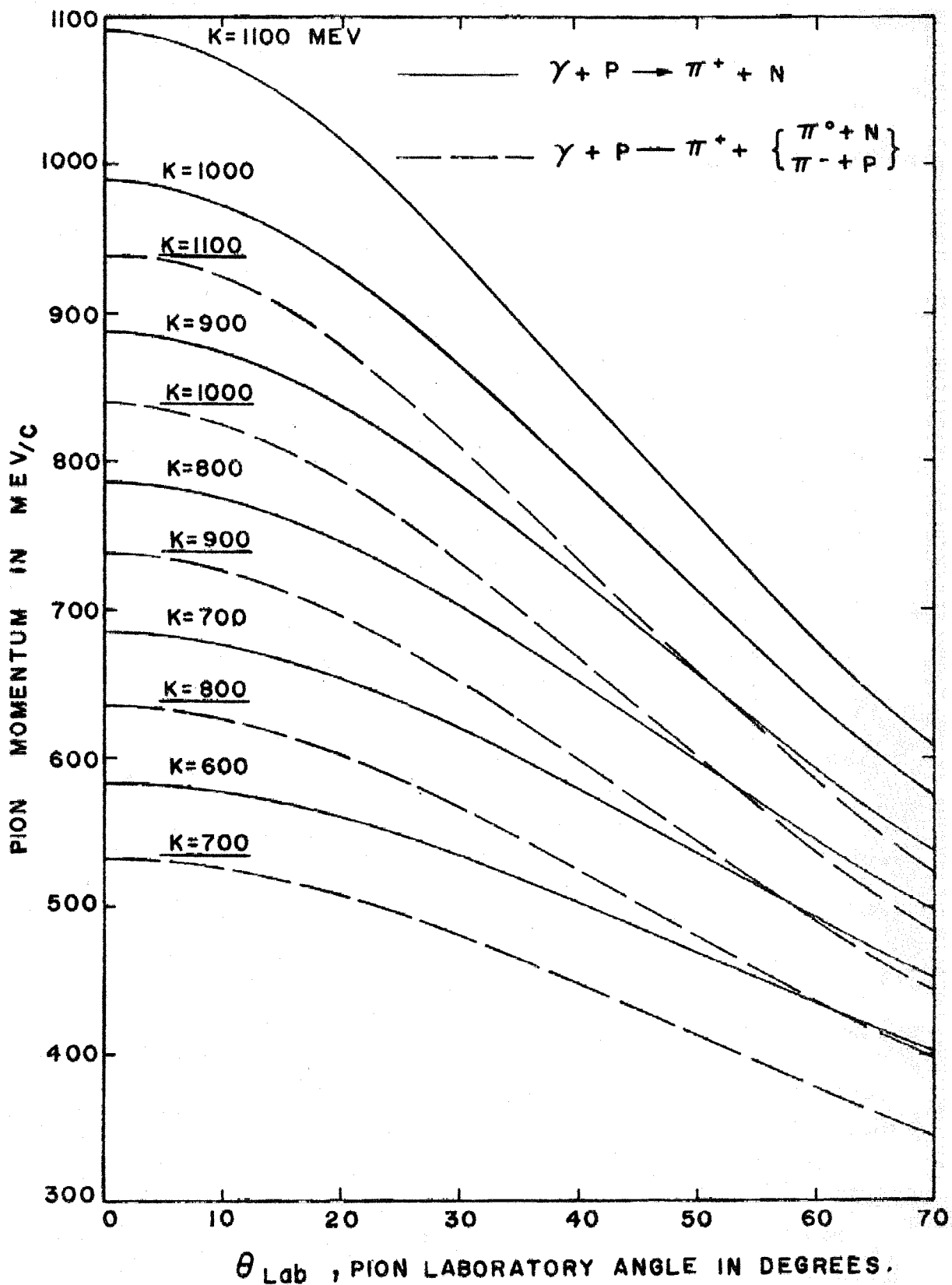
B. PROBLEMS AT SMALL ANGLES

There are several experimental problems which are peculiar to measurements at small angles:

(1) A large number of particles, mostly electrons (and positrons), are produced at forward angles. Some of these are produced in the hydrogen. Others are due to the presence of target material other than the hydrogen, and to production in the collimator and scrapers which define the beam.

Figure 3. Pion Momentum Vs. Laboratory Angle

k is the laboratory photon energy.



The great majority of these particles are of low energy and are rejected by the magnetic selection. However they would flood any scintillation counter placed in front of the magnet to define the aperture, as was done in the previous experiments (5), and make coincidence measurements unreliable. Those electrons whose momenta are within the spectrometer acceptance must be distinguished from the pions. Since pions of these energies have a velocity very nearly equal to c (within 2%) it is difficult to construct a velocity discrimination system.

(2) When the spectrometer is set at angles smaller than 15° (lab angle) the beam strikes the magnet yoke or coils. This creates two problems:

a) The large number of shower particles created can cause a flooding of aperture defining counters if they escape from the steel or copper and enter the magnet gap.

b) The interruption of the beam causes difficulties in the intensity monitoring system.

(3) The angular resolution of an aperture of fixed dimensions deteriorates as the angle decreases. This is illustrated in fig. 4.

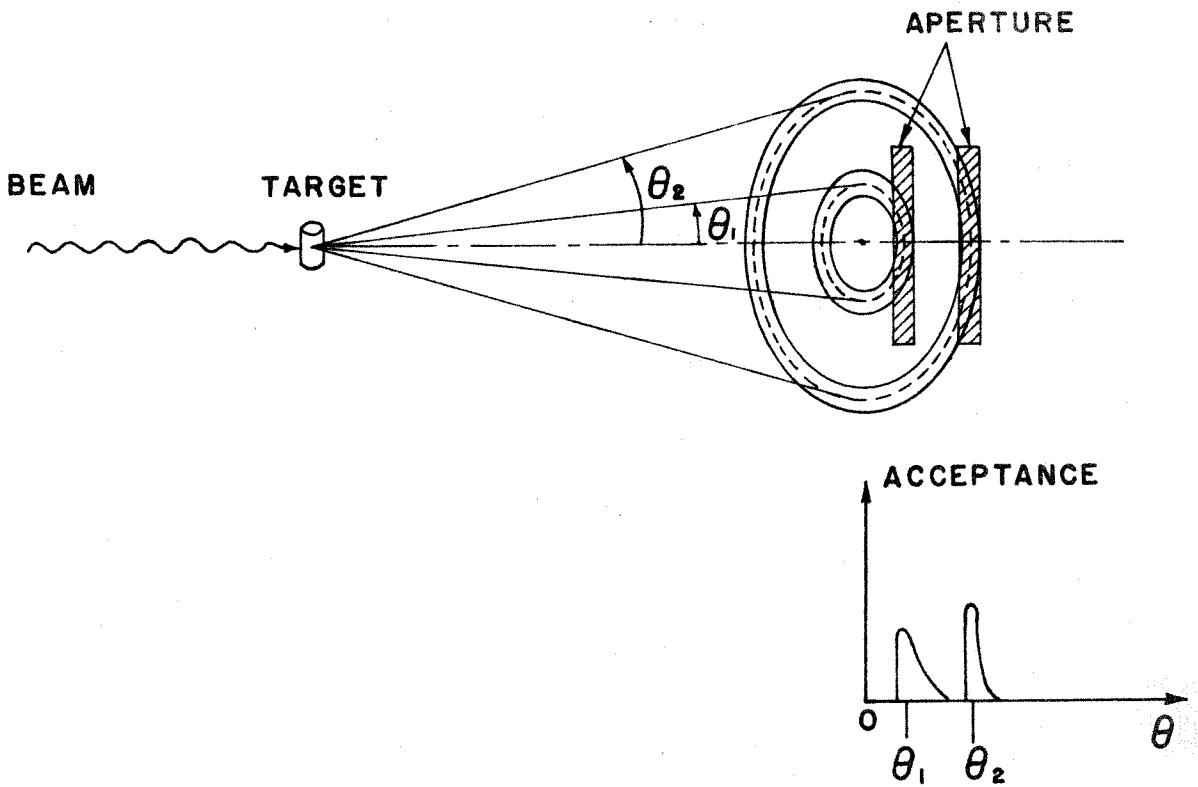
The solution to each of these problems will be discussed in the following sections, together with a description of the experimental arrangement.

C. THE SYNCHROTRON BEAM GEOMETRY

In fig. 5 is shown an overall view of the synchrotron and the experimental area. The photon beam emerges from the synchrotron, passing through the primary collimator which defines the beam size. Then it passes through two Pb scrapers, which clean the beam of scattered photons and particles created in the collimation process. A set

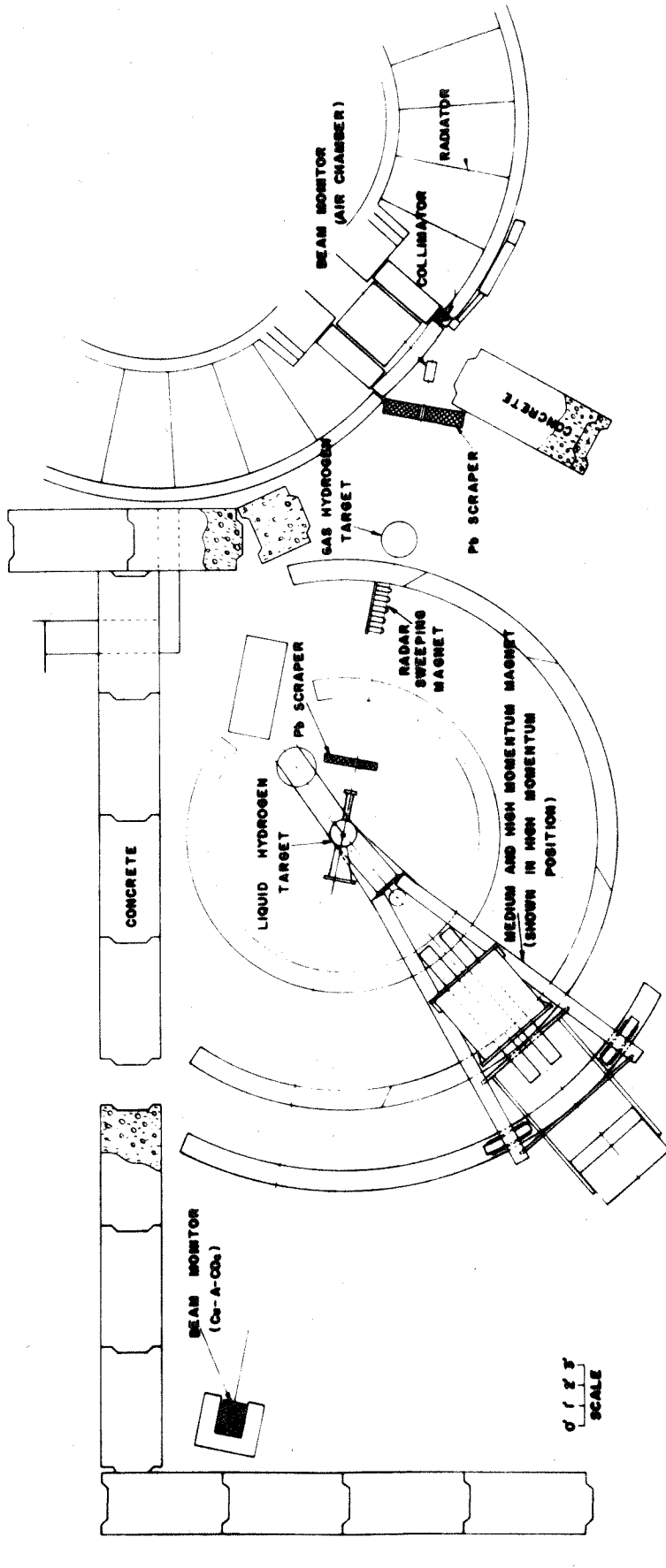
Figure 4. Angular Resolution of an Aperture of Fixed Size

This drawing shows why the angular resolution of an aperture (the cross-hatched areas) deteriorates as one moves from an angle θ_2 to a smaller angle θ_1 , due to the poor matching of the rectangular area to the circular projections from the target.



ANGULAR RESOLUTION FOR AN
APERTURE OF FIXED SIZE

Figure 5. The Experimental Area



of permanent "radar" magnets serves to sweep out electrons produced either in the collimator or in targets for other experiments. Actually, two arrangements were used during the experiment. The one shown in fig. 5 replaced an earlier version dictated by the requirements of other experiments. The radar magnets were closer to the second scraper in the earlier arrangement and did not give adequate sweeping. It was necessary to use the additional sweeping effect of the low energy spectrometer magnet which was mounted along the beam line just south of the first scraper at that time.

D. THE HYDROGEN TARGET

The target consists of a 3" diameter cylinder of liquid hydrogen contained in a Mylar cup. Surrounding this is a vacuum and a series of heat shields cooled by liquid nitrogen. The target was designed by V. Z. Peterson, and modified by R. L. Walker. The target used in this experiment differs from that previously used (5) mainly in that a "foghorn" shaped aluminum shield with large Mylar windows replaces a 360° Mylar window. This is shown in fig. 6. The amount of material in the path of the beam is substantially reduced, yielding a smaller background from the target structure. The Mylar windows are quite far from the target center and are not "seen" by the spectrometer except at the smallest angles, thus further reducing the background. At small angles, where the electron background becomes a major problem, this reduction of material in the beam is quite essential and was one of the reasons for redesigning the target.

The target can be used in either of two positions. For angles

smaller than 15° or larger than 45° the target is set so that the large Mylar window faces the spectrometer. In this position the small angle particles pass through the thin window and those at large angles through the $1/16$ " aluminum outer shield. Between 15° and 45° some of the particles would have to pass through the thick flange holding the Mylar window or the weld bead joining the horn to the outer shield. In order to avoid this the target is rotated 180° into its alternate position with the small window facing the spectrometer. This position is suitable for measurements at any angle greater than 15° .

E. THE SPECTROMETER

The magnetic spectrometer with its counter system is shown in fig. 6. Its properties as used in this experiment are summarized in Table 1. A detailed description of the magnet and measurements to determine its characteristics is given in an internal report (6). Angular settings are made by rotating the magnet about its pivot, below the target, on steel tracks. By this means angles can be set quite quickly, with an error of less than 0.1 degrees. When the spectrometer was set to 3° , the smallest angle used, the beam hit the magnet coil only 1" from the inside edge and there were many singles counts induced by the shower particles which escaped from the copper windings and entered the magnet gap. Pb shielding was placed along the magnet coils on the beam side, and a 4" Pb beam stopper was placed in front of the coils. This reduced the singles counts to an acceptable level.

F. THE COUNTER SYSTEM

The particle detection system consisted of five scintillation

Figure 6. The Hydrogen Target and Spectrometer

The spectrometer is shown in the high energy position, in which it was used throughout the experiment.

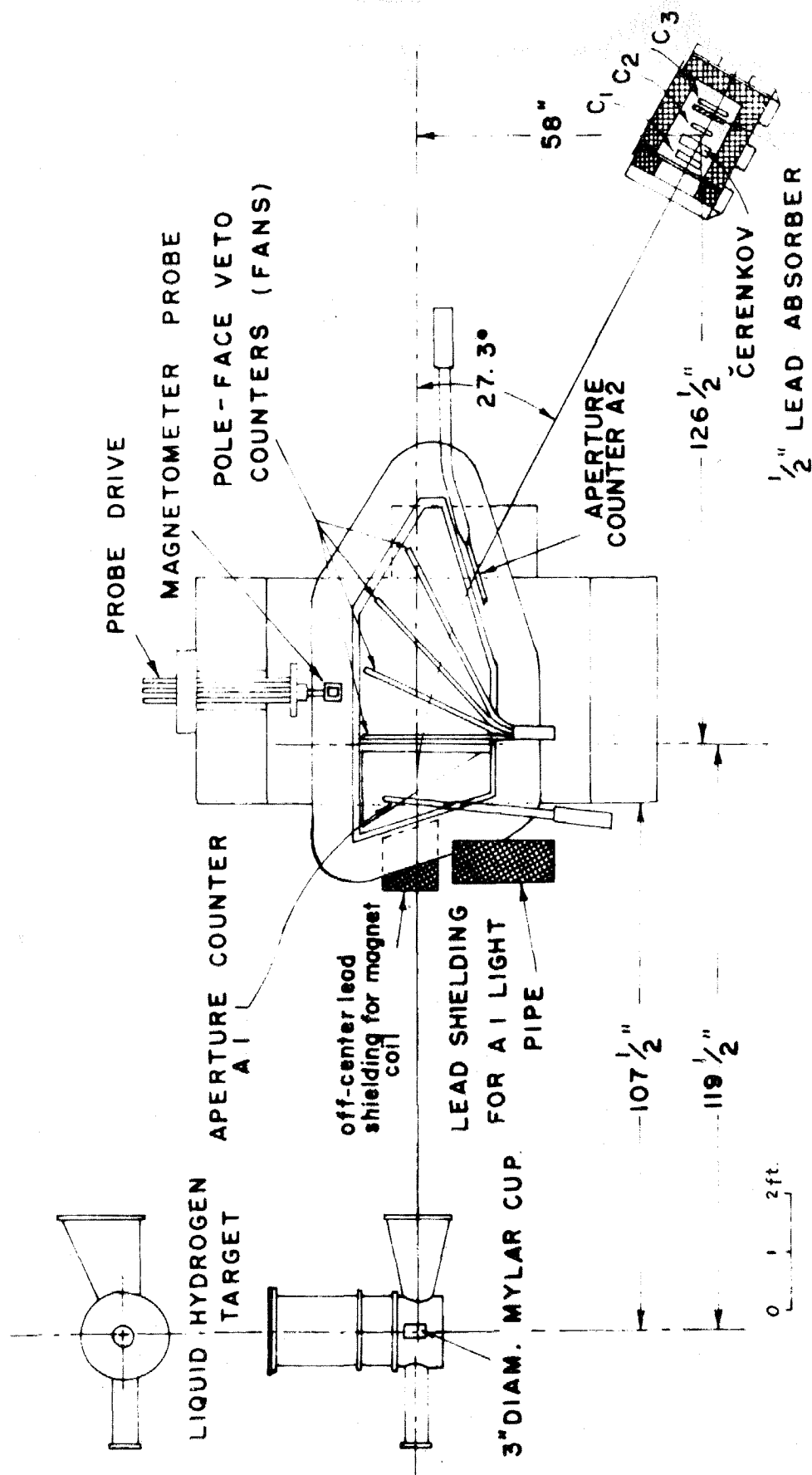


Table 1

Properties of the Spectrometer as Used For This Experiment

Acceptance $\frac{\Delta p}{p_0} \Delta \Omega$: (1) 1.08×10^{-4} ster.

(2) 0.54×10^{-4} ster.

(for two sizes of A2 scintillator)

Angular resolution: 1° (in lab. system)

Momentum dispersion $\frac{\Delta p}{p_0} = 0.099$

Maximum momentum: 1200 Mev/c

Maximum angle: 57°

Current regulation: 0.1 %

Field measurement: proton resonance magnetometer

whose resonant frequency, F , is given by

$F_{mc.} = a p_0$ where p_0 is in Mev/c

a is obtained from floating wire measurements and can be represented, with sufficient accuracy, by

$$a = \begin{cases} 0.05426, & p_0 \leq 575 \\ 0.05426 + b(p_0 - 575)^2 + c(p_0 - 575)^3 \\ \quad + d(p_0 - 575)^4, & p_0 \geq 575 \end{cases}$$

where $b = 5.616 \times 10^{-9}$

$c = -11.30 \times 10^{-12}$

$d = 17.17 \times 10^{-15}$

counters and one Cherenkov counter, and is shown in fig. 6

There was also a set of pole-face veto counters ("fan counters") which served to eliminate particles which scattered from the pole faces. A description of the individual counters appears in Table 2. Counter A1, which served to define the vertical angular aperture in previous experiments could not be used in this way at small angles because the large number of low energy particles (mainly electrons) produced at small angles flooded this counter and made it unreliable for coincidence measurements. This prompted the use of a new aperture counter, A2, placed behind the magnet. The low energy particles were swept out by the magnetic field, giving an acceptable counting rate in A2 even at small angles. The aperture is made slightly "fuzzy" due to the momentum dependence of the angular limits but this effect is insignificant.

A2 was designed to give a smaller vertical aperture than A1 because at small angles the angular resolution would deteriorate if the counters were too long, as mentioned in section B. It is of course advantageous to have as large an aperture as possible in order to increase the counting rate. Therefore, two sizes of scintillators were used, the smaller one being necessary only at 3° or 3.2° . The scintillators could be interchanged quickly, being attached by a pair of collars and set screws.

G. PARTICLE SELECTION AND ELECTRONICS

Particles of the same momentum and charge but different mass were distinguished on the basis of the pulse heights produced in the five counters.

Table 2
Description of the Counter

Desig.	Type	Size, in	Use
A1	scint.	12.34 x 3.24 x 0.250	calibrations and efficiency measurements
Fans	scint.	two arrays of 4 rods, 1/2 x 3/4 (see fig. 3)	veto of particles scattered from pole tips
A2	scint.	(1) 11.84 x 2.99 x 0.46 (2) 6.00 x 2.99 x 0.46 (interchangeable)	aperture definition
C1	scint.	5.75 x 11.0 x 0.787	dE/dx particle selection
C2	scint.	4.75 x 11.0 x 0.787	dE/dx particle selector (and shower detector)
C	Cherenkov	6.0 x 11.0 x 1.50	velocity particle selector
C3	scint.	5.75 x 11.0 x 0.394	dE/dx particle selector (and shower detector)

A1, A2, C1, C2 and C3 were scintillation counters in which the pulse height was proportional to the specific ionization, dE/dx . \check{C} was a Cherenkov counter of the total internal reflection type, giving an output pulse only if the particle velocity exceeded a velocity of about 0.85 c. The pulses were analyzed and counted by the electronics system shown in fig. 7.

Pions were selected on the basis of their pulse heights exceeding lower limiting values in all five counters, and not producing a pulse in the "fan" counters. Protons were rejected by the velocity selection of \check{C} . Since the major problem at small angles is the electron background special attention will be devoted to the electron detection scheme.

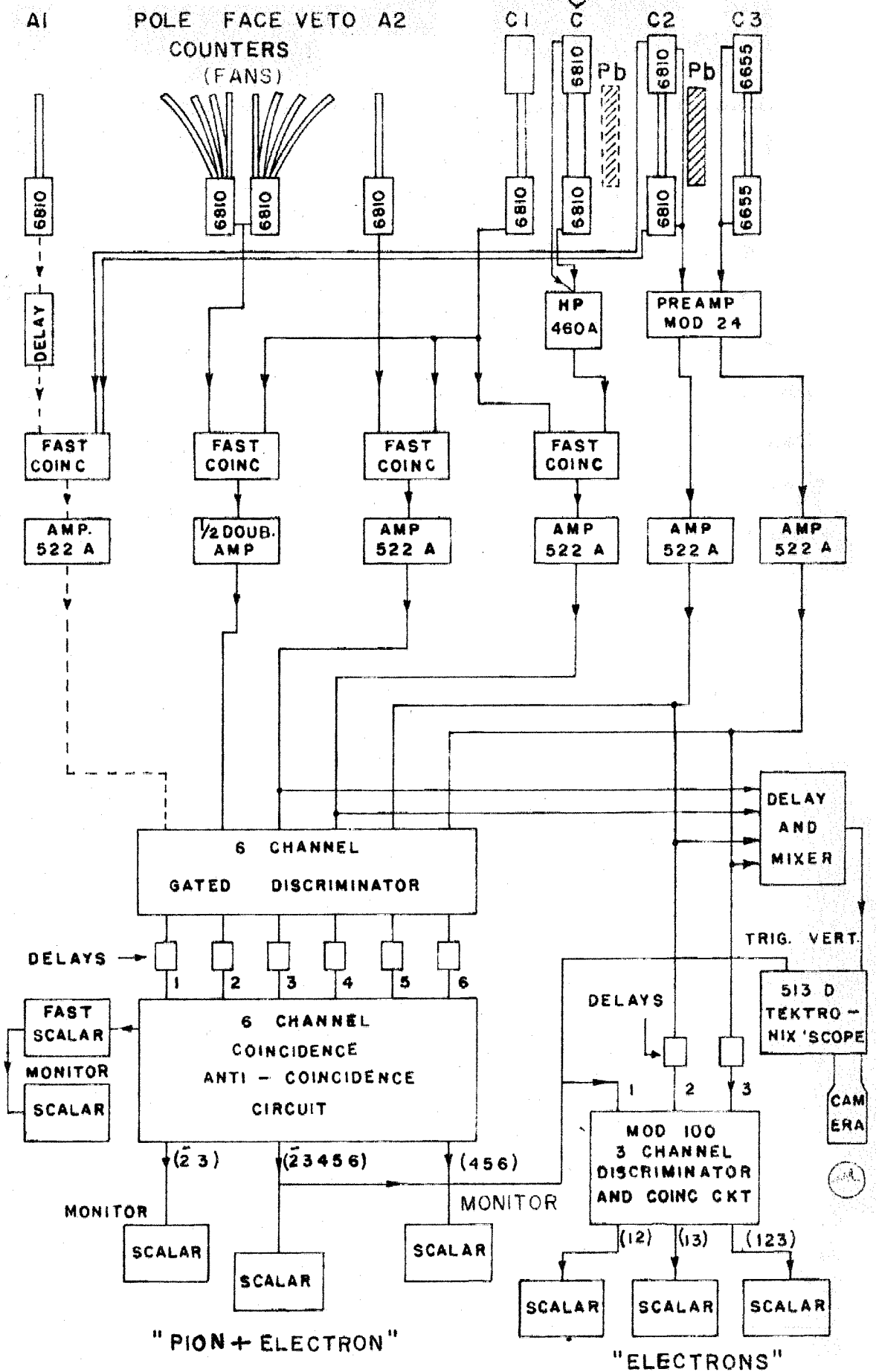
The electrons cannot be distinguished from the pions by means of velocity selection unless gaseous Cherenkov counters are used. The complications in the design of such a counter prompted the use of a much simpler scheme which relied upon the tendency of an electron to initiate a shower.

At most angles, a 1/2" Pb convertor was placed in front of C3. The shower initiated by an electron produced a large pulse in this counter. Those pulses which exceeded a high limiting bias (corresponding to approximately three times the pulse height produced by a minimum ionizing particle) were counted in a special "electron" scalar.

At the smallest angles it was necessary to use a second 1/2" Pb convertor placed in front of C2. Events producing larger pulses in either C2 or C3 or both C2 and C3 were counted as "electrons". This additional convertor was used to increase the detection efficiency and to eliminate some spurious counts that were observed at the smallest

Figure 7. Electronics Block Diagram

The numbers 6810 and 6655 are phototube types. HP means Hewlett Packard. All other units, except of course the oscilloscope, were specially built. The phototube circuit shown in dotted lines was used only for calibration and efficiency runs.



angle, 3° . These events were discovered when reverse magnetic field (negative charge) runs were taken and "negative pions" were observed, after backgrounds were subtracted, when using the single convertor. It is believed that these spurious counts arose from low energy photons or electrons produced in showers in the magnet material, but no definite identification could be made. At 5° no "negative pions" were observed even with the single convertor. At 3° , the single convertor positive "pion counting rate" was approximately 10% higher than the double convertor rate, due to these events. The double convertor "negative pion" counting rate was zero within statistics (approximately 4%). In fact the result was actually slightly negative.

III. DATA

A list of the data points and the associated kinematical quantities and experimental configurations is given in Table 3. The counting rates obtained for each point for full target and "empty" target runs are given in Table 4. (The empty target contained one atmosphere of hydrogen gas at liquid hydrogen temperature.)

The proton runs were made separately by requiring the Cherenkov counter in veto rather than coincidence.

The errors listed are purely statistical, i. e. simply $(\text{counting rate})/\sqrt{N}$, where N is the number of counts. Since C and E are not statistically independent the errors given reflect only the number of counts for each of these quantities separately, and are not indicative of the errors in the final pion counting rate.

Table 3

Data Point Kinematics and Configuration

Point:	The designation of the data point according to laboratory photon energy and angle.
k :	Mean laboratory photon energy, Mev.
θ_o :	Central angle of spectrometer.
θ_{cm} :	Pion center of momentum angle corresponding to θ_o .
p_o :	Mean momentum of spectrometer, Mev/c.
p_o^s :	Pion momentum at center of hydrogen target, before losing momentum in the target and counter material in front of the magnet.
E_o :	Maximum photon energy in the beam (or the electron energy of the internal beam).
Config:	<p>The two variables in the configuration are the size of the scintillator on counter A2 and the number of Pb converters used.</p> <p>1 12" scint.</p> <p>2 6" scint.</p> <p>S single 1/2" converter, in front of C3</p> <p>D double converter. One in front of C3, one in front of C2 (each 1/2").</p> <p>e.g. 1D means a 12" scintillator was used with a double converter.</p>

Table 3

Point	k	θ_o	θ_{cm}	p_o	p_o^s	E_o	config.
700-5	700	5°	8.0°	680.2	683.8	800	1D
700-7.5	700	7.5°	12.0°	677.7	681.3	800	1S
800-3.2	800	3.2°	5.3°	782.9	786.5	900	2D
800-5	800	5°	8.3°	781.5	785.0	900	1D
800-7.5	800	7.5°	12.5°	778.2	781.8	900	1S
900-3	900	3°	5.2°	884.2	887.8	990	2D
900-5	900	5°	8.6°	882.1	885.7	990	1S
900-7.5	900	7.5°	12.9°	878.0	881.6	990	1S
900-10	900	10°	17.2°	872.3	876.0	990	1S
900-15	900	15°	25.6°	856.5	860.2	990	1S
960-3	960	3°	5.3°	944.8	948.4	1050	2D
960-5	960	5°	8.8°	942.4	946.0	1050	1S
960-7.5	960	7.5°	13.2°	937.7	941.3	1050	1S
960-10	960	10°	17.6°	931.3	934.9	1050	1S
960-15	960	15°	26.2°	913.3	917.0	1050	1S
1025-3	1025	3°	5.4°	1010.2	1013.8	1130	2D
1025-5	1025	5°	9.0°	1007.5	1011.1	1130	1S
1025-7.5	1025	7.5°	13.5°	1002.2	1005.8	1130	1S
1025-10	1025	10°	17.9°	994.9	998.5	1130	1S
1025-15	1025	15°	26.7°	974.5	978.2	1130	1S
1025-20	1025	20°	35.3°	947.0	951.4	1130	1S
1025-25	1025	25°	43.6°	914.8	919.2	1130	1S
1025-35	1025	35°	59.3°	840.2	844.5	1130	1S
1025-45	1025	45°	73.7°	760.0	764.3	1130	1S
1025-55	1025	55°	86.7°	682.0	686.2	1130	1S

Table 4

Data

Point: As in Table 3, the energy and laboratory angle.

C: The number of $\overline{23456}$ coincidence counts per BIP.*

E: The number of "Electron" counts per BIP* for either single or double convertor.

C_p: The number of proton counts per BIP* when running with the Cherenkov counter in veto rather than in coincidence.

The errors listed are discussed on page 29.

*One BIP is approximately 0.95×10^{12} Mev. See Appendix I for the exact definition, which depends slightly on the end point energy, E_o .

Table 4
Foreground

Point	C	E	C _p
700-5	1.92 ± 0.05	0.94 ± 0.05	1.68 ± 0.16
700-7.5	1.08 ± 0.04	0.17 ± 0.02	1.34 ± 0.15
800-3.2	2.95 ± 0.05	2.42 ± 0.04	0.86 ± 0.11
800-5	1.25 ± 0.04	0.54 ± 0.02	1.40 ± 0.13
800-7.5	0.82 ± 0.03	0.12 ± 0.01	1.43 ± 0.14
900-3	1.92 ± 0.04	1.48 ± 0.03	0.74 ± 0.09
900-5	0.99 ± 0.03	0.24 ± 0.02	1.07 ± 0.12
900-7.5	0.69 ± 0.03	0.08 ± 0.01	0.98 ± 0.11
900-10	0.56 ± 0.02	0.06 ± 0.005	1.11 ± 0.12
900-15	0.54 ± 0.03	0.04 ± 0.01	0.80 ± 0.10
960-3	1.64 ± 0.03	1.32 ± 0.03	0.82 ± 0.10
960-5	0.90 ± 0.03	0.18 ± 0.01	1.27 ± 0.12
960-7.5	0.52 ± 0.02	0.08 ± 0.01	1.08 ± 0.11
960-10	0.48 ± 0.02	0.05 ± 0.01	0.83 ± 0.10
960-15	0.53 ± 0.02	0.05 ± 0.01	0.76 ± 0.09
1025-3	0.98 ± 0.02	0.71 ± 0.01	0.73 ± 0.08
1025-5	0.60 ± 0.02	0.14 ± 0.01	1.36 ± 0.15
1025-7.5	0.45 ± 0.01	0.08 ± 0.005	1.01 ± 0.08
1025-10	0.44 ± 0.015	0.04 ± 0.004	0.93 ± 0.08
1025-15	0.49 ± 0.015	0.05 ± 0.005	0.68 ± 0.08
1025-20	0.50 ± 0.02	0.04 ± 0.006	0.81 ± 0.09
1025-25	0.53 ± 0.02	0.05 ± 0.007	0.69 ± 0.08
1025-35	0.35 ± 0.02	0.04 ± 0.006	0.34 ± 0.06
1025-45	0.161 ± 0.008	0.015 ± 0.003	0.22 ± 0.05
1025-55	0.088 ± 0.009	0.008 ± 0.003	0.04 ± 0.02

Table 4

Point	Background		E	C _p
	C			
700-5	0.99 ± 0.05		0.90 ± 0.05	0.58 ± 0.08
700-7.5	0.15 ± 0.025		0.07 ± 0.02	0.63 ± 0.12
800-3.2	2.19 ± 0.04		2.07 ± 0.04	0.44 ± 0.09
800-5	0.37 ± 0.04		0.28 ± 0.03	0.63 ± 0.11
800-7.5	0.15 ± 0.03		0.04 ± 0.01	0.37 ± 0.10
900-3	1.38 ± 0.05		1.29 ± 0.04	0.34 ± 0.08
900-5	0.22 ± 0.02		0.10 ± 0.02	0.38 ± 0.08
900-7.5	0.09 ± 0.02		0.02 ± 0.008	0.26 ± 0.08
900-10	0.05 ± 0.01		0.002 ± 0.002	0.26 ± 0.06
900-15	0.03 ± 0.01		0.008 ± 0.006	0.12 ± 0.04
960-3	0.98 ± 0.04		0.91 ± 0.03	0.44 ± 0.08
960-5	0.16 ± 0.02		0.07 ± 0.01	0.60 ± 0.10
960-7.5	0.04 ± 0.01		0.012 ± 0.006	0.34 ± 0.08
960-10	0.02 ± 0.01		0.002 ± 0.002	0.20 ± 0.07
960-15	0.03 ± 0.01		0.007 ± 0.005	0.04 ± 0.03
1025-3	0.50 ± 0.02		0.45 ± 0.02	0.48 ± 0.09
1025-5	0.10 ± 0.01		0.05 ± 0.007	0.33 ± 0.08
1025-7.5	0.072 ± 0.008		0.031 ± 0.006	0.19 ± 0.03
1025-10	0.044 ± 0.008		0.010 ± 0.004	0.17 ± 0.03
1025-15	0.020 ± 0.007		0.004 ± 0.003	0.04 ± 0.015
1025-20	0.026 ± 0.009		0.009 ± 0.005	0.10 ± 0.04
1025-25	0.023 ± 0.009		0.003 ± 0.003	0.05 ± 0.03
1025-35	0.010 ± 0.006		0.000 ± 0.003	0.05 ± 0.02
1025-45	0.013 ± 0.006		0.000 ± 0.003	0.04 ± 0.03
1025-55	0.013 ± 0.006		0.006 ± 0.004	0.02 ± 0.02

IV. DATA REDUCTION

A. CROSS SECTION FORMULAS

The counting rate can be expressed in terms of the cross section, kinematical quantities, and geometrical factors:

$$C_{\pi} = \int \dots \int \sigma(d\theta') \frac{\partial \Omega'}{\partial \Omega} R_D A_{\pi} N_H N(k) n(x, y) dx dy dz dk d\Omega$$

where

C_{π} = number of counts per BIP observed

$\sigma(k, \theta') d\Omega'$ = differential cross section for producing a pion in $d\Omega'$ at θ' from a photon of energy k . Primed quantities refer to c.m. system.

$\frac{\partial \Omega'}{\partial \Omega}$ = transformation from c.m. solid angle to laboratory solid angle

R_D = correction for pion decay, including resulting muon background

A_{π} = correction for pion absorption

N_H = the number of hydrogen nuclei per unit volume effective in the reaction

$N(k)dk$ = the number of photons per BIP with energy from k to $k+dk$.

$n(x, y)$ = the relative intensity of the beam at point x, y in a plane perpendicular to the beam at the target.

$d\Omega$ = laboratory solid angle increment.

An integral over the variables indicated yields the observed counting rate. This integral is quite complicated if carried out in detail. In practice, if the spectrometer acceptance region is illuminated nearly uniformly with pions, the quantities $\sigma(d\theta')$, $\frac{\partial \Omega'}{\partial \Omega}$, R_D , A_{π} , and $N(k)$

are nearly constant over the range of integration where there is a non-zero integrand. Therefore we may write a more convenient expression containing average quantities:

$$\sigma(k, \theta') = C_{\pi}/\kappa$$

where

$$\kappa = \left[\left(\frac{\partial \Omega}{\partial \Omega} \right) \left(\frac{\partial k}{\partial p} \right) \right]_{av} (\Delta \Omega \frac{\Delta p}{p_o}) R_D A_{\pi} N_H \bar{l} \overline{N(k)} p_o$$

$\Delta \Omega$ = the average solid angle of the spectrometer.

\bar{l} = the mean path length for the beam through the hydrogen.

$\overline{N(k)}$ = an average over $N(k)$, taking into account the photon spectrum and the spectrometer resolution.

$\frac{\Delta p}{p_o}$ = the momentum dispersion of the spectrometer.

In this experiment all configurations were such that the use of average quantities rather than the integral expression is quite adequate. Since there is some energy loss of the pion in the target and in the counter A1, the momentum setting of the magnet, p_o , corresponds to a pion produced with higher average momentum, p_o^s . This is taken into account by multiplying by $\frac{p_o}{p_o^s}$ to obtain the effective momentum dispersion. Corrections for the pion decay, expressed by the factor R_D , are discussed in Appendix III. The absorption corrections, A_{π} , are discussed in Appendix IV.

B. CALCULATION OF κ

1. Acceptance of Spectrometer

The value of the product $\frac{\Delta p}{p_o} \Delta \Omega$ is known from floating wire

measurements for the configuration in which A1 is used to define the aperture (5). Rather than perform a similar measurement of this quantity for A2 the ratio of the acceptance using A2 to that using A1 was measured directly with a statistical accuracy of 1.5% by counting particles produced in a carbon target at 25° (lab) with both configurations simultaneously. The results agree well with estimates from graphical ray tracing. The ratio obtained was

$$\frac{(\Delta\Omega \frac{\Delta p}{p_o})_{A1}}{(\Delta\Omega \frac{\Delta p}{p_o})_{A2}} = 1.81 (\pm 1.5\%)$$

for the larger scintillator on A2. This result was used to calculate the values for the acceptance given in Table 1.

2. Effective Length

\bar{l} is calculated by averaging the target thickness over the cylinder of liquid hydrogen, weighted according to the beam density. This procedure requires a knowledge of the spatial distribution of the beam density, which has been measured recently as part of an experiment to determine the beam spectrum. A computer program was written to calculate \bar{l} , using the measured beam density, for rectangular or circular collimation, both of which were used during this experiment. The change of density with machine energy causes \bar{l} to be a function of energy. The results are included in Table 5.

3. Hydrogen Density

The liquid hydrogen operates at 1/2 psi above atmospheric pressure, which corresponds to a density of 0.0707 gms/cc. The "empty"

Table 5
Calculation of κ

Point	$\frac{\partial \kappa}{\partial p} \left(\frac{\partial \Omega}{\partial \Omega} \right)$	A_{π}	R_D	$\frac{\Delta P}{P_0} (\Delta \Omega) \times 10^4$	\bar{l} , cm	W , Mev/BIP $\times 10^{-12}$	$B(k, E_0)$	$\overline{N(k)} \times 10^{-6}$	$\kappa \times 10^{-28}$
700-5	2.525	0.842	0.920	1.08	7.16	0.945	0.912	1.539	6.583
700-7.5	2.525	0.892	0.920	1.08	7.16	0.945	0.912	1.539	6.949
800-3.2	2.734	0.842	0.930	0.54	7.17	0.953	0.907	1.200	3.236
800-5	2.734	0.842	0.928	1.08	7.17	0.953	0.907	1.200	6.445
800-7.5	2.734	0.892	0.928	1.08	7.17	0.953	0.907	1.200	6.800
900-3	2.949	0.842	0.936	0.54	7.17	0.951	0.894	0.933	3.083
900-5	2.949	0.892	0.936	1.08	7.17	0.951	0.894	0.933	6.516
900-7.5	2.948	0.892	0.935	1.08	7.17	0.951	0.894	0.933	6.477
900-10	2.947	0.892	0.936	1.08	7.17	0.951	0.894	0.933	6.441
900-15	2.946	0.892	0.935	1.08	7.17	0.951	0.892	0.931	6.302
960-3	3.086	0.842	0.939	0.54	7.18	0.949	0.890	0.838	3.110
960-5	3.085	0.892	0.939	1.08	7.18	0.949	0.890	0.838	6.570
960-7.5	3.085	0.892	0.938	1.08	7.18	0.949	0.890	0.838	6.530
960-10	3.085	0.892	0.938	1.08	7.18	0.949	0.890	0.838	6.486
960-15	3.083	0.892	0.937	1.08	7.18	0.949	0.888	0.836	6.335
1025-3	3.219	0.842	0.942	0.54	7.18	0.940	0.896	0.727	3.018
1025-5	3.218	0.892	0.943	1.08	7.18	0.940	0.896	0.727	6.381
1025-7.5	3.218	0.892	0.942	1.08	7.18	0.940	0.896	0.727	6.341
1025-10	3.217	0.892	0.941	1.08	7.18	0.940	0.896	0.727	6.286
1025-15	3.214	0.892	0.941	1.08	7.18	0.940	0.894	0.726	6.144
1025-20	3.211	0.892	0.938	1.08	7.18	0.940	0.892	0.724	5.935
1025-25	3.207	0.892	0.936	1.08	7.18	0.940	0.892	0.724	5.715
1025-35	3.198	0.892	0.929	1.08	7.18	0.940	0.890	0.722	5.182
1025-45	3.183	0.892	0.920	1.08	7.18	0.940	0.886	0.719	4.604
1025-55	3.165	0.892	0.911	1.08	7.18	0.940	0.881	0.715	4.047

target used for background runs actually contained one atmosphere of hydrogen gas at liquid hydrogen temperature, with density 0.0015 gms/cc. Therefore the effective density for calculating the cross section is:

$$\rho_H = 0.0707 - 0.0015 = 0.0692 \text{ gms/cc.}$$

Using an atomic weight of 1.008 and Avogadro's number 6.024×10^{23} , we obtain:

$$N_H = 0.4136 \times 10^{23} \text{ nuclei/cc.}$$

4. $\overline{N(k)}$

The photon population is discussed in Appendix I, Beam Monitoring.

5. Correction Factors

The values for R_D and A_π are obtained from the results of calculations and measurements discussed in Appendices III and IV respectively.

The values of the separate factors and the final values for κ are given in Table 5, for each of the data points.

C. COUNTING RATE FORMULAS

Because the counter system does not perfectly discriminate between the pions, protons and electrons that pass through the spectrometer, the counting rate for pions must be calculated from the observed number of counts, taking into account the system efficiencies.

Definitions:

C_π, C_p, C_e = the number of pions, protons, and electrons, respectively, passing through the system per BIP, within the acceptance range of the spectrometer. In the case of the pions C_π refers to the number remaining after absorption.

$\eta_{E\pi}, \eta_{Ep}, \eta_{Ee}$ = the efficiencies of the electron detection system for counting pions, protons and electrons respectively.

$\eta_{C\pi}^\vee, \eta_{Cp}^\vee, \eta_{Ce}^\vee$ = the efficiencies of the Cherenkov counter for counting pions, protons and electrons respectively.

[All other efficiencies are assumed to be 1.00.]

C = total number of counts per BIP (23456 coincidence, referring to the electronics diagram, fig. 7).

E = "electron" counts per BIP.

We can write C and E in terms of the other quantities above:

$$C = \eta_{C\pi}^\vee C_\pi + \eta_{Ce}^\vee C_e + \eta_{Cp}^\vee C_p$$

$$E = \eta_{C\pi}^\vee \eta_{E\pi} C_\pi + \eta_{Ce}^\vee \eta_{Ee} C_e + \eta_{Cp}^\vee \eta_{Ep} C_p$$

We can express C_π in terms of measured quantities:

$$C_\pi = \frac{1}{\eta_{C\pi}^\vee} \frac{1}{(1 - \frac{\eta_{E\pi}}{\eta_{Ee}})} \left\{ C - \frac{E}{\eta_{Ee}} - \eta_{Cp}^\vee (1 - \frac{\eta_{Ep}}{\eta_{Ee}}) C_p \right\}$$

Errors:

In order to calculate the statistical error, we use the fact that

$\eta_{C\pi}^\vee, \eta_{E\pi}, \eta_{Ee}, \eta_{Cp}^\vee, \eta_{Ep}$ and C_p are independent quantities. C and

E however are not independent since all of E must also be a part of C.

We divide $C - \frac{E}{\eta_{Ee}}$ as follows:

$$C - \frac{E}{\eta_{Ee}} = [C - E] + \left[\left(1 - \frac{1}{\eta_{Ee}}\right) E \right]$$

It is easy to see that the two quantities in brackets are statistically independent, since $[C - E]$ could have been counted directly by using a veto circuit and then this quantity would certainly be an independent variable. Once the counting rate is written in terms of independent quantities the error formula can be calculated in a straightforward manner. The result is:

$$\begin{aligned} \epsilon_{C\pi}^2 = & \frac{1}{\eta_{C\pi}^2 \left(1 - \frac{\eta_{E\pi}}{\eta_{Ee}}\right)^2} \left\{ \epsilon_{C-E}^2 + \left(1 - \frac{1}{\eta_{Ee}}\right)^2 \epsilon_E^2 + \eta_{Cp}^2 \left(1 - \frac{\eta_{Ep}}{\eta_{Ee}}\right)^2 \epsilon_{Cp}^2 \right. \\ & + \frac{E^2}{\eta_{Ee}^4} \epsilon_{\eta_{Ee}}^2 + C_p^2 \left[\left(1 - \frac{\eta_{Ep}}{\eta_{Ee}}\right)^2 \epsilon_{\eta_{Cp}}^2 + \eta_{Cp}^2 \left(\frac{\epsilon_{\eta_{Ep}}^2}{\eta_{Ee}^2} + \frac{\eta_{Ep}^2}{\eta_{Ee}^4} \epsilon_{\eta_{Ee}}^2 \right) \right] \Big\} \\ & + \left[(C-E) + \left(1 - \frac{1}{\eta_{Ee}}\right) E - \eta_{Cp} \left(1 - \frac{\eta_{Ep}}{\eta_{Ee}}\right) C_p \right]^2 \\ & \left\{ \frac{1}{\eta_{C\pi}^2 \left(1 - \frac{\eta_{E\pi}}{\eta_{Ee}}\right)^4} \left(\frac{1}{\eta_{Ee}^2} \epsilon_{\eta_{E\pi}}^2 + \frac{\eta_{E\pi}^2}{\eta_{Ee}^4} \epsilon_{\eta_{Ee}}^2 \right) + \frac{1}{\eta_{C\pi}^4 \left(1 - \frac{\eta_{E\pi}}{\eta_{Ee}}\right)^2 \eta_{C\pi}^2} \right\} \end{aligned}$$

where ϵ_x = statistical error in x.

V. RESULTS

A. TABULAR LISTING

The final values for the differential cross section as obtained from this experiment are listed in Table 6.

The errors listed arise solely from counting statistics and do not include systematic errors. Errors due to counter efficiency measurement statistics are included.

The absorption correction error has been treated in a special way. No error has been assigned to those points which were obtained using the single convertor since such an error would shift all of the points together without changing the shape. However at the smallest angles, where the double convertor was used, the error in the difference in absorption for the single and double convertors has been included in the overall error since such an error would shift one point with respect to the rest.

The error in the measurement of the spectrometer acceptance has been regarded as a systematic error and is not included in the errors listed.

The results of the preceding experiment of Dixon and Walker (5) are listed in Table 7. Corrections have been made to these results for improved values for the decay correction and for the more accurate spectrum shape.

B. GRAPHICAL DISPLAY

The results from both experiments are displayed in figs. 8(a) to 8(e). The curves are least squares Moravcsik type fits, the details of which are given in Section VI B.

Table 6

Results

Point	θ' (cm)	C_{π} , counts/BIP	$\sigma(\theta')$, $\mu\text{b/ster}$
700-5	8.0°	0.997 ± 0.052	15.14 ± 0.79
700-7.5	12.0°	0.903 ± 0.049	12.99 ± 0.70
800-3.2	5.3°	0.451 ± 0.032	13.94 ± 0.99
800-5	8.3°	0.700 ± 0.042	10.86 ± 0.65
800-7.5	12.5°	0.638 ± 0.043	9.38 ± 0.63
900-3	5.2°	0.399 ± 0.027	12.94 ± 0.88
900-5	8.6°	0.674 ± 0.039	10.34 ± 0.60
900-7.5	12.9°	0.577 ± 0.036	8.91 ± 0.56
900-10	17.2°	0.478 ± 0.021	7.42 ± 0.33
900-15	25.6°	0.508 ± 0.031	8.04 ± 0.49
960-3	5.3°	0.268 ± 0.023	8.62 ± 0.74
960-5	8.8°	0.496 ± 0.034	7.55 ± 0.52
960-7.5	13.2°	0.445 ± 0.028	6.81 ± 0.43
960-10	17.6°	0.443 ± 0.026	6.83 ± 0.40
960-15	26.2°	0.481 ± 0.028	7.59 ± 0.44
1025-3	5.4°	0.249 ± 0.015	8.25 ± 0.50
1025-5	9.0°	0.427 ± 0.020	6.69 ± 0.31
1025-7.5	13.5°	0.352 ± 0.017	5.55 ± 0.27
1025-10	17.9°	0.392 ± 0.019	6.24 ± 0.30
1025-15	26.7°	0.452 ± 0.019	7.36 ± 0.31
1025-20	35.3°	0.466 ± 0.026	7.85 ± 0.44
1025-25	43.6°	0.497 ± 0.027	8.70 ± 0.47
1025-35	59.3°	0.320 ± 0.021	6.18 ± 0.40
1025-45	73.7°	0.143 ± 0.012	3.10 ± 0.26
1025-55	86.7°	0.080 ± 0.011	1.98 ± 0.27

Table 7

Results From the Experiment of Dixon and Walker (5)

Point: In this table the point designation refers to the c.m. angle instead of the laboratory angle.

The results given here have been corrected for an improved calculation of the decay corrections and for a more accurate photon spectrum shape.

* Indicates a point obtained from an average of data from more than one experimental configuration.

Table 7

<u>Point</u>	<u>$\sigma(\theta^1)$, $\mu\text{b}/\text{ster.}$</u>
700-20	12.42 ± 0.67
700-30	10.86 ± 0.61
700-45	11.14 ± 0.59
700-60*	10.66 ± 0.18
700-75*	9.86 ± 0.31
700-90	8.60 ± 0.30
700-105	6.40 ± 0.30
700-120	4.46 ± 0.21
700-135	3.51 ± 0.18
700-150	2.74 ± 0.20
700-163	2.35 ± 0.19
800-20	9.31 ± 0.46
800-30	8.00 ± 0.47
800-45	7.25 ± 0.39
800-60	5.88 ± 0.41
800-75*	5.35 ± 0.17
800-90*	4.65 ± 0.14
800-105	4.06 ± 0.18
800-120	3.39 ± 0.16
800-135	2.69 ± 0.15
800-150	2.56 ± 0.16
800-163	2.26 ± 0.17
900-20	8.61 ± 0.47
900-30	8.06 ± 0.51
900-45	7.78 ± 0.46
900-60	5.04 ± 0.29
900-75	3.00 ± 0.20
900-90	2.69 ± 0.13
900-105	2.72 ± 0.14
900-120	2.66 ± 0.13
900-135	2.97 ± 0.11
900-150	2.15 ± 0.14
900-164	2.14 ± 0.15

Figure 8. Angular Distributions

The measured differential cross section, from this experiment and that of Dixon and Walker (5), are shown for 700, 800, 900, 960 and 1025 Mev laboratory photon energies. The errors shown are statistical and do not indicate systematic errors other than counter efficiency errors, which are themselves statistical in nature.

The solid curves are least squares fits with the Morovcsik form

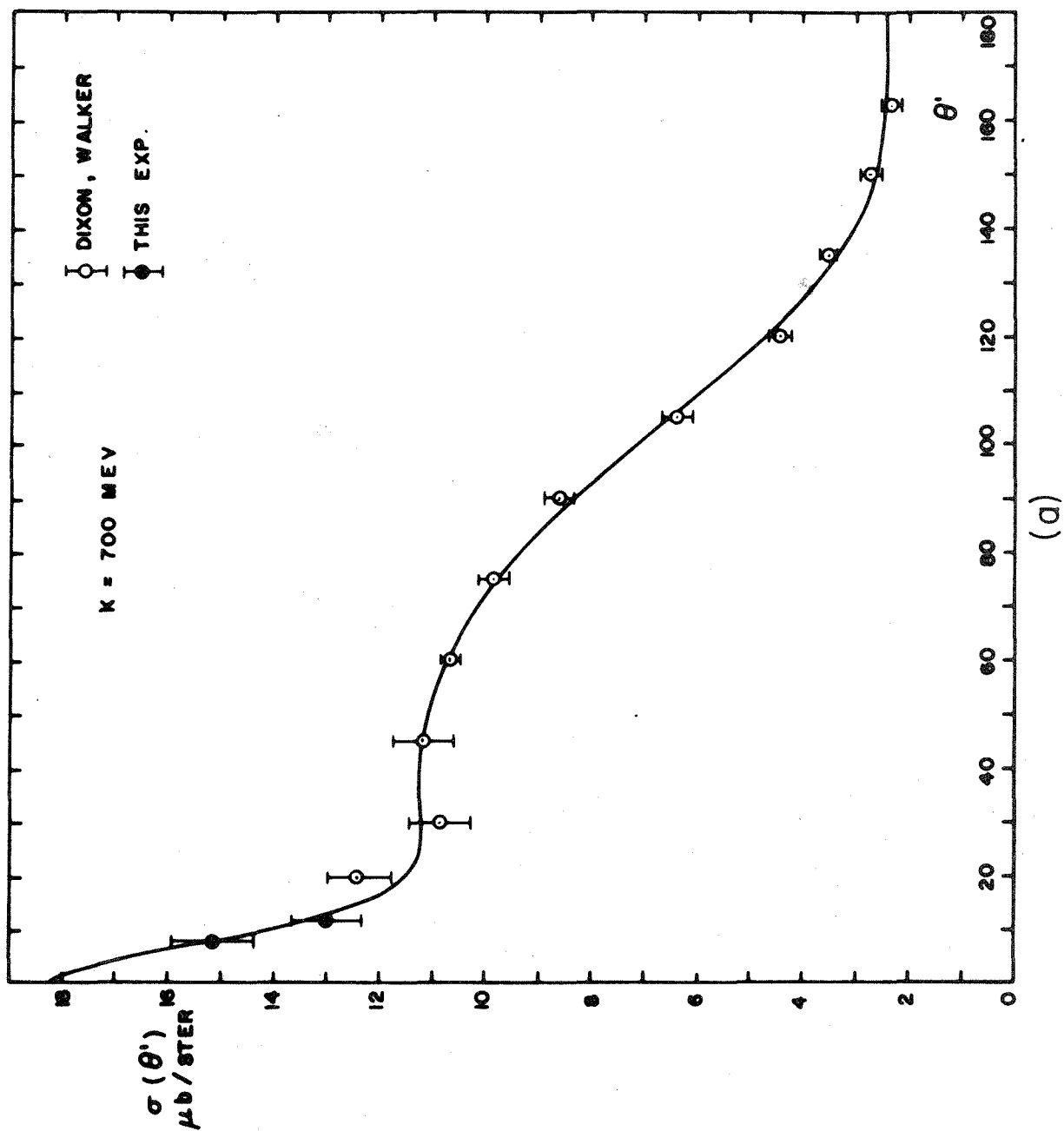
$$\sigma(\theta') = \frac{\sum_{n=0}^N B_n \cos^n \theta'}{(1 - \beta' \cos \theta')^2}$$

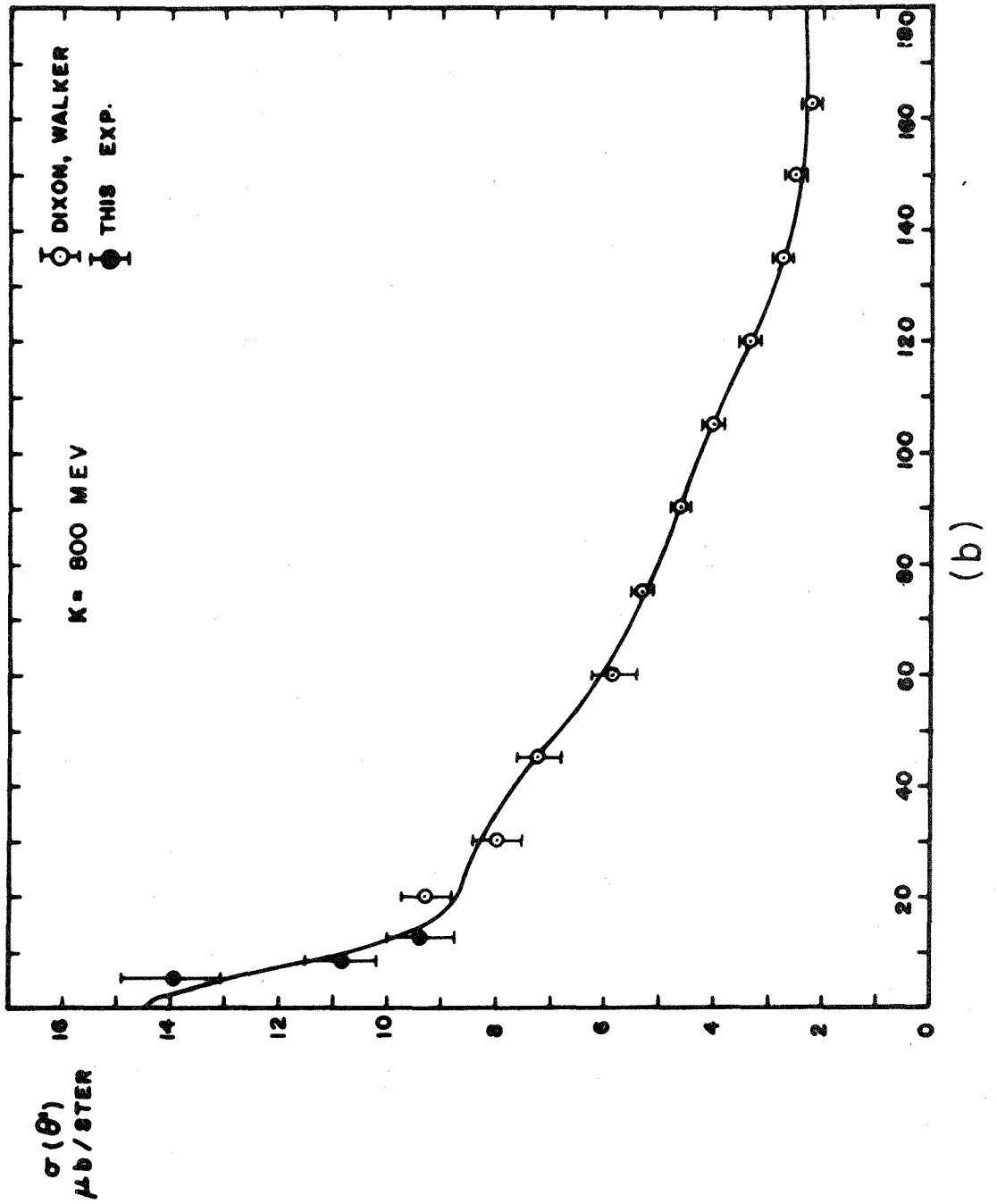
In each case $N = 6$.

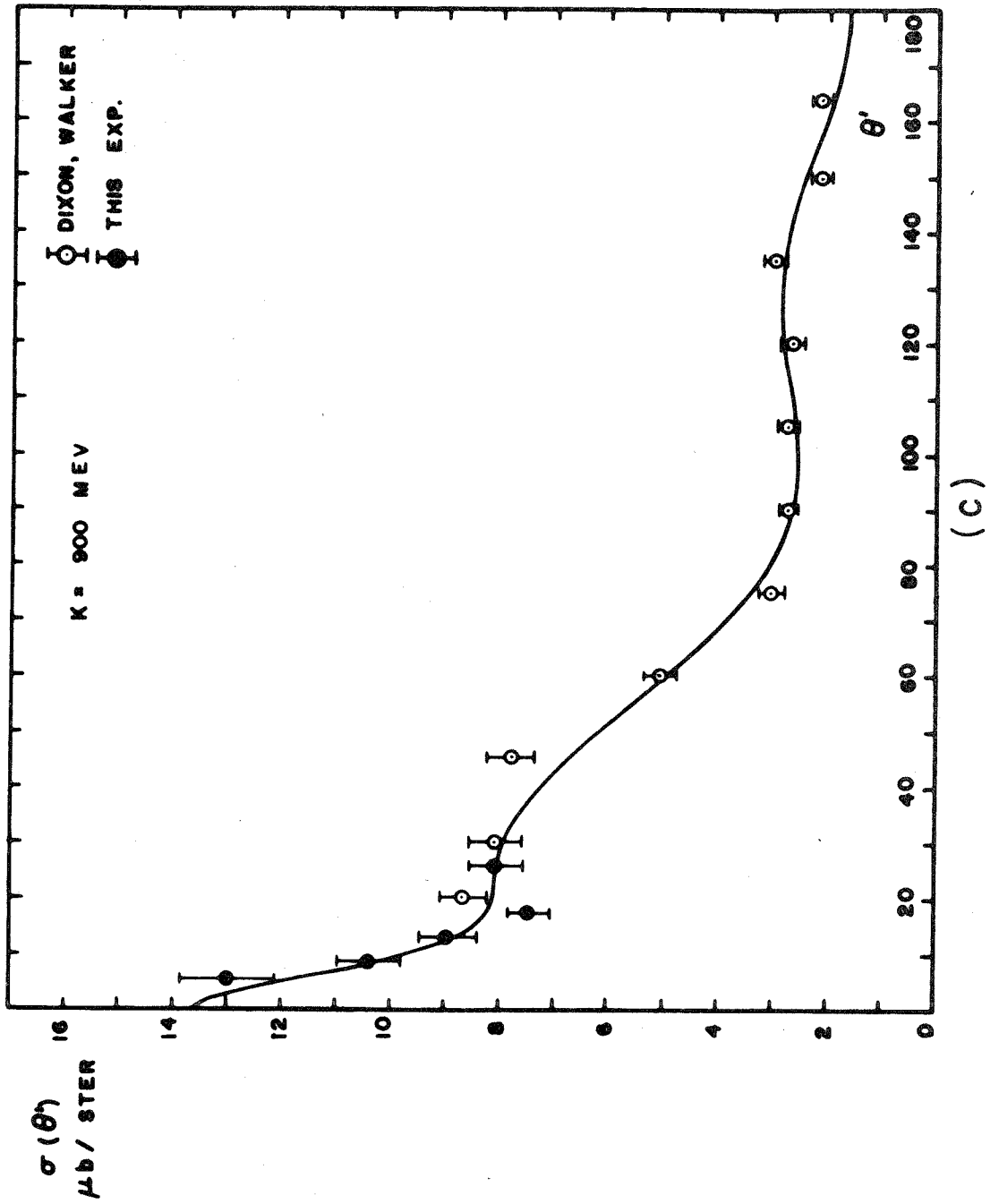
Some artificial data points not shown have been included in making the fits (see text). For $k = 1025$ Mev, fig. 8(e), the simple polynomial fit

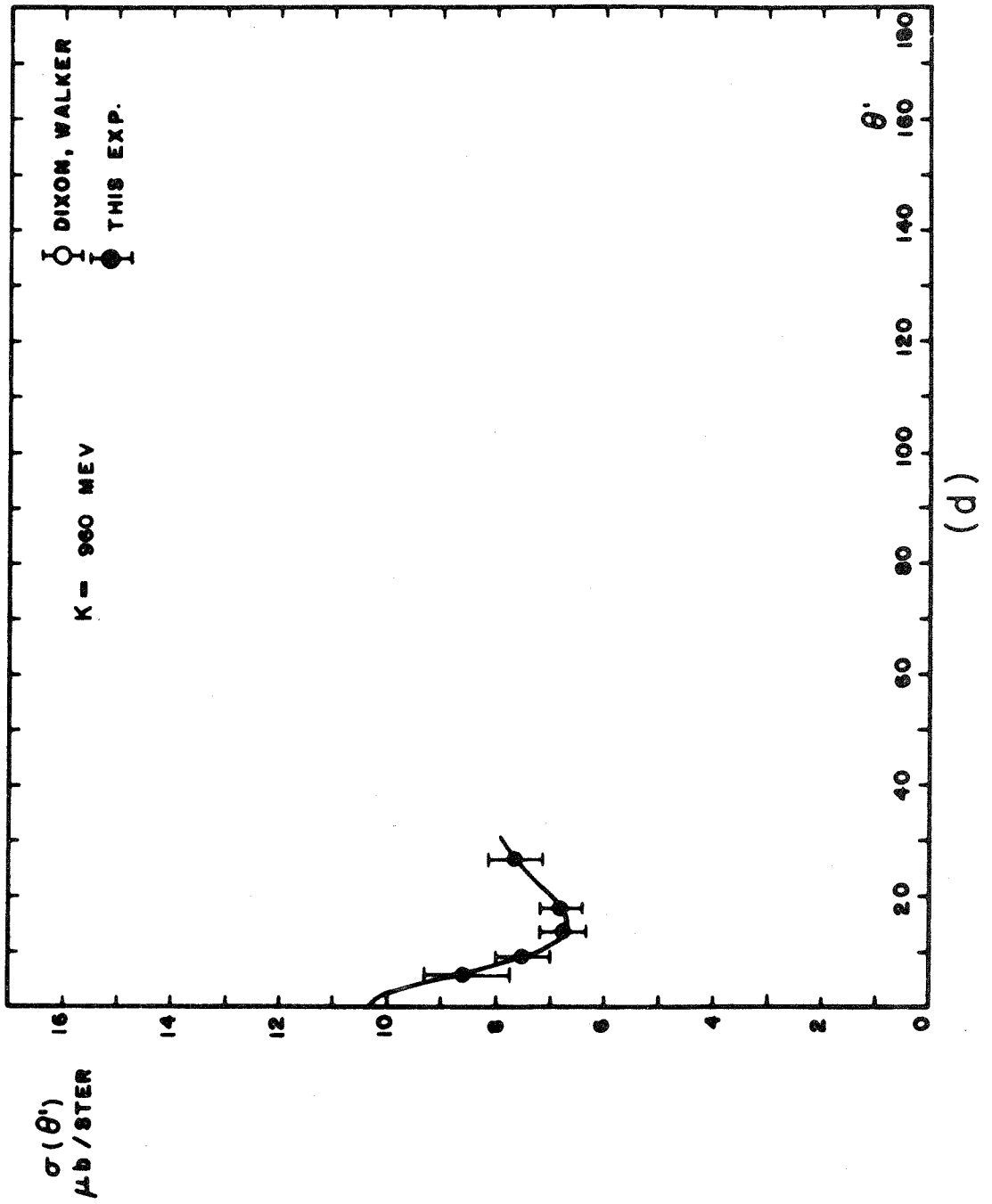
$$\sigma(\theta') = \sum_{n=0}^N A_n \cos^n \theta'$$

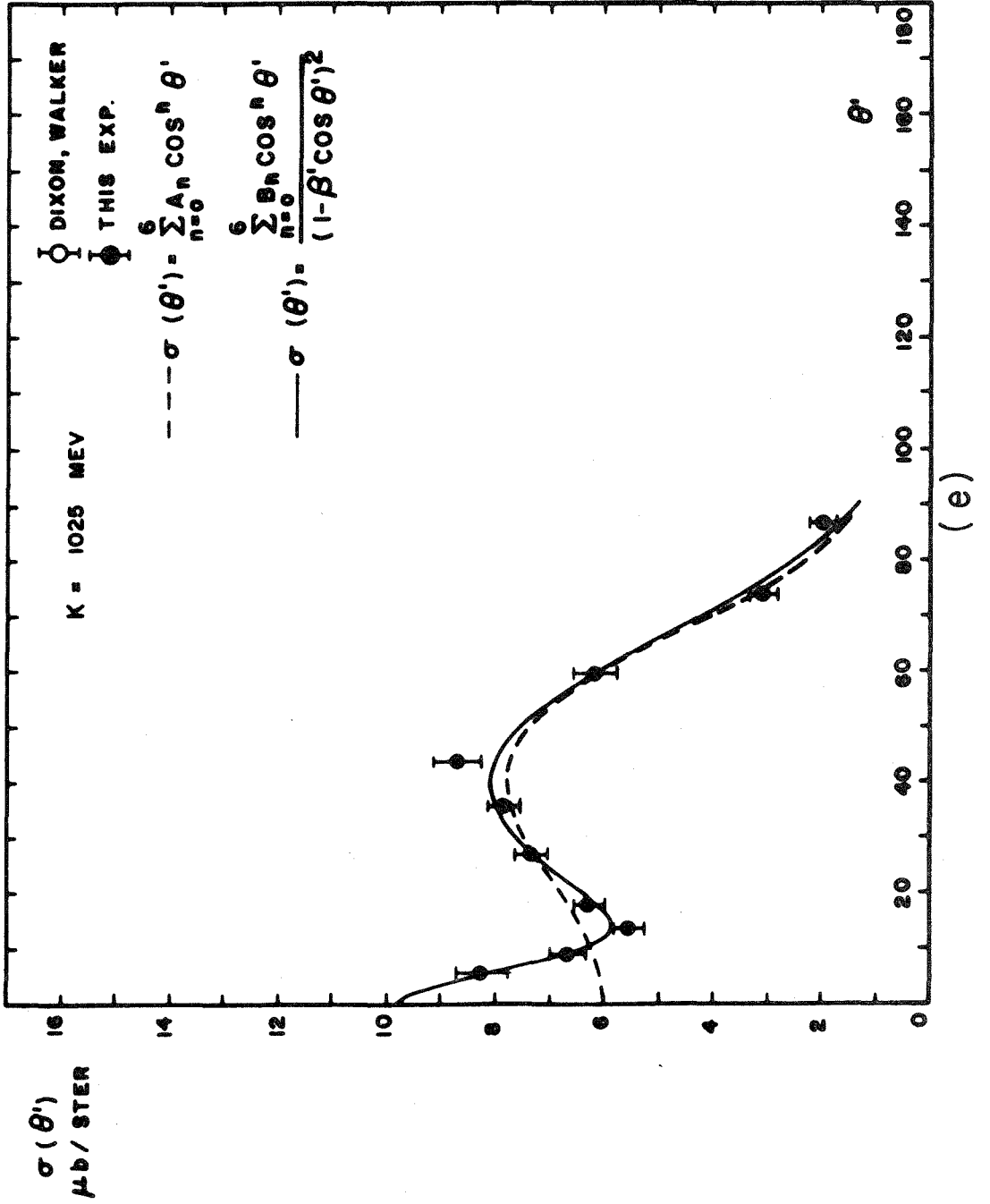
is also shown to illustrate the poor fit obtained as compared with the Morovcsik form.











IV. ANALYSIS

A. GENERAL

Since there exists no satisfactory theory for predicting the photo-production cross section in the energy range of this experiment, one must extract as much information as possible on the basis of a phenomenological analysis of the data.

The cross section can be written in terms of all of the multipoles that can contribute. (7) However, there are so many unknown complex coefficients that it is not possible to uniquely determine them from the data at present. The only method of attack which has any hope of success is to simplify the form of the cross section as much as possible by assuming that all of the interactions take place in resonant states in which one multipole predominates in the vicinity of each of the resonance energies. In addition to these resonant states one must insert the retardation term and "background" states of low angular momentum, the only available procedure being to use the Born approximation, perhaps with variations in the amplitudes of the two terms. Such a program of analysis is being carried out by J. Link and R. L. Walker, using standard resonance formulas to suggest the energy dependence of the multipole amplitudes and phases. By using the currently accepted state assignments for the first and second resonances the possible choices for the multipoles become sufficiently restricted that there is some chance that one can distinguish between the possible state assignments for the third resonance by comparing the calculated angular distributions with experimental results. In fact, this possibility was

one of the reasons for initiating this experiment. It was hoped that interferences with the retardation term at small angles would distinguish between multipoles in the vicinity of the third resonance. However, interference with the low angular momentum states obscures any such effects, as may be seen by examining the Born approximation results, fig. 2.

A description of the detailed procedure used by Link and Walker would be rather lengthy. It is sufficient to say that at the present stage of the program no definite decisions can be made with regard to the third resonance assignments. None of the synthesized expressions agree well enough with experiment, or for that matter disagree violently enough, that an unambiguous choice can be made. The analysis will continue, aided in the future by measurements at 1100 and 1200 Mev. (11)

There are some features of the theory which are especially related to the small angle measurements of this experiment, and even though a multipole analysis is not possible the data will be analyzed with regard to these special points, namely the effect of the retardation term and the importance of the 0° cross section.

B. MORAVCSIK CURVE FITTING

Moravcsik (8) has pointed out that the presence of the retardation term should be specifically taken into account when making a fit to π^+ photoproduction data. The simplest procedure in fitting angular distributions is to use the polynomial form

$$\sigma(\theta') = \sum_{n=0}^N A_n \cos^n \theta'$$

However, the retardation term introduces a term into the cross section of the form

$$\frac{F(k, \theta')}{(1 - \beta' \cos \theta')^2}$$

where $F(k, \theta')$ is a smooth function of photon energy and c.m. angle, and β' is the velocity/c of the pion in the c.m. system. Since β' is quite close to 1.0, an expansion of this function in terms of powers of $\cos \theta'$ is very slowly converging and requires a large number of terms to give an adequate approximation. If the functional form

$$\sigma(\theta') = \frac{\sum_{n=0}^N B_n \cos^n \theta'}{(1 - \beta' \cos \theta')^2}$$

is used, many fewer terms (smaller N) will give a satisfactory fit. The terms in the cross section that do not have this characteristic denominator will be effectively multiplied by $\cos \theta'$ or $\cos^2 \theta'$. Thus we can expect that a satisfactory fit will be obtained for N greater by no more than two than the value which would be obtained if the retardation term were not present. Fits were made to the data by the usual method of least squares, using the Moravcsik form.

The principles of the least squares procedure has been treated by many authors but a most convenient summary of all of the features necessary for the analysis here is given in a paper by P. Cziffra and M. Moravcsik (9). The fitting involved the inversion of matrixes and was performed on the IBM 709 computer at the Western Data Processing Center. Even though the data points have a statistical accuracy on the

order of 5%, it was necessary to use double precision arithmetic (sixteen significant figures) in order to obtain meaningful results. This is due to the large range in orders of magnitude of the elements of the initial matrix. It would have been possible to avoid double precision by multiplying the rows and columns of the matrix by appropriate factors to reduce the range of the elements but it was more straightforward to use available double precision routines. The program also calculated statistical properties which allowed the application of the χ^2 test to determine the relative goodness-of-fit for different values of N . The value of the fitting function, together with its statistical error, could be calculated at any point.

$B_0, B_1, \dots, B_N, \chi^2$ and the χ^2 probability have been computed for several values of N for the data listed in Tables 6 and 7. The results are given in Table 8.

At each energy an artificial data point has been inserted in the non-physical region at $\cos \theta^i = 1/\beta^i$. The origin of this point will be made clear in section (C) below.

At 960 Mev and 1025 Mev there are no data at large angles. In order that the fitting curve would have a reasonable behavior in this region several data points, obtained by interpolation and extrapolation of data at nearby energies, have been added with appropriately large error assignments. These artificial points are listed in Table 9.

The fitting curves for $N = 6$ are shown in Figure 8.

There are three items which should be pointed out with regard to the uniqueness of these curves:

Table 8. Least Squares Fitting Coefficients and χ^2

The results of least squares fits to the data, including the artificial points mentioned in the text and listed in Table 9, are listed.

The fitting function used was

$$\sigma(\theta') = \frac{\sum_{n=0}^N B_n \cos^n \theta'}{(1 - \beta' \cos \theta')^2}$$

The coefficients B_n , χ^2 and p , the χ^2 attaining probability, are listed for several values of N . D is the number of degrees of freedom. [$D = \text{no. of data points} - (N + 1)$]

Table 8

700 Mev Data

	4	5	6	7	8
N					
B ₀	7.93 ± 0.14	8.15 ± 0.16	8.32 ± 0.20	8.48 ± 0.21	8.50 ± 0.23
B ₁	-9.06 ± 0.37	-8.76 ± 0.39	-9.42 ± 0.59	-8.60 ± 0.73	-8.78 ± 1.02
B ₂	-4.57 ± 0.24	-6.93 ± 0.88	-7.48 ± 0.96	-11.22 ± 2.19	-11.44 ± 2.35
B ₃	5.48 ± 0.57	6.47 ± 0.68	9.71 ± 2.17	8.48 ± 2.37	10.13 ± 7.04
B ₄	0.27 ± 0.35	3.02 ± 1.05	1.90 ± 1.29	13.59 ± 6.26	13.39 ± 6.32
B ₅	--	-1.90 ± 0.69	-4.87 ± 2.11	-9.19 ± 3.10	-12.9 ± 15.21
B ₆	--	--	1.88 ± 1.27	-6.88 ± 4.77	-5.0 ± 8.75
B ₇	--	--	--	5.39 ± 2.83	7.7 ± 9.84
B ₈	--	--	--	--	-1.55 ± 6.21
D	9	8	7	6	5
χ ²	16.3	8.53	6.33	2.70	2.64
P	0.05	0.40	0.50	0.85	0.70

800 Mev Data

	4	5	6	7	8
N					
B ₀	4.66 ± 0.08	4.56 ± 0.10	4.68 ± 0.10	4.70 ± 0.11	4.70 ± 0.12
B ₁	-5.57 ± 0.26	-5.96 ± 0.30	-6.80 ± 0.46	-6.64 ± 0.52	-6.63 ± 0.63
B ₂	-1.28 ± 0.22	0.33 ± 0.64	-0.21 ± 0.68	-0.99 ± 1.43	-0.97 ± 1.63
B ₃	1.13 ± 0.41	0.76 ± 0.43	4.98 ± 1.80	4.76 ± 1.83	4.64 ± 4.51
B ₄	1.09 ± 0.27	-0.96 ± 0.82	-2.49 ± 1.03	-0.15 ± 4.38	-0.14 ± 4.40
B ₅	--	1.30 ± 0.49	-2.65 ± 1.71	-3.71 ± 2.40	-3.43 ± 10.31
B ₆	--	--	2.52 ± 1.04	-0.46 ± 3.48	0.34 ± 5.33
B ₇	--	--	--	1.30 ± 2.09	1.12 ± 6.97
B ₈	--	--	--	--	0.14 ± 4.09
D	10	9	8	7	6
χ ²	19.08	11.98	6.14	5.75	5.75
P	0.03	0.23	0.6	0.58	0.45

Table 8

900 Mev Data

	4	5	6	7	8
N					
B ₀	3.08 ± 0.02	2.71 ± 0.09	2.62 ± 0.10	2.53 ± 0.10	2.60 ± 0.11
B ₁	-3.09 ± 0.07	-4.26 ± 0.25	-3.67 ± 0.38	-4.24 ± 0.44	-5.06 ± 0.58
B ₂	-0.26 ± 0.06	4.87 ± 0.59	5.37 ± 0.64	8.24 ± 1.29	7.02 ± 1.42
B ₃	-2.12 ± 0.11	-3.38 ± 0.38	-6.55 ± 1.56	-5.42 ± 1.62	2.84 ± 4.18
B ₄	2.41 ± 0.07	-3.94 ± 0.72	-2.93 ± 0.87	-12.70 ± 3.95	-12.73 ± 3.97
B ₅	--	4.02 ± 0.43	7.04 ± 1.50	10.46 ± 2.02	-9.11 ± 9.35
B ₆	--	--	-1.87 ± 0.89	5.83 ± 3.16	14.38 ± 5.09
B ₇	--	--	--	-4.68 ± 1.84	8.14 ± 6.26
B ₈	--	--	--	--	-8.07 ± 3.76
D	12	11	10	9	8
X ²	119.97	34.05	29.66	23.23	19.60
P	<0.01	<0.01	<0.01	<0.01	0.02

960 Mev Data

	4	5	6	7	8
N					
B ₀	2.76 ± 0.35	2.55 ± 0.35	2.21 ± 0.40	2.20 ± 0.40	2.20 ± 0.40
B ₁	-1.65 ± 0.71	-3.18 ± 1.15	-1.14 ± 1.57	0.12 ± 4.46	-33.86 ± 144
B ₂	-0.48 ± 0.77	3.25 ± 2.39	6.55 ± 2.94	4.72 ± 6.67	105.60 ± 426
B ₃	-4.87 ± 1.32	-4.24 ± 1.32	-16.83 ± 6.74	-22.45 ± 19.91	58.76 ± 344
B ₄	4.25 ± 0.64	-1.02 ± 3.28	0.39 ± 3.35	11.16 ± 36.04	-493.80 ± 2134
B ₅	--	2.66 ± 1.62	16.13 ± 7.25	17.63 ± 8.81	369.80 ± 1488
B ₆	--	--	-7.31 ± 3.84	-18.39 ± 37.12	343.25 ± 1529
B ₇	--	--	--	5.02 ± 16.74	-528.35 ± 2254
B ₈	--	--	--	--	176.42 ± 745
D	5	4	3	2	1
X ²	6.49	3.78	0.16	0.068	0.0125
P	0.25	0.45	0.98	0.97	0.91

Table 8
1025 Mev Data

N	4	5	6	7	8
B ₀	2.07 ± 0.19	2.03 ± 0.21	1.38 ± 0.24	1.73 ± 0.28	1.75 ± 0.29
B ₁	0.08 ± 0.50	0.42 ± 1.04	0.99 ± 1.06	-2.06 ± 1.75	-1.92 ± 1.79
B ₂	-1.20 ± 0.59	-1.73 ± 1.53	9.08 ± 2.39	12.16 ± 2.76	10.67 ± 4.62
B ₃	-5.94 ± 0.80	-6.12 ± 0.93	-26.27 ± 3.51	-13.61 ± 6.79	-12.02 ± 7.88
B ₄	5.00 ± 0.39	5.76 ± 2.09	3.33 ± 2.15	-19.02 ± 10.53	-14.60 ± 15.23
B ₅	--	-0.36 ± 0.97	22.78 ± 4.01	20.76 ± 4.06	12.98 ± 19.78
B ₆	--	--	-11.27 ± 1.89	9.63 ± 9.82	9.10 ± 9.93
B ₇	--	--	--	-9.58 ± 4.43	-3.06 ± 16.83
B ₈	--	--	--	--	-2.90 ± 7.20
D	9	8	7	6	5
X ²	45.43	45.29	8.94	4.24	4.08
P	<0.01	<0.01	0.25	0.6	0.55

Table 9. Artificial Data Points

The data points inserted at the pole were calculated from theory using a value of the coupling constant $f^2 = 0.081$.

The points added to the 960 and 1025 Mev data to force the proper wide angle behavior were obtained from the Dixon-Walker data by interpolation and extrapolation.

Table 9

A. Residues at the Pole $\cos \theta' = \frac{1}{\beta}$

<u>k, Mev</u>	<u>$1/\beta'$</u>	<u>$(1-\beta' \cos \theta')^2 \sigma(\theta') \mu\text{b/ster.}$</u>
700	1.0521	0.04414 ± 0.00290
800	1.0429	0.02836 ± 0.00190
900	1.0363	0.01925 ± 0.00130
960	1.0332	0.01559 ± 0.00110
1025	1.0304	0.01258 ± 0.00084

B. Wide Angle Points

960 Mev (Interpolated)

<u>θ'</u>	<u>$\sigma(\theta') \mu\text{b/ster.}$</u>
60°	6.13 ± 1.00
90°	2.20 ± 0.40
120°	2.70 ± 0.40
150°	2.46 ± 0.40

1025 Mev (Extrapolated)

<u>θ'</u>	<u>$\sigma(\theta') \mu\text{b/ster.}$</u>
120°	2.50 ± 0.50
150°	2.70 ± 0.60
164°	2.20 ± 0.50

(i) The χ^2 test gives an ambiguous decision about the best degree polynomial to use in some cases. This is especially true for the 900 Mev data. The χ^2 probability indicates that there is no order of polynomial which gives a really satisfactory fit. This indicates that there is probably some inconsistency in the data, as might be guessed from the appearance of the points in fig. 8(c).

The 1025 Mev data, on the other hand, yields a quite definitive answer to the question of which is the most suitable order of polynomial. The greatest effort was expended on the measurements at this energy and the statistical errors are somewhat less than for the other data. Also since all points were measured with the same apparatus there is less chance for systematic errors to affect the shape of the angular distribution.

(ii) The advisability of using the Moravscik form rather than a simple polynomial is demonstrated in fig. 8(e), in which the same number of terms are used in the two forms at 1025 Mev. It is obvious that more terms would be required in the simple polynomial to give as good a fit as does the special form.

(iii) There is some question of absolute normalization between this experiment and that of Dixon and Walker. Moving all of the points obtained here upward with respect to the earlier data by 4% reduced the value of χ^2 slightly. For example, at 800 Mev χ^2 changed from 11.98 to 10.35 for $N = 5$. This is not sufficient evidence to warrant a renormalization. The general shape of the curves was unchanged by such a shift, and therefore none of the arguments presented will be affected.

C. THE COUPLING CONSTANT

Moravcsik et al (10) have discussed the possibility of obtaining from π^+ photoproduction data a value of the pion-nucleon coupling constant. It is shown that in any theory which one can propose there exists a term in the differential cross section which has a second order pole, i. e. becomes infinite, when $\cos \theta' = 1/\beta'$. This term is of course just the retardation term which we have been discussing. At this pole the contributions from all other terms, no matter how complicated, are negligible. The coefficient of this term is simply related to kinematical quantities and the pion-nucleon coupling constant. One can express this behavior by

$$(1 - \beta' \cos \theta')^2 \sigma(\theta') \Big|_{\cos \theta' = 1/\beta'} = 147 f^2 \frac{q}{k^3} \frac{1 - \beta'^2}{(1 + \omega/M)^2} + O(0)$$

where

f^2 = derivative coupling constant (squared)

q = pion momentum in (Mev/c)/pion mass (Mev)

k = photon energy / pion mass

β' = pion velocity/c

M = nucleon mass/pion mass

$$\frac{\omega}{M} = \frac{k}{M} - 1 + \sqrt{1 + \left(\frac{k}{M}\right)^2}$$

all in the c. m. system. The prescription for obtaining f^2 from measured quantities is to extrapolate the cross section data, multiplied by $(1 - \beta' \cos \theta')^2$, into the region $\cos \theta' > 1$, which is obviously inaccessible to physical apparatus. The value of the extrapolated function, i. e., the residue at the pole, yields f^2 immediately from the preceding

formula.

Such a procedure is relatively straightforward if one has very accurate data at many angles, especially near 0° . Then the fitting function can be chosen relatively unambiguously and the error in the extrapolation will be small.

As the energy becomes higher, β' approaches 1. Therefore the pole is closer to the physical region at high energies. However, the value of the residue becomes smaller with increase in energy. The combination of these two effects gives an optimum energy for obtaining f^2 for a given number of data points of specified accuracy. Moravscik et al give this energy as about 500 Mev (laboratory photon energy), but point out that the maximum is very broad.

The data from this experiment has been used in an attempt to obtain a value of f^2 , whose current value, obtained from pion scattering and low energy photoproduction experiments is 0.081 ± 0.01 . An illustration of an extrapolation curve is shown in fig. 9. The results are listed in Table 10, for various values of N at the different energies. The errors given are based on the statistical properties of the fit, calculated from inverse matrix elements, etc. (see Cziffra and Moravscik (9)). It is obvious that the procedure leaves something to be desired with regard to self consistency. As may be seen by examining the values obtained for different N , the choice of fitting function is important and it is probably this ambiguity which leads to the inconsistency. In the case of the 1025 Mev data the order of fit chosen by the χ^2 test was quite definite. Also the choice, $N = 6$, is consistent with the currently accepted ($J = 5/2$) assignment for the third resonance. In order to see

Figure 9. Extrapolation to the Pole $\cos \theta' = \frac{1}{\beta}$.

The solid curve is the polynomial $\sum_{n=0}^6 B_n \cos^n \theta'$ resulting from a least squares fit of the Moravscik type to the 1025 Mev data, some of which extends beyond the limits plotted. The dotted curves indicate the probable error limits on the fitting curve, based on the statistical properties of the least squares procedure. The value of the ordinate at $\cos \theta' = \frac{1}{\beta} = 1.0304$ yields a measure of the pion nucleon coupling constant when multiplied by some kinematical factors.

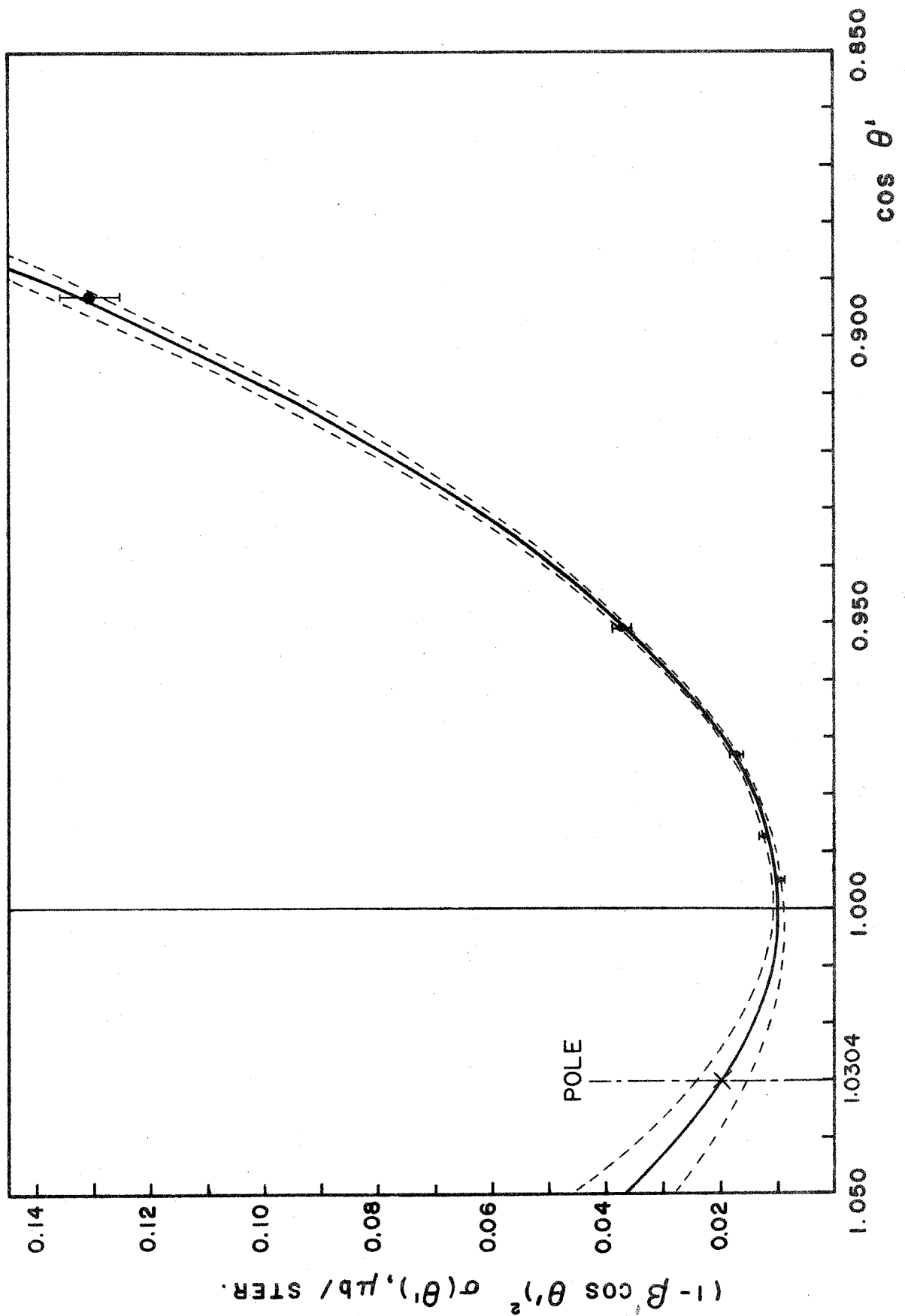


Table 10. Experimental Values of the Coupling Constant

The values of f^2 obtained from an extrapolation to the pole at $\cos \theta' = \frac{1}{\beta}$ are listed for each order of polynomial. The most likely choice, based on the χ^2 test, is underlined.

The numerical coefficient a , in the formula

$$f^2 = a \cdot (1 - \beta' \cos \theta')^2 \sigma(\theta')$$

is given for each energy.

Table 10

k =	700	800	900	960	1025
a =	1.835	2.856	4.208	5.196	6.439
N = 4	0.098 ± 0.024	0.019 ± 0.020	0.018 ± 0.016	0.078 ± 0.029	0.154 ± 0.016
N = 5	<u>0.050 ± 0.037</u>	0.033 ± 0.028	0.167 ± 0.023	0.113 ± 0.035	0.185 ± 0.020
N = 6	0.023 ± 0.056	<u>0.076 ± 0.037</u>	0.179 ± 0.032	<u>0.064 ± 0.045</u>	<u>0.122 ± 0.027</u>
N = 7	0.071 ± 0.080	0.103 ± 0.052	0.159 ± 0.041	0.048 ± 0.130	0.084 ± 0.036
N = 8	0.034 ± 0.112	0.123 ± 0.071	0.115 ± 0.055	?	0.071 ± 0.046

-68-

Average (weighted) of underlined values:

$$f^2 = 0.087 \pm 0.017$$

that this is the case we remember that the Moravscik fitting form effectively adds two powers of $\cos \theta'$ to allow for the retardation term. Thus $N = 6$ implies an angular distribution, due to interactions other than the "photoelectric effect", with powers of $\cos \theta'$ up to the 4th. This is just what would be produced by a $D_{5/2}$ state, from either a magnetic quadrupole or electric octopole, or an $F_{5/2}$ state from an electric quadrupole. In order to produce higher powers of $\cos \theta'$ it is necessary to have both a photon interaction of higher order than quadrupole and a pion angular momentum greater than 2 (D wave).

More accurate data with a finer angular mesh is needed before a useful measurement of f^2 can be obtained from this method.

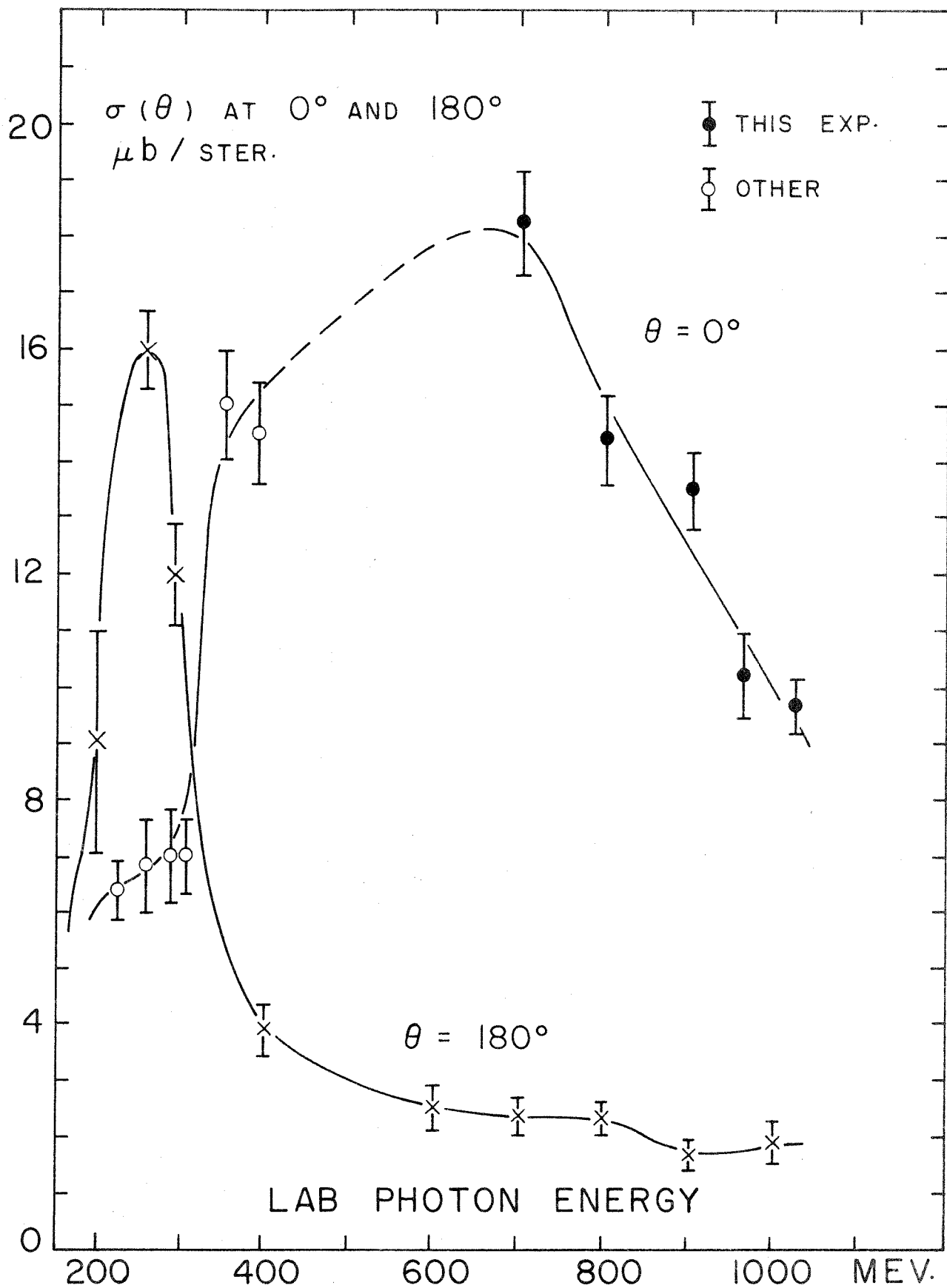
Since f^2 could not be obtained independently from this experiment, although there was no gross inconsistency with the currently accepted value, it was decided to use the residue at the pole as an artificial data point in order to obtain the best value of the cross section at 0° . The interpolation procedure introduced by having points on both "sides" of 0° is superior to an extrapolation from the small angle data alone. The actual values of $(1 - \beta' \cos \theta')^2 \sigma(\theta') \Big|_{\cos \theta' = 1/\beta'}$ used in the analysis are listed in Table 9.

D. $0^\circ, 180^\circ$ CROSS SECTIONS

At 0° and 180° the effect of the retardation term disappears. Therefore the cross section at these two angles is a measure of the interaction in states which do not arise from the "meson current" coupling. In fig. 10 is plotted the 0° and 180° cross section vs. energy, using the extrapolated values from this experiment together with some

Figure 10. 0° and 180° Cross Sections vs. Energy

The values of the 0° cross section obtained from this experiment were obtained from the intercept at 0° of the least squares fitting curves, using artificial data points at the pole, $\cos \theta^i = 1/\beta^i$.



data from low energies. There are features of this plot which are most interesting. One of these is the cross over, or reversal of asymmetry, at the first resonance. Another is the notable lack of fluctuations in the curves over the region of the second resonance. At the highest energies there is a drop in the 0° curve.

It is possible to express the photoproduction amplitude in terms of the contributions from each of the multipoles that can occur. As pointed out previously, it is advisable to separate out the retardation term in order to reduce the order of the multipoles required, and to give better correspondence to the physical situation. If one does this at 0° and 180° , comparatively simple expressions result (from R. L. Walker (7)):

$$\sigma(0^\circ) \sim |O|^2 + |E|^2 + 2\text{Re}(O \times E)$$

$$\sigma(180^\circ) \sim |O|^2 + |E|^2 - 2\text{Re}(O \times E)$$

where O and E are the odd and even parity multipole contributions from interactions other than the "meson current" coupling, of the form:

$$O = \sqrt{2} E_{11} - \sqrt{2} E_{13} + \sqrt{6} M_{23} - \sqrt{6} M_{25} + \sqrt{12} E_{35} + \dots$$

$$E = \sqrt{2} M_{11} - \sqrt{2} M_{13} + \sqrt{6} E_{23} - \sqrt{6} E_{25} + \sqrt{12} M_{35} + \dots$$

where $E_{j,j_{\text{Tot}}}$ is the amplitude for production from an electric multipole having photon angular momentum j in a state of total angular momentum $\frac{1}{2} j_{\text{Tot}}$. $M_{j,j_{\text{Tot}}}$ is the similar amplitude for a magnetic multipole. The numerical coefficients depend of course on the normali-

zation of the multipoles. (7)

The comparative simplicity of the 0° ; 180° expressions makes them useful for testing the agreement between experiment and trial combinations of multipoles, prior to examining the complete angular distributions.

One would hope that, even though each of the multipole amplitudes cannot be obtained from the data at present, at least the quantum numbers of the resonant states, in particular the poorly known third resonance, could be obtained in this way. However, even this does not seem possible. A preliminary attempt at synthesizing the observed cross sections from various multipoles has shown that the behavior at 0° and 180° , as well as in the rest of the angular range, is insensitive to the choice of angular momentum and parity within the experimental uncertainties. There seems to be little hope of making a definite assignment of parity on the basis of this analysis. The effort will be continued however.

E. TOTAL CROSS SECTION

The total cross section can be obtained by integrating the least squares fitting curves:

$$\sigma_{\text{Total}} = 2\pi \int_0^\pi \sigma(\theta') \sin \theta' d\theta'$$

The forward angle region contributes little to the total cross section so the values at 700, 800, and 900 Mev will not be very different from those previously obtained (5). The 960 Mev data are too incomplete to give a significant value, while the 1025 Mev data yield a total cross section with a rather large error, as calculated from the properties of the least squares fit.

Table 11 lists the values obtained, together with the values obtained by Dixon and Walker.

Table 11

Total Cross Section

<u>k, Mev</u>	<u>$\sigma_{\text{Total}}, \mu\text{b}$</u>	<u>$[\sigma_{\text{total}}, \text{Dixon}, \mu\text{b}]$</u>
700	96.94 ± 1.17	94.62 ± 1.19
800	62.10 ± 0.93	60.11 ± 0.89
900	49.48 ± 0.86	48.88 ± 0.92
960	50.20 ± 3.55	--
1025	47.89 ± 2.11	--

VII. CONCLUSIONS AND SUGGESTIONS

This experiment has demonstrated conclusively the strong effect of the retardation term on the π^+ photoproduction differential cross section, especially in the small angle region, at high energies. The rather marked resemblance of the small angle behavior to the results of a simple Born approximation calculation suggests that the influence of the interference between the retardation term and low angular momentum states, which predominate in the Born approximation, is so great as to mask or at least obscure effects due to higher angular momenta such as the high energy resonance states.

The much improved values of the 0° cross section given by this experiment are useful for comparison with theory. In particular, a phenomenological synthesis of the contributing states from experimental data can be carried out at 0° , unhampered by considerations of the retardation term.

A knowledge of the behavior of the forward-backward asymmetry of the cross section at still higher energies, above the third resonance, would be helpful in determining the contributing states. An experiment is now in progress to measure the differential cross section at higher energies, including the small angle region (11).

APPENDIX I

BEAM MONITORING AND BREMSSTRAHLUNG SPECTRUM

A. GENERAL

The beam intensity was monitored by a thick walled sealed copper ion chamber filled with an argon - CO_2 mixture. This chamber was calibrated against the Cornell type quantameter (12). This heavy chamber (called Chamber III) also served to stop the beam and was placed as far down stream as possible. When the spectrometer was set to angles smaller than 15° the beam was stopped by the magnet yoke or coil windings rather than in the ion chamber and another monitoring system was required. A second "thin" chamber consisting of two parallel plates which collected ions produced in the air as the beam passed between them, was placed near the primary collimator. Because this type of chamber is sensitive to atmospheric changes and to charged particles as well as photons, it was calibrated against Chamber III before and after each run by moving the spectrometer magnet out of the beam path.

The charge on the ion chamber collector plates was integrated and recorded in units called BIPS, which are related by the integrator constant and the ion chamber calibration to the total beam intensity, including all photon energies. A knowledge of the beam spectrum then yields the number of photons per BIP in the energy region of interest.

B. CHAMBER CALIBRATION

The sensitivity of the quantameter can be calculated from shower theory, and is designed (12) to be independent of the spectrum, giving a

response which is proportional to the total energy in the beam. The calculated response for $p/T = 2.782 \text{ mm}/^\circ\text{K}$ is

$$U_Q = 4.93 \times 10^{12} \text{ Mev/coulomb}$$

Unexpected difficulties were encountered in the calibration of Chamber III. Three separate calibrations were carried out, none of which agree within the errors ascribed to the measurements.

The first was performed soon after the installation of the chamber, before its use with any experiments, and involved only a few runs. It is not known whether the beam was properly centered on the chamber at that time.

After this experiment was completed the other two calibrations were made, one month apart. Although the runs were self consistent within 1% or better for one calibration, the two separate measurements disagree by 4%, after allowance is made for a slow leakage of the gases out of the chamber between calibrations. No explanation of this discrepancy can be found. The response before and after emptying and re-filling the chamber was the same (third calibration). It is known that the quantameter was not unstable because a calibration of a small portable chamber that had been calibrated reproducibly several times before gave excellent agreement with previous results. An inspection of the interior of Chamber III showed no signs of mechanical or electrical failure.

There was one other calibration by T. Terman, whose experiment ran concurrently with the beginning of this one. This was a very limited measurement, consisting of only one run on each chamber, but a careful reduction of the data yields agreement with the second calibration men-

tioned above, with an estimated accuracy of about 2%.

Since the choice among calibrations is somewhat arbitrary, and the second seems to agree with the only available independent measurement, that is the one I have chosen for reducing the data. The values are given in Table A1. A systematic error of approximately 3% should be assigned to the absolute normalization due to this unfortunate circumstance. This error affects the matching of the data from this experiment to that of Dixon and Walker (5), and in retrospect more overlapping data points should have been taken.

C. THE SPECTRUM

The number of photons per BIP in an energy range k to $k + dk$ is given by

$$N(k)dk = \frac{WB(k, E_0)}{E_0 k} dk$$

Expressed in this way, the function $B(k, E_0)$ is nearly constant up to $k = E_0$, where it vanishes. The normalization factor W is chosen so that

$$\int_0^{E_0} B(k, E_0) dk = E_0$$

In principle $B(k, E_0)$ could be calculated if the detailed behavior of the electrons striking the radiator were known. However such is not the case, and one must measure the spectrum in order to obtain an accurate value of $B(k, E_0)$. Such a measurement has been performed by R. L. Walker and the author, and the reduction of the data is still in progress.

A preliminary analysis however gives some information which is

Table A1
Ion Chamber Calibration

Quantameter:

$$U_Q = 4.93 \times 10^{18} \pm 2\% \text{ Mev/coulomb @ } p/T = 2.782 \text{ mm/}^\circ\text{K}$$

independent of energy

Chamber III: @ $p/T = 2.555 \text{ mm/}^\circ\text{K}$

<u>E_o, Mev</u>	<u>U, Mev/coulomb</u>	<u>W, Mev/BIP</u>
800	4.45×10^{18}	0.945×10^{12}
900	4.49	0.953
990	4.48	0.951
1050	4.47	0.949
1130	4.43	0.940

W was computed from the integrator calibration:

$$\text{Integrator \#0249 : } 0.2123 \times 10^{-6} \text{ coulombs/BIP}$$

of use here. Using the theoretical formula for the pair production cross section (13), including production from the electrons and screening effects, one can calculate a value of $B(k, E_0)$ from the measured counting rates, the calculated pair spectrometer response and the theoretical sensitivity of the quantameter. Using the average of many runs with several types of convertor materials one obtains a value:

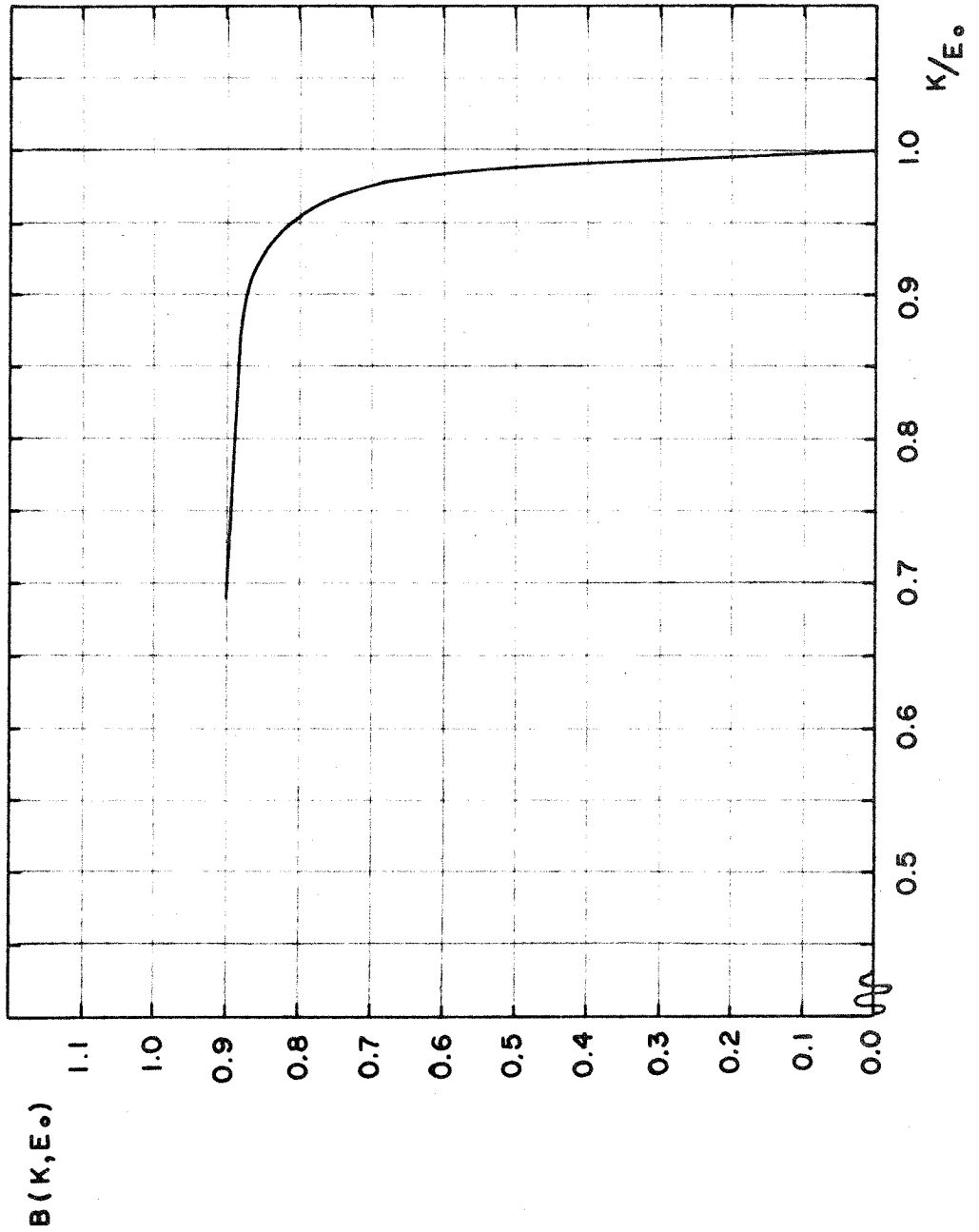
$$B(k, E_0) \bigg|_{k/E_0 = 0.7} = 0.900 \pm 0.040$$

independent of E_0 within errors in the energy range $800 \leq E_0 \leq 1200$. The error assignment is based on errors in the absolute calibration of the quantameter, the errors in the pair cross section formula and on uncertainty in the pair spectrometer efficiency. Since all of these errors are somewhat uncertain the value 0.04 should be considered an estimate.

The spectrometer shape near the end point can be obtained from the pair spectrometer data by approximating the resolution curve of the spectrometer and "unfolding" the measured spectrum by trial and error. One must take into account the variation of the spectrum with angle in the photon beam and average over the collimating aperture. Within the errors inherent at the present stage of the analysis there is no dependence of the spectrum on end point energy when plotted versus k/E_0 , for $800 \leq E_0 \leq 1200$. The final spectrum shape used in the data analysis is shown in fig. A1. The absolute accuracy is the same as that quoted for $B(k, E_0) \big|_{k/E_0 = 0.7}$. The relative accuracy, i. e. the shape, has accuracy sufficient to contribute less than 1% to the errors in the cross section. Since the error due to the spectrum shape is rather independent of pion

Figure A1. Bremsstrahlung Spectrum $B(k, E_0)$.

This curve was obtained from a preliminary analysis of data from a pair spectrometer measurement of the spectrum. A weighted average over the collimated beam cross section has been taken, and the normalization at k/E_0 is based on the theoretical pair production cross section and the calculated response of the Cornell quantameter.



angle, the error made in the shape of the differential cross section will be quite small.

The value of $\overline{N(k)}$ is obtained for each data point by integrating $N(k)$ over the spectrum weighted by the spectrometer resolution function, which can be obtained either from the magnet report (6) or from the decay correction curves in Appendix III.

APPENDIX II

COUNTER EFFICIENCIES

A. THE CHERENKOV COUNTER

1. $\eta_{C\pi}^{\vee}$, Cherenkov counter efficiency for pions.

The inefficiency, $1 - \eta_{C\pi}^{\vee}$, was measured by selecting pions with a time-of-flight circuit using A1, with the spectrometer set at a large angle so that electrons were not present. The ratio of counts with the Cherenkov counter in veto to those with it in coincidence is the inefficiency (neglecting second order terms).

2. η_{Cp}^{\times} , Cherenkov counter efficiency for protons.

The same time-of-flight circuit that was used for the $\eta_{C\pi}^{\vee}$ measurement was set to select protons. The ratio of Cherenkov coincidence counts to veto counts is the efficiency.

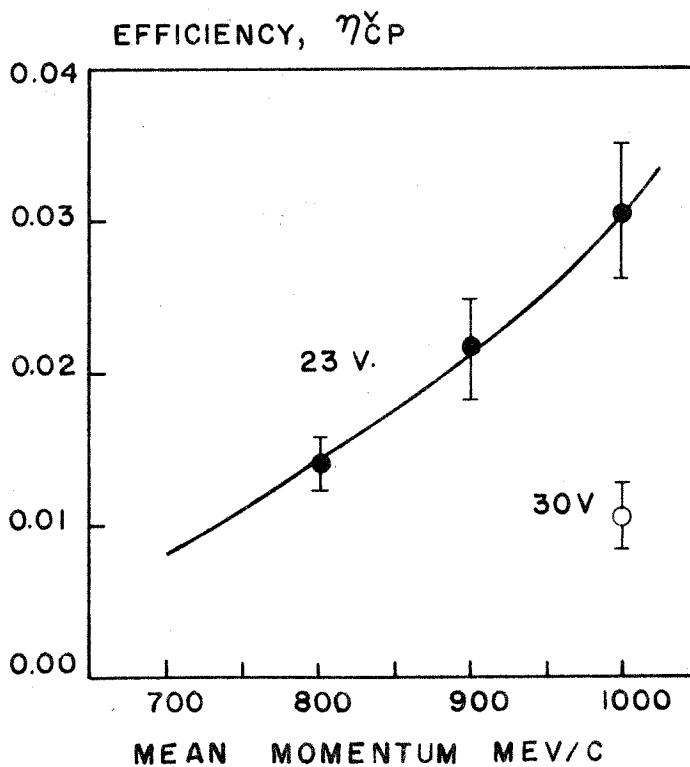
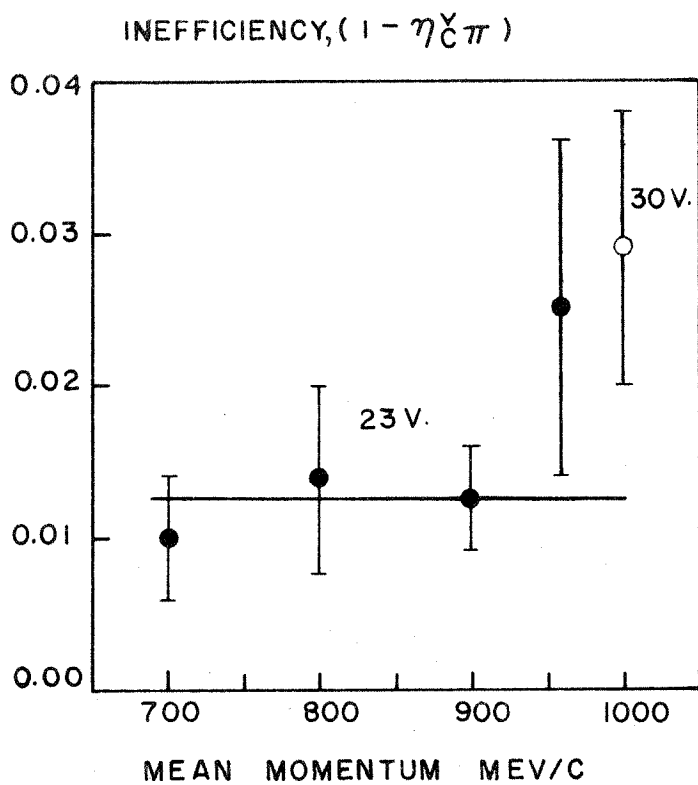
When only a few particles are counted, as in these efficiency measurements, there is some worry about whether the time-of-flight selector is adequate. The pulse heights in counters other than the time-of-flight circuit showed that the particles being counted were indeed those desired. That is, the particles that were all supposed to be protons were heavily ionizing in C2 and C3, and those that were supposed to be pions gave a pion-like pulse distribution in C2 and C3; i. e. they were not heavily ionizing in both C2 and C3. The results of the measurements are shown in fig. A2.

B. THE ELECTRON COUNTER

η_{Ee} , the efficiency of the electron counter for counting electrons,

Figure A2. Cherenkov Counter Efficiencies $\eta_{C\pi}^{\vee}$, η_{Cp}^{\vee}

The quantities actually measured, $(1 - \eta_{C\pi}^{\vee})$ and η_{Cp}^{\vee} are plotted. The bias values refer to the lower limit placed on the pulse resulting from a coincidence between the Cherenkov counter and C1. Most of the experiment was carried out with a bias of 23 v.



was measured by setting the spectrometer at 0° and using a $1/8''$ Pb target. A rough calculation shows that the number of electrons accepted by the spectrometer is greater by 10^6 than the number of other particles. By severely collimating the beam and detuning the synchrotron the counting rate could be reduced to acceptable levels. The efficiency is then given simply by the ratio of "electrons" counts (the large pulses) to the total number of counts. The results are shown in fig. A3.

Since this efficiency was a critical point it was measured repeatedly throughout the experiment. These measurements never differed from the overall average by more than expected statistical fluctuations. Each measurement had a statistical accuracy of about 0.3%.

$\eta_{E\pi}$, the efficiency for counting a pion as an electron, was measured by using a time-of-flight circuit to eliminate protons, and operating at a large angle to eliminate electrons. The ratio of "electrons" counts to the total number of counts is $\eta_{E\pi}$, shown in fig. A4. The bias chosen for the electron counter was a compromise between too small η_{Ee} and too large $\eta_{E\pi}$.

η_{Ep} , the efficiency for counting a proton as an electron, was measured in the same way as $\eta_{E\pi}$ except that the time-of-flight was set for protons and the Cherenkov counter was used in veto rather than coincidence. The results are shown in fig. A5.

C. GAIN AND BIAS STABILITY

In order to insure that the system efficiencies would be stable against day to day variations in the electronics a simple but sensitive procedure was adopted which would allow an adjustment of gains and

Figure A3. Electron Detector Efficiency η_{Ee}

The single convertor was 1/2" of Pb placed in front of counter C3. The double convertor system had an additional 1/2" piece in front of counter C2. The efficiency η_{Ee} is the probability that an electron will produce a large pulse in C3, for the single convertor, or a large pulse from either C2 or C3 or both, when the double convertor was used.

EFFICIENCY, η_{Ee}

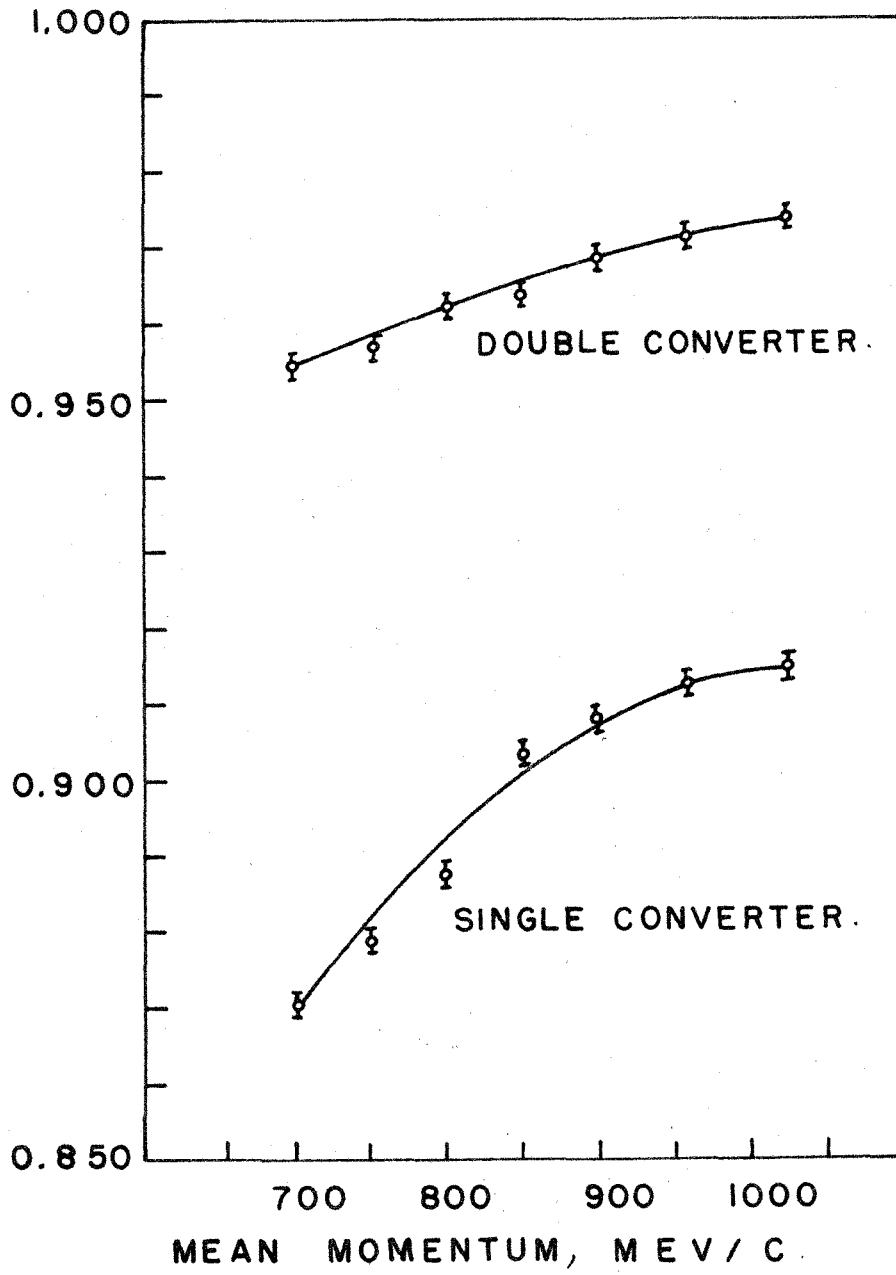


Figure A4. Electron Detector Efficiency $\eta_{E\pi}$

$\eta_{E\pi}$ is the efficiency for pions to count in the electron detection system.

EFFICIENCY, $\eta_{E\pi}$

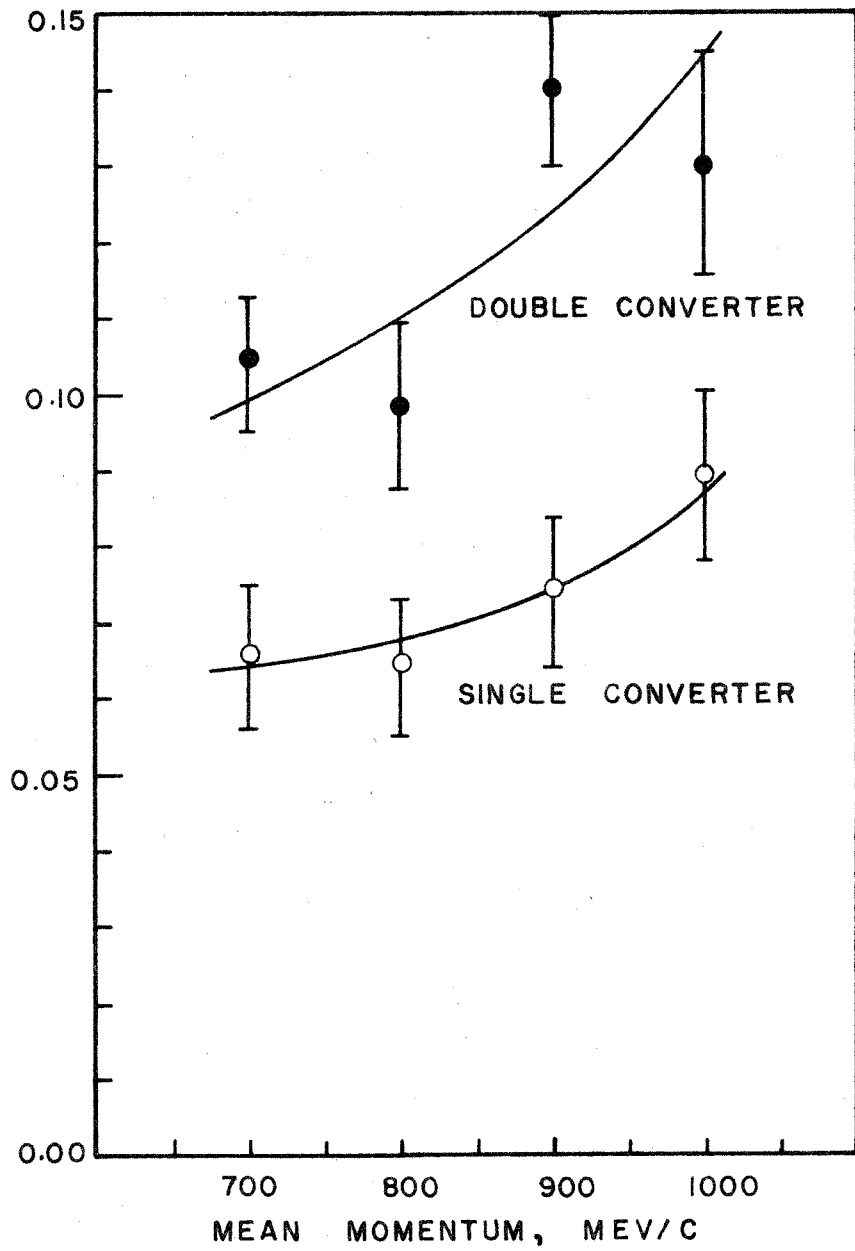
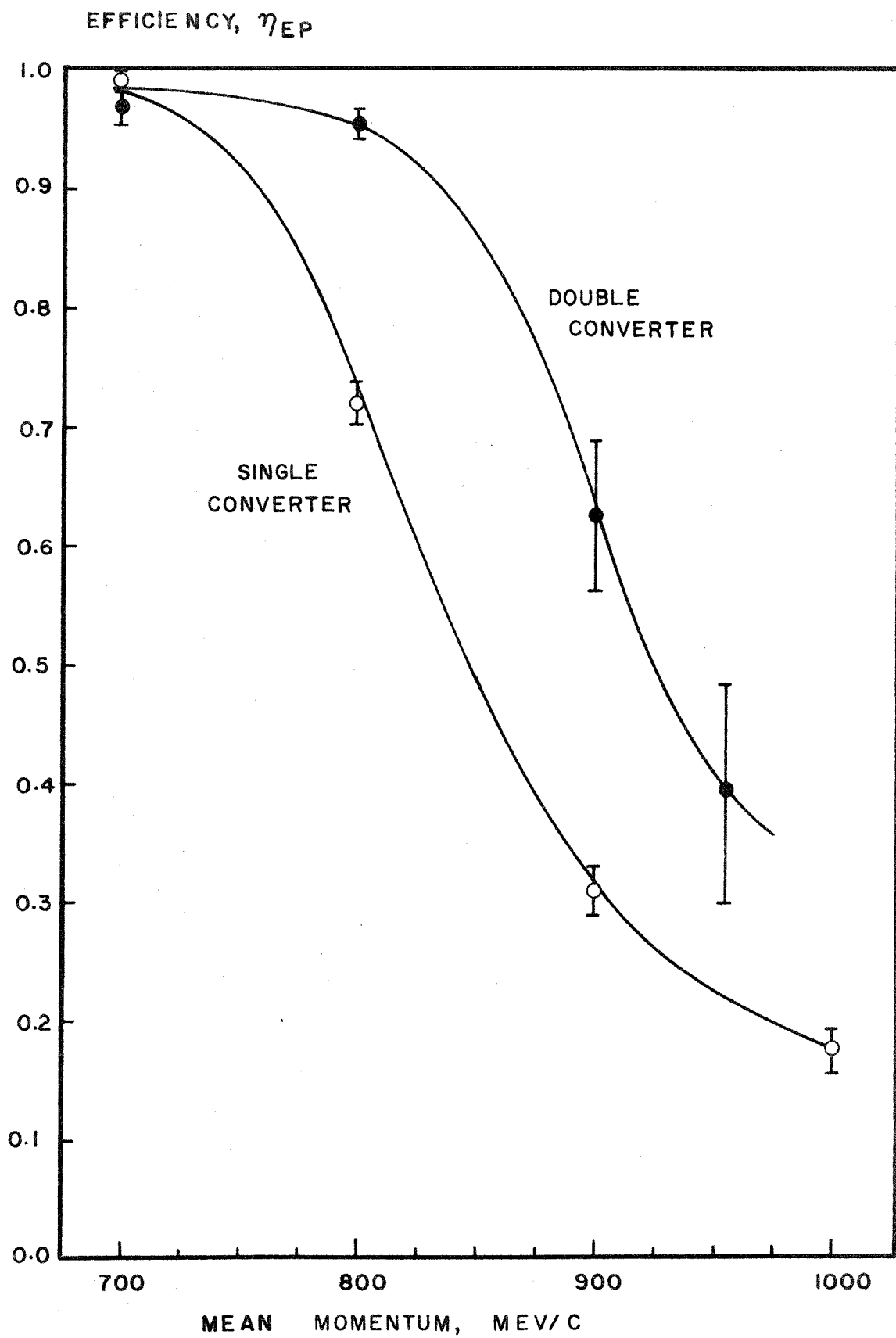


Figure A5. Electron Detector Efficiency η_{Ep}

η_{Ep} is the efficiency for protons to count in the electron detection system.



biases at the beginning of each day's running and after several hours of extended running.

The abundant supply of electrons at 0^0 was used as a source. At preselected bias values, amplifier gains were adjusted one by one to give 50% efficiency for each counter. Then biases were restored to normal operating values, on the assumption that variations in biases would occur merely as a linear change in scale and not as a uniform displacement. The long term stability of the electron detector efficiencies indicates that this method has merit.

It should be mentioned that in adjusting the gains of C2 and C3 the Pb convertors were removed since otherwise almost all pulses saturated the amplifiers.

<u>Pulse</u>	<u>Bias Adjusted</u>	<u>Running Bias, v</u>	<u>Test Bias</u>	<u>Test</u>
C·C1 coinc.	Ch. 4 of 6 Ch. Coinc. Box	23	40	$\frac{(3246)_{40}}{(3456)_{23}} = \frac{1}{2}$
A2·A1 coinc.	Ch. 3 of 6 Ch. Coinc. box	40	85	$\frac{(3456)_{85}}{(3456)_{40}} = \frac{1}{2}$
C2	Ch. 2 of MOD100	65	34-1/2	$\frac{"E_2"}{(3456)} = \frac{1}{2}$
C3	Ch. 3 of MOD100 Coinc. box	60	34	$\frac{"E_3"}{(3456)} = \frac{1}{2}$

Refer to electronics block diagram, p. 26.

APPENDIX III

DECAY CORRECTIONS

Charged pions decay into muons by the reaction

$$\pi^+ \rightarrow \mu^+ + \nu$$

with a mean life at rest of $(2.56 \pm 0.05) \times 10^{-8}$ sec. This means that a fraction of the pions will decay before they reach the counter telescope. Since the counter system cannot distinguish between pions and muons one must investigate in some detail the effect of the decay on the counting rate. There are two effects, which tend to compensate: (1) Pions which would have been counted were it not for the decay can be lost due to the angle of decay and/or change in momentum. (2) pions which were not within the acceptance range of the spectrometer, in angle and/or momentum, decay into muons which might then be accepted.

For the geometry of this experiment and a typical pion momentum, about 10% of the pions decay in passing through the system.

The correction to the pion counting rate can be calculated exactly by setting up a multiple integral containing the decay kinematics and the spectrometer geometry. However, the variable limits of integration and the complicated integrand make the evaluation of the integral very difficult. Previous attempts at this problem (5) approximated the integration procedure, not treating the region inside the magnet except as an extension from the regions outside. Even in these approximations a digital computer was used to reduce the labor involved.

Availability of the higher speed IBM 709 at the Western Data

Processing Center prompted the use of Monte Carlo techniques for this problem. This method has the advantage that the physical situation can be simulated to a rather good approximation and the computation procedure becomes quite simple in comparison with an evaluation of the multiple integral.

The computer program:

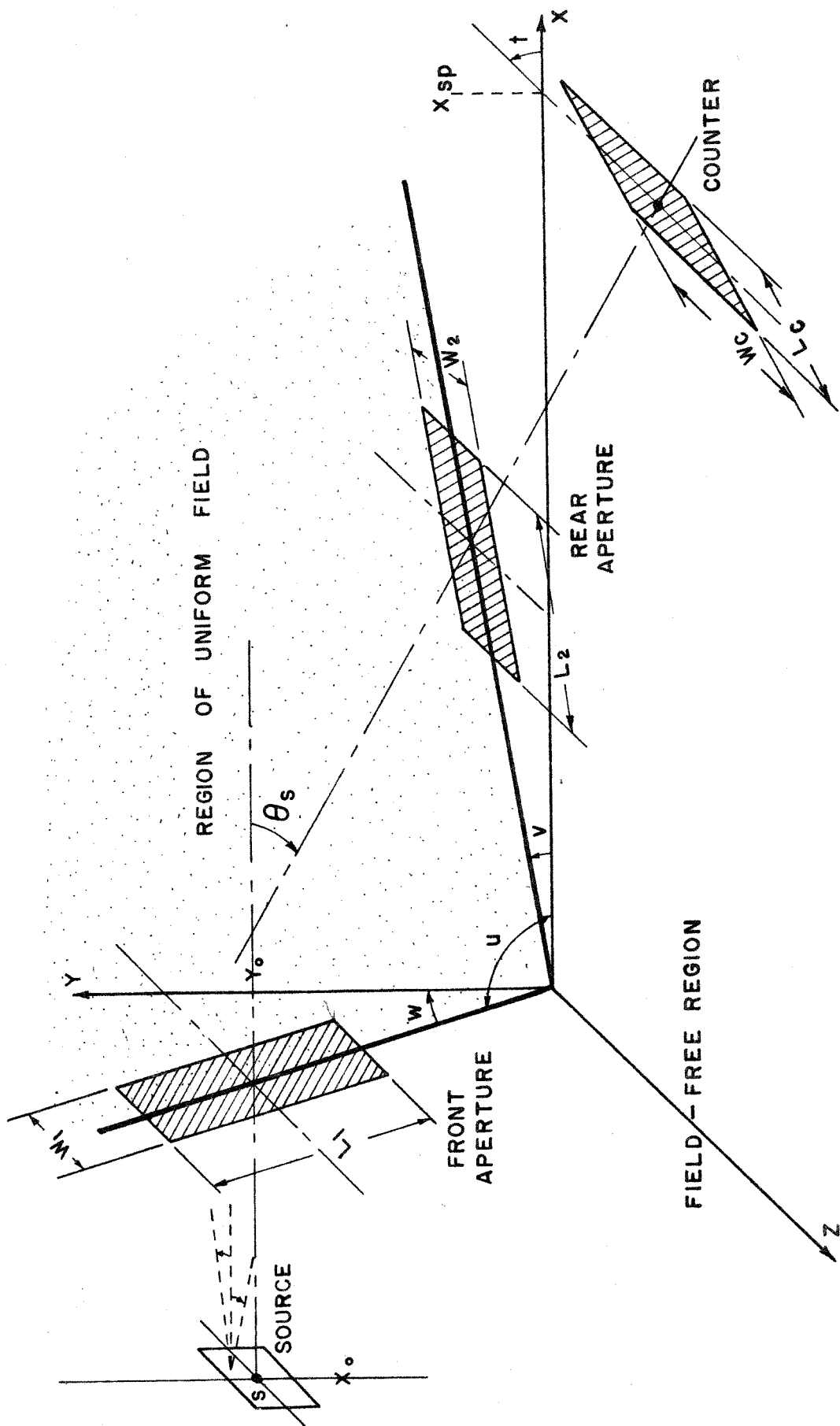
The spectrometer magnet is simulated by two "effective edges" inside of which the field is uniform and outside of which there is no field. Horizontal deflection due to the fringing field is included approximately. The coordinate system used is shown in Fig. A6. The H_2 target is replaced by a uniform rectangular source of pions at the focus of the magnet, and the aperture defining counters are merely limits within which the paths of the particles must lie in order to be accepted.

The computational procedure is best shown by means of the flow diagram for the computer program, fig. A7.

Briefly, the computer is given a decay distance, R , and the number of trials to make. From the value of R and the size of the entrance aperture the computer calculates the range of angles into which a pion could be emitted with a finite chance of being accepted, taking into account the maximum decay angle. Then the position in the source and the two projected angles of emission are selected at random, within the previously calculated limits. The pion is advanced by a distance R . If the counter has not been passed already decay takes place at a randomly selected direction in the rest system of the pion. Conversion to the laboratory system gives the angle and momentum of


Figure A6. Decay Correction Coordinate System

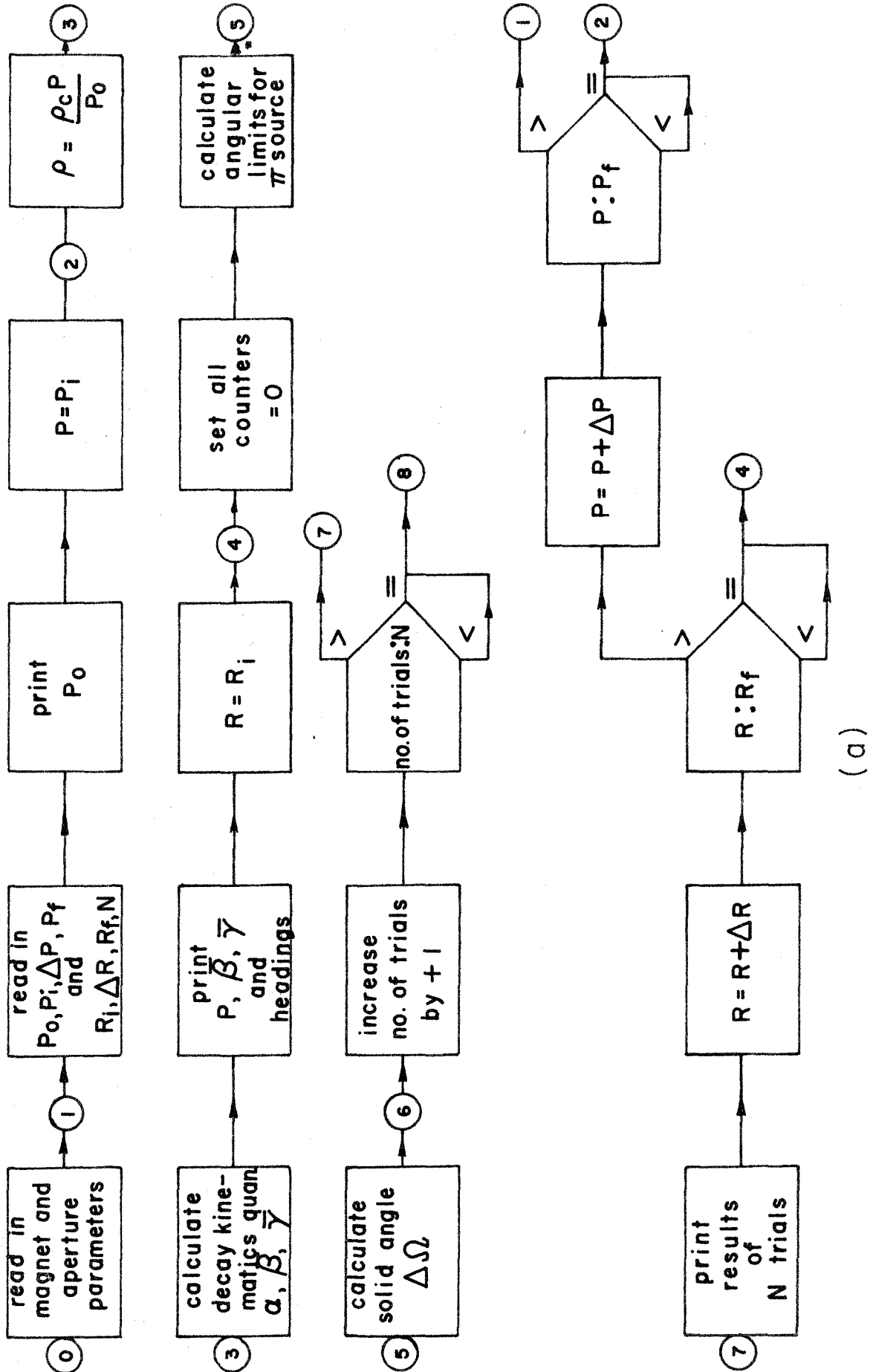
The effective edges of the magnet are shown in heavy lines. The randomly selected mission angles at the source are shown without any label since they were not named specifically in the computer program. The variables shown refer to notation used in the detailed program which is not given here.

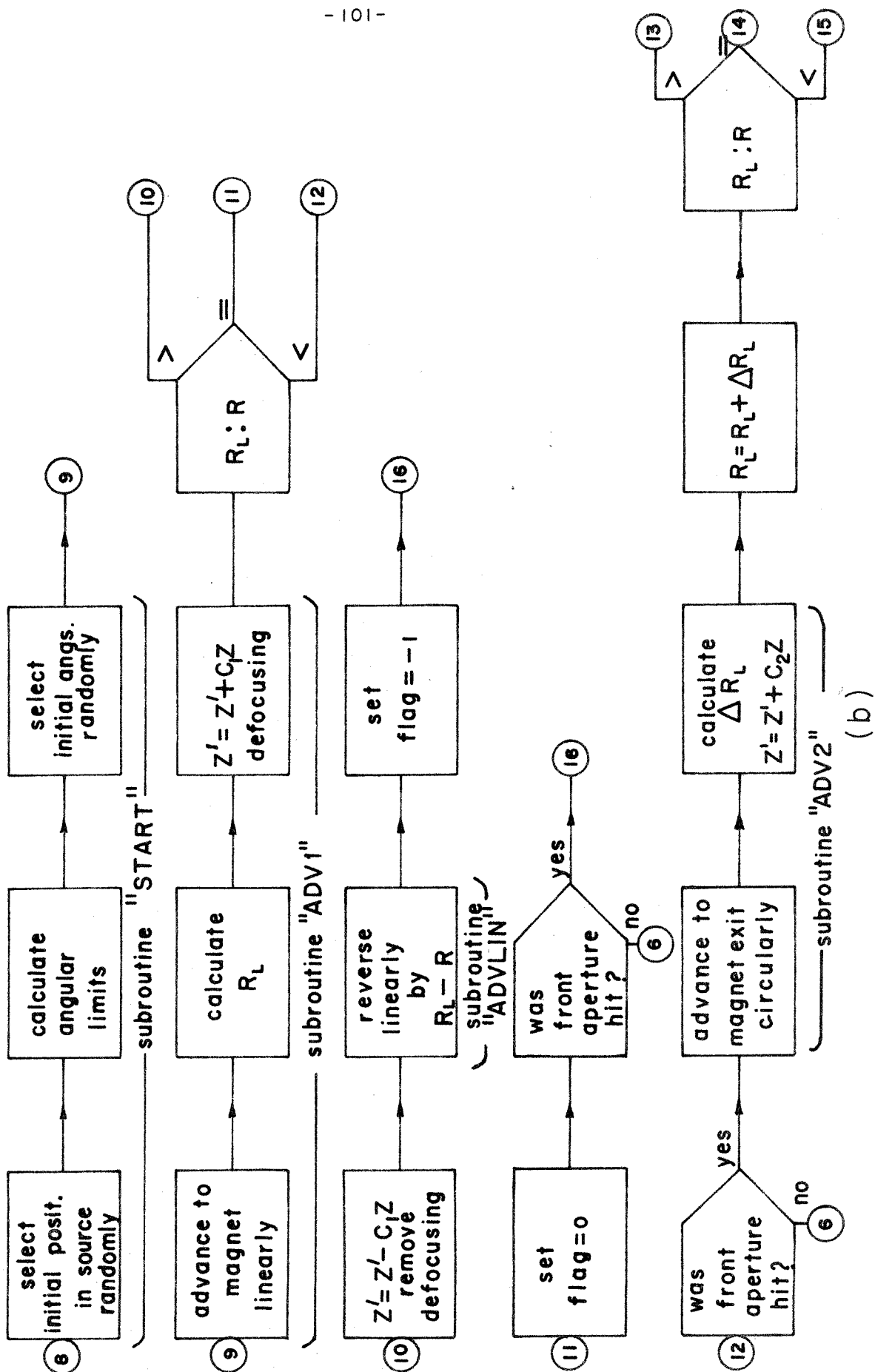


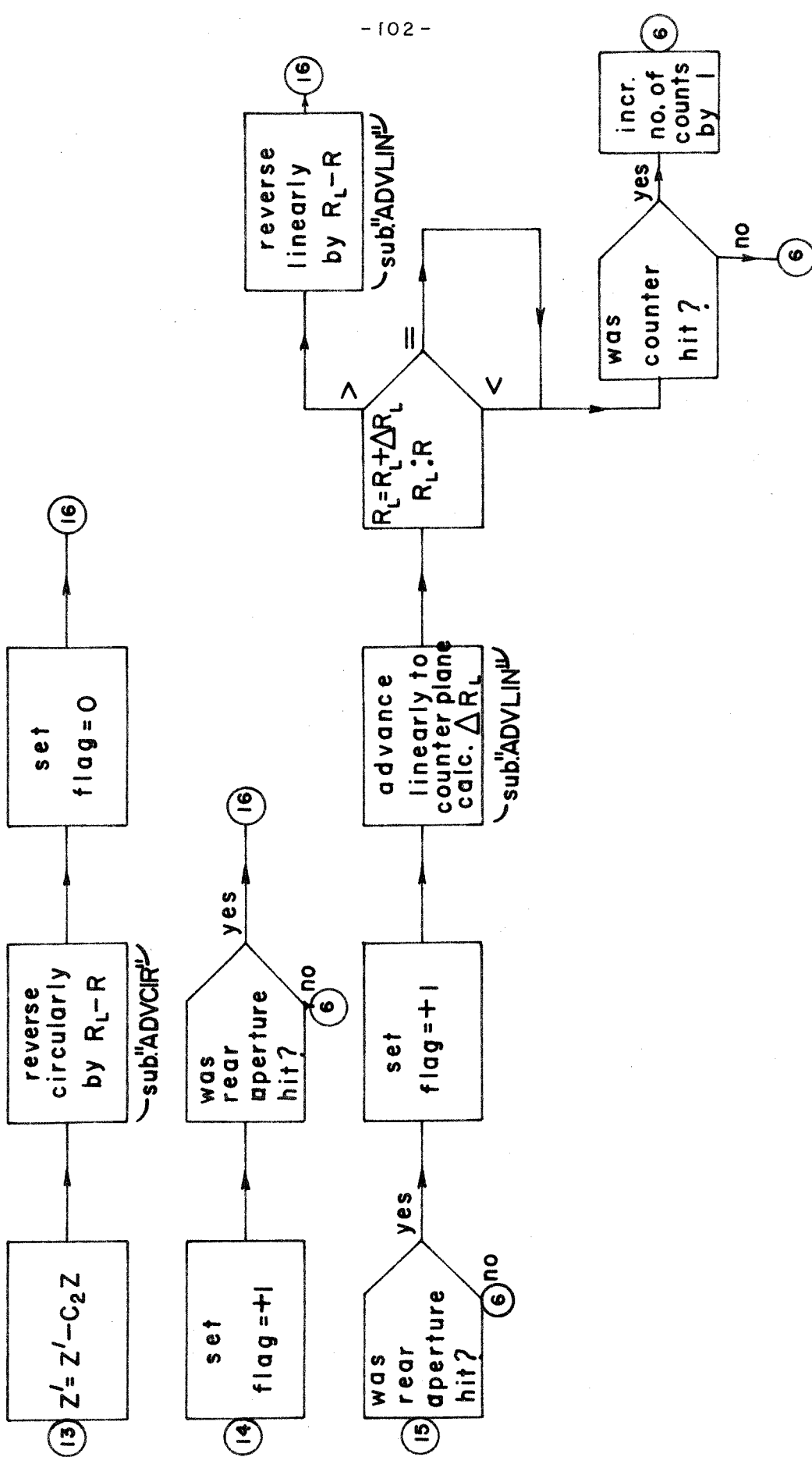
COORDINATE SYSTEM FOR DECAY CORRECTION

Figure A7. Block Diagram of Computer Program for the
Decay Corrections

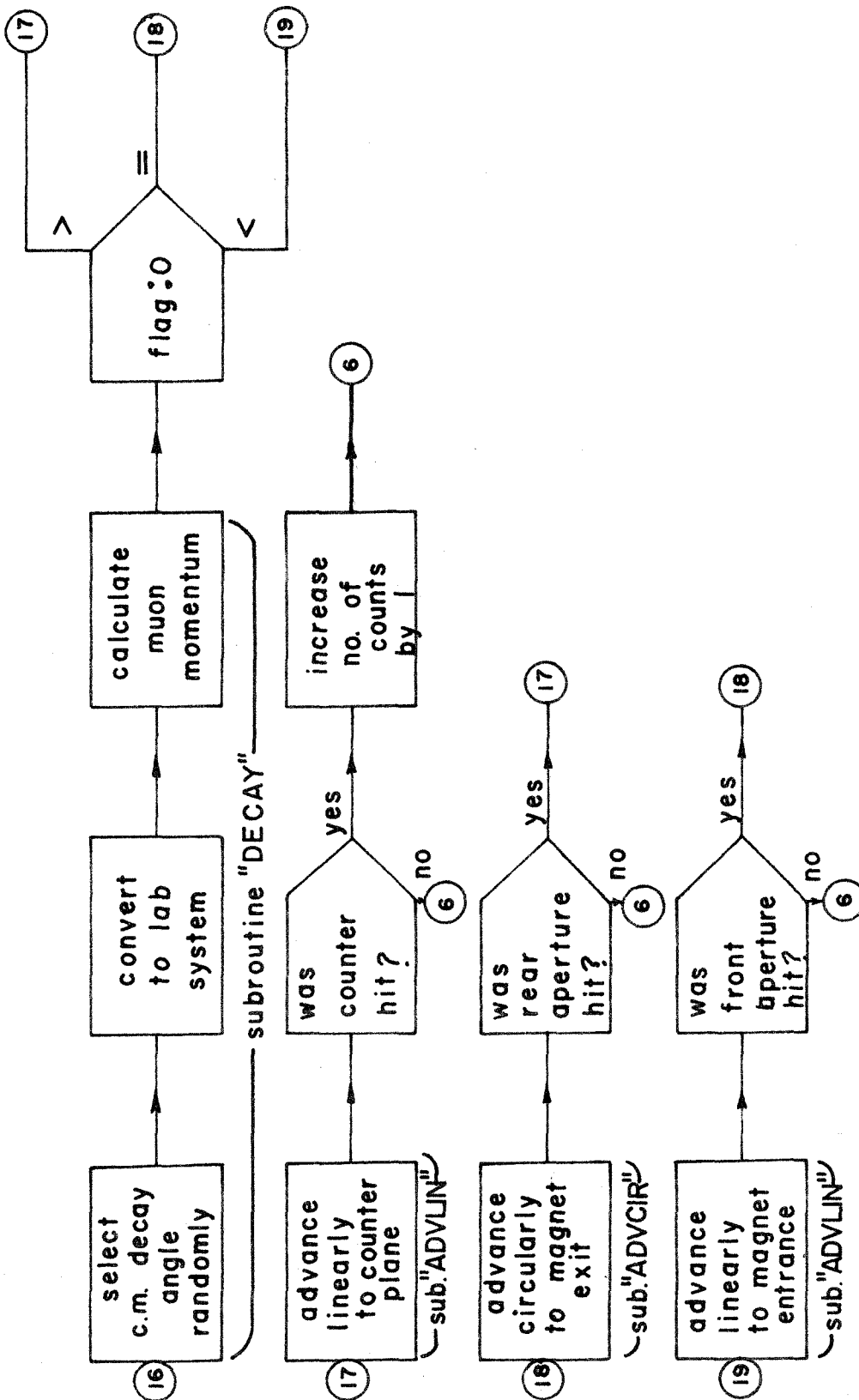
The symbol  indicates a branch comparison of the
algebraic quantities x and y .







(C)



(b)

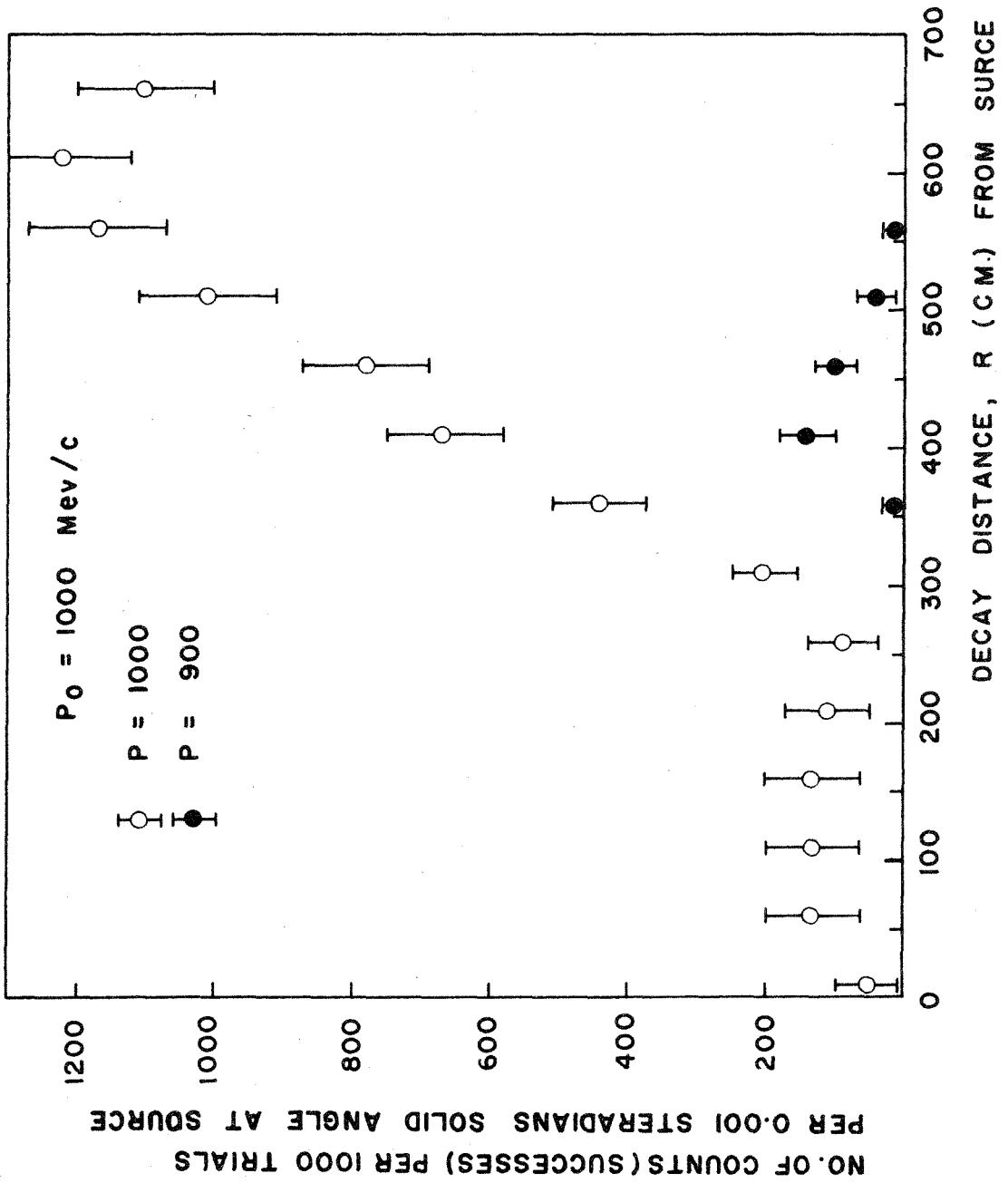
the decay muon. The muon is then advanced to the counter plane and tested for a hit. Then, unless enough trials have been made, another pion is "emitted" from the source. If any of the apertures are missed during the advance of the particle, a miss is recorded and another trial started. After the requested number of trials has been completed a new value of R is selected and the process begins again.

Note that the distance from the source at which decay occurs is fixed rather than chosen randomly (with proper weight). This simplifies the program, speeds the computation, and yields a physical picture of the way in which the decay affects the counting rate. The weighted integration over R can be carried out easily by hand. The time required to trace a particle to a successful count is about 0.1 second. If an intermediate aperture is missed the time is correspondingly reduced. For a typical set of parameters, about 1000 trials per minute can be made, half of which are successes if the pion momentum is the same as the central momentum of the spectrometer and the decay occurs near the rear focus. The total computer time required to generate the set of curves necessary to make the corrections is on the order of several hours. A previous attempt at a Monte Carlo solution to this problem by P. L. Donaho in this laboratory, using a computer 100 times slower, yielded results whose statistical accuracy was not adequate because of the prohibitive computational time involved.

A sample of the intermediate results of the computation, before the integration over decay length was performed, is shown in fig. A8. From such curves a physical picture of the way in which the decay process affects the correction can be obtained. Or, conversely, physical

Figure A8. Sample Results from Monte Carlo Calculations

A small sample of the computer output, before integration by hand over the decay distance R , is shown for a spectrometer setting of 1000 Mev/c (high energy position) and two values of initial pion momentum.



intuition gives a check on the operation of the computer program. The final results of the computer and hand calculations are shown in the set of curves in figs. A9 and A10. The correction is obtained by integrating over the decay curve, fig. A9, for a given spectrometer setting, weighting the integration by the actual pion spectrum emitted from the source, and dividing this result by the value of the similar integral over the normalization curve (no decay), fig. A10, for the same spectrum. This procedure of normalizing with a computer calculated curve rather than with measured values of the spectrometer response tends to cancel errors in the magnet simulation process, although this simulation yields the same effective aperture as in the real system within 2%. The final corrections are given in Section IV, Data Reduction.

Additional decay correction curves have been included here in figs. A11, A12, A13, and A14. These were used to correct the Dixon-Walker data.

Figure A9. Muon Counting Rate, High Energy Position
with Counter A2

The number of muon counts per 1000 pions emitted from the source, per 0.001 steradians, weighted by the probability of decay at distance R and integrated over R is shown for several values of spectrometer central momentum as a function of initial pion momentum. The errors of the points due to the Monte Carlo statistics are of the order of 10%.

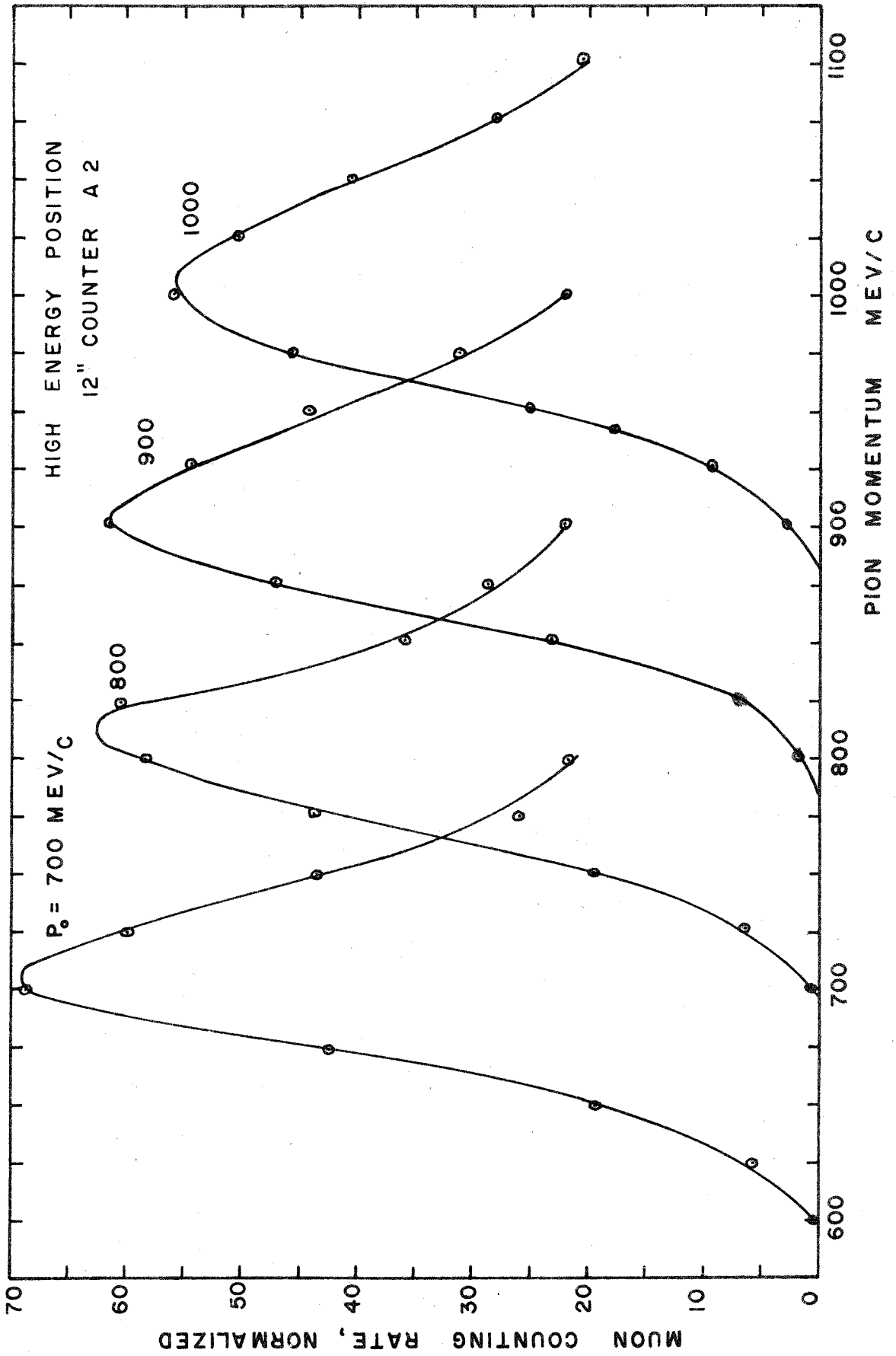


Figure A10. Momentum Response, High Energy Position
with Counter A2

The response of the spectrometer to particles that do not decay is normalized in the same way as for the decay curves shown in fig. A9 except that there is no weighting for the decay probability. The errors of each of the points are on the order of 10%.

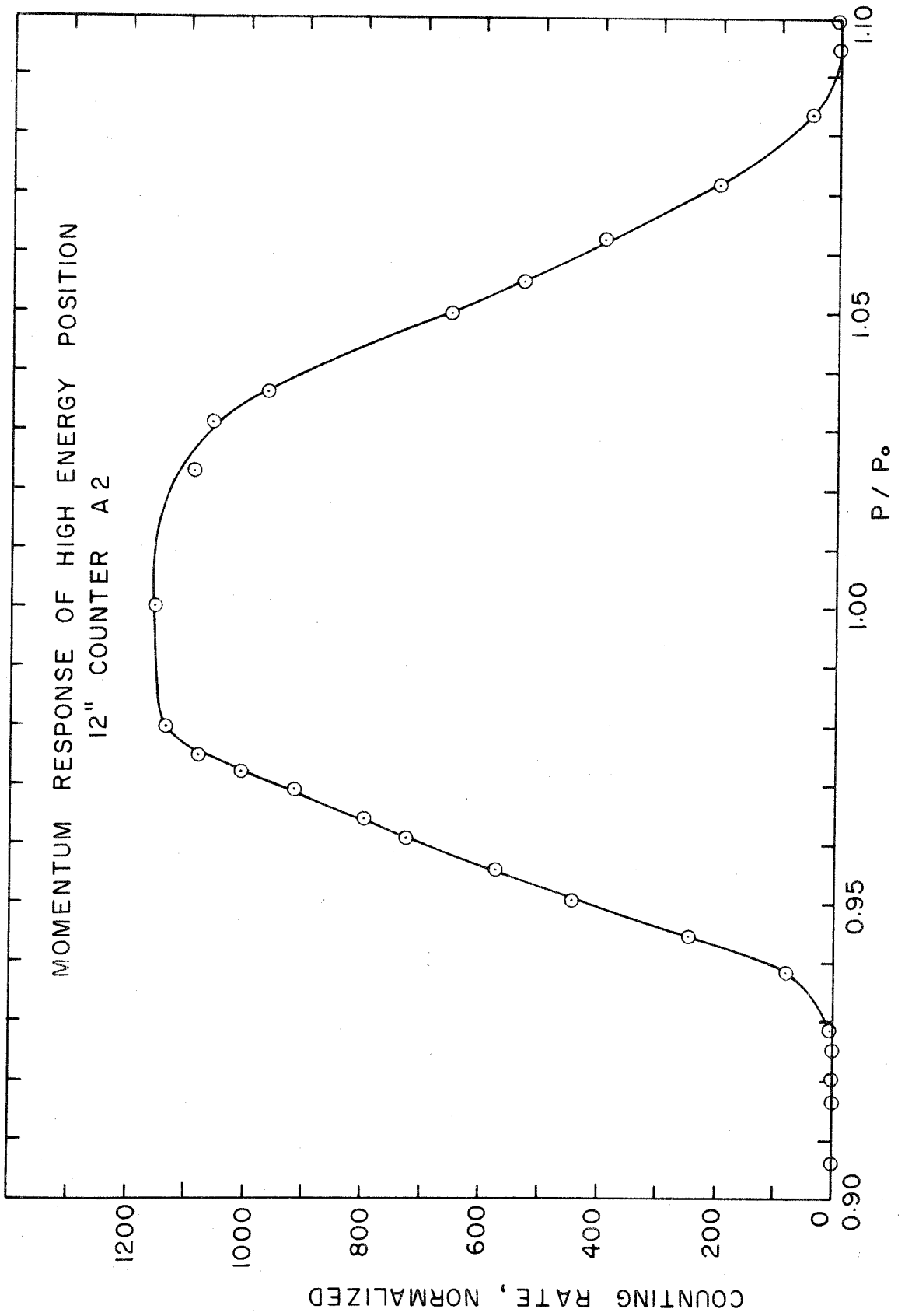
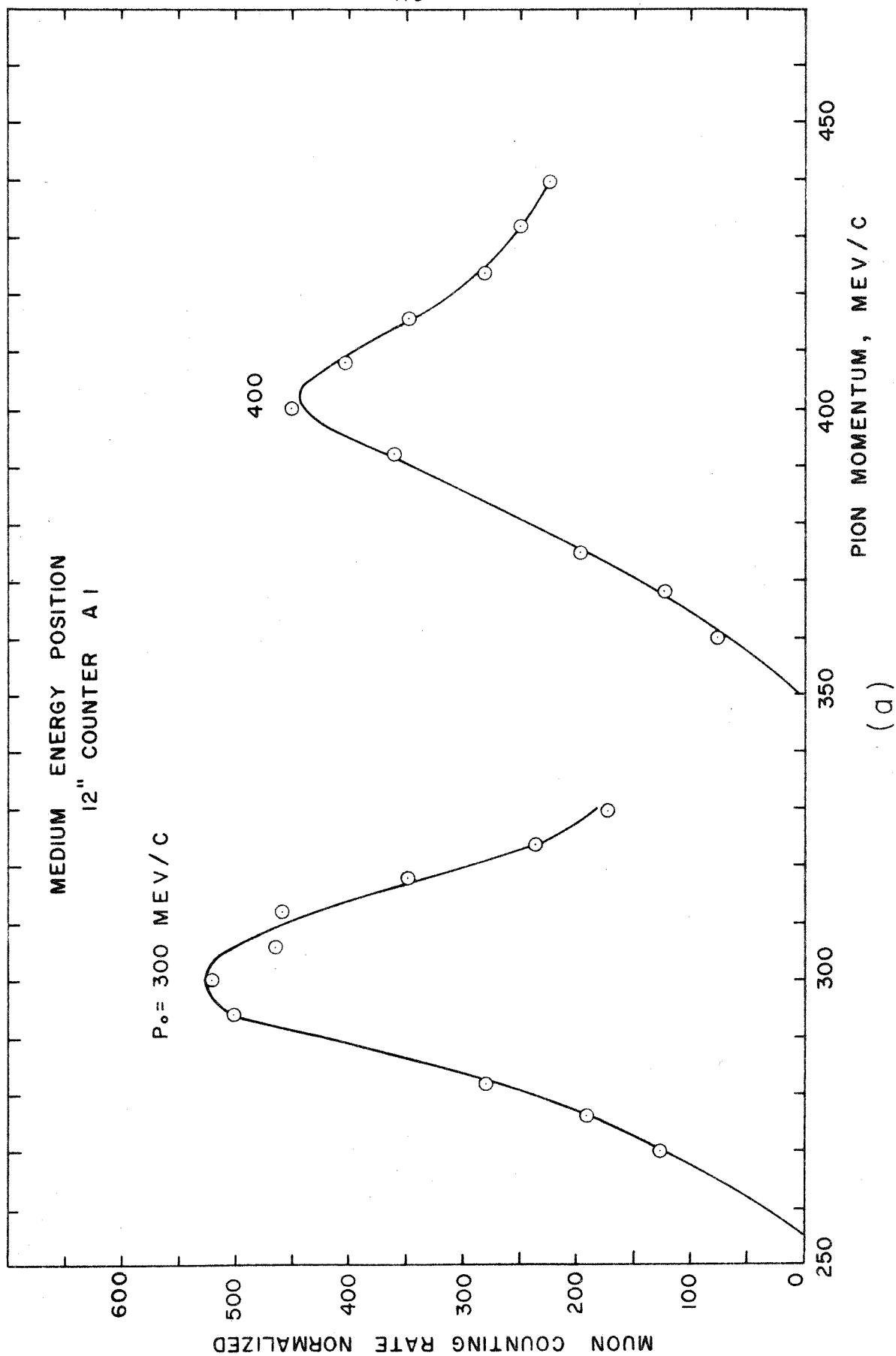


Figure A11. Muon Counting Rate, Medium Energy Position

The decay curves similar to those in fig. A9 are shown for the medium energy position, using A1 instead of A2. These curves were used to correct the Dixon-Walker data.



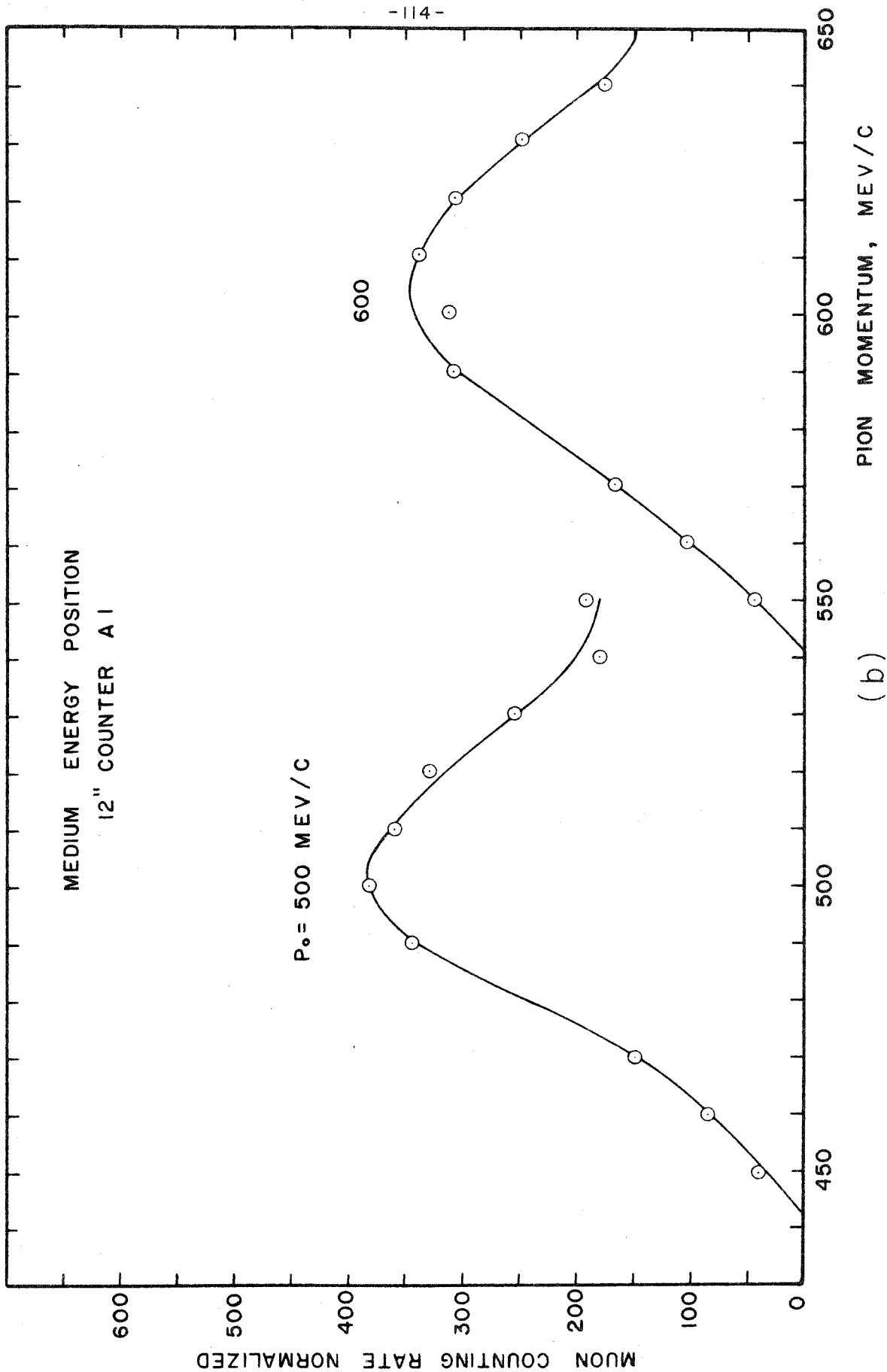


Figure A12. Momentum Response, Medium Energy Position

This curve, similar to fig. A10, complements the decay curves in fig. A11.

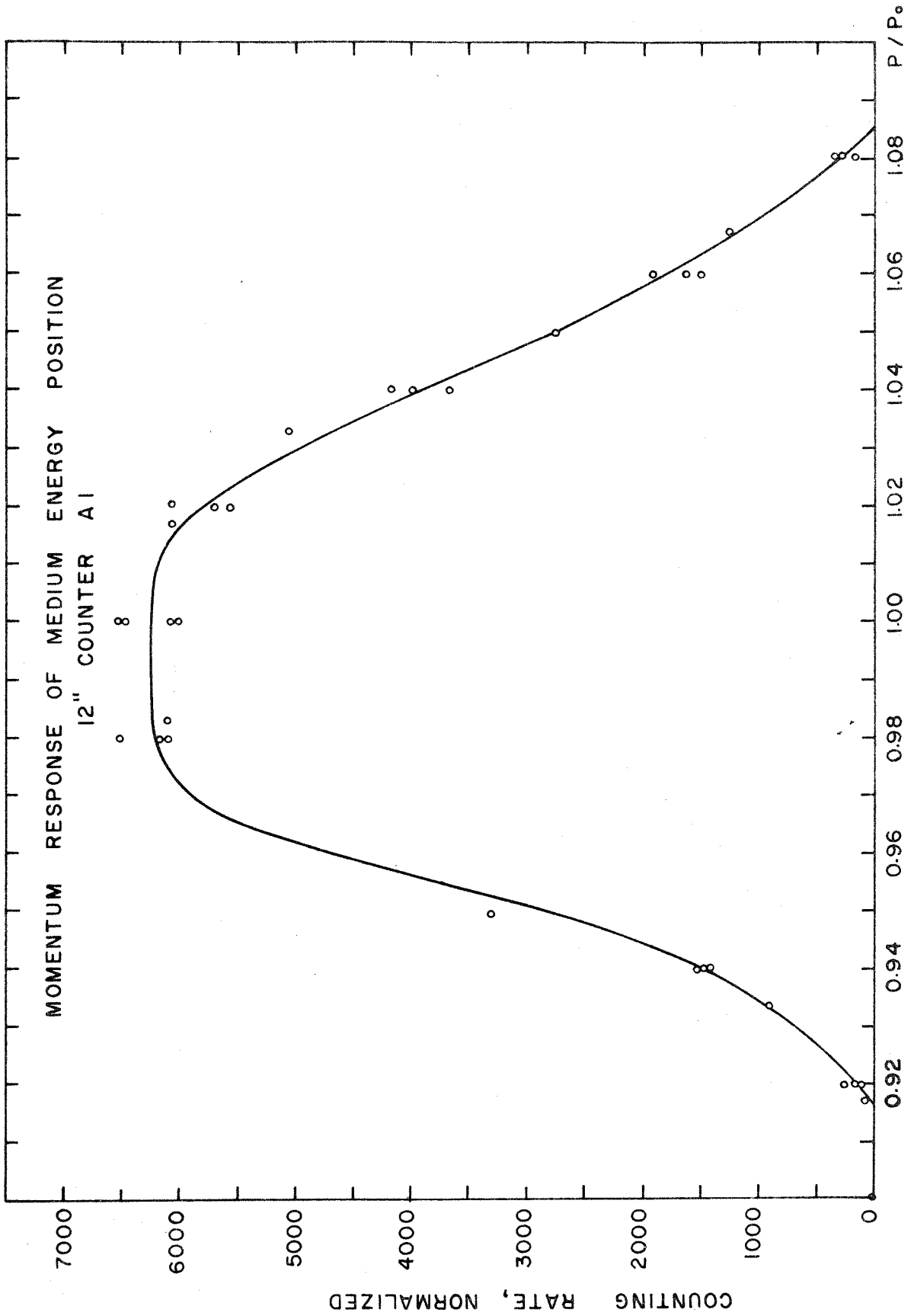


Figure A13. Muon Counting Rate, High Energy Position
with Counter A1

The decay curves similar to those of fig. A9 are shown for the case in which the aperture is defined by a 12ⁿ counter A1, instead of A2, and by the fan counters. These curves were used to correct the Dixon-Walker data.

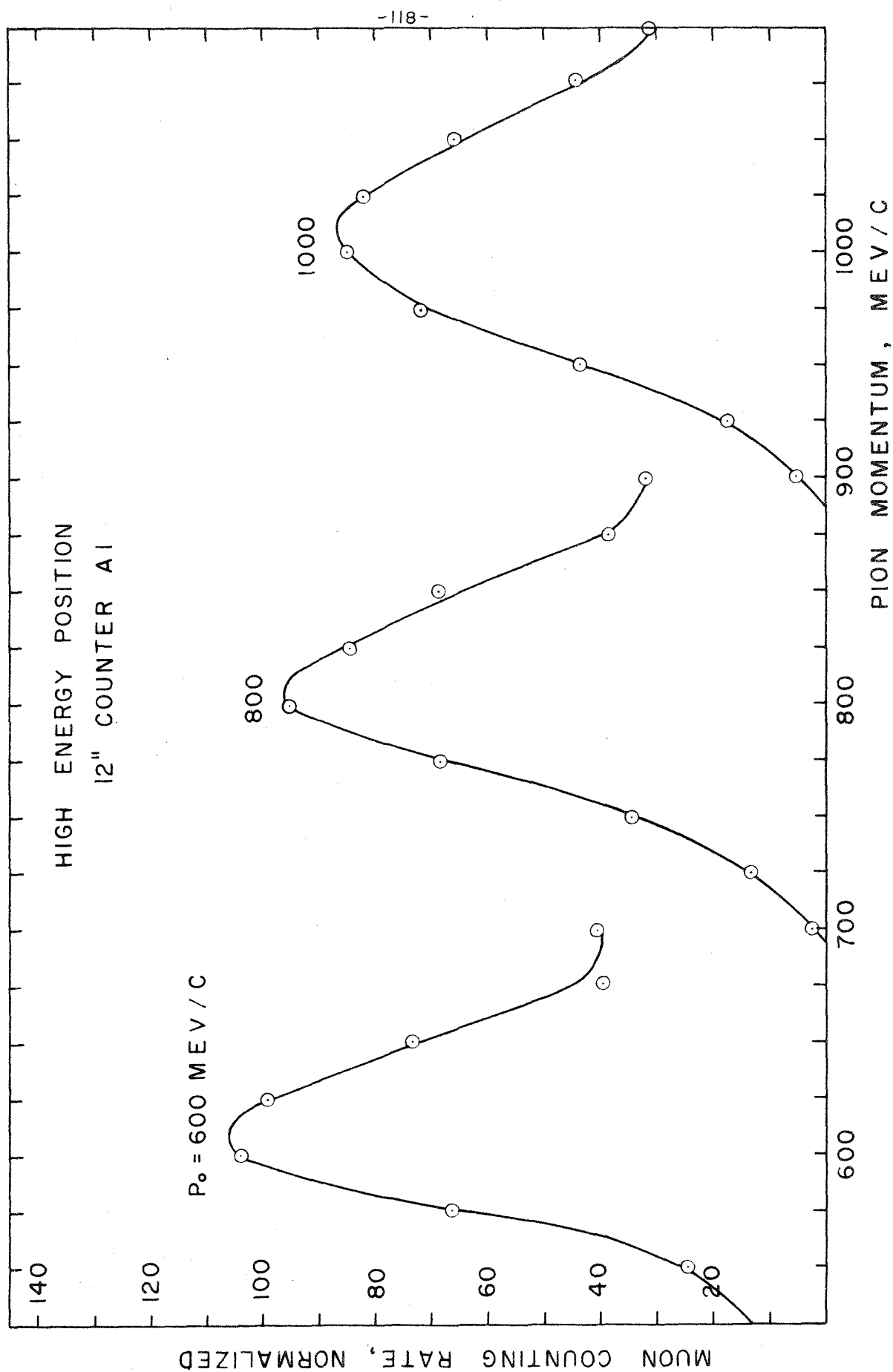
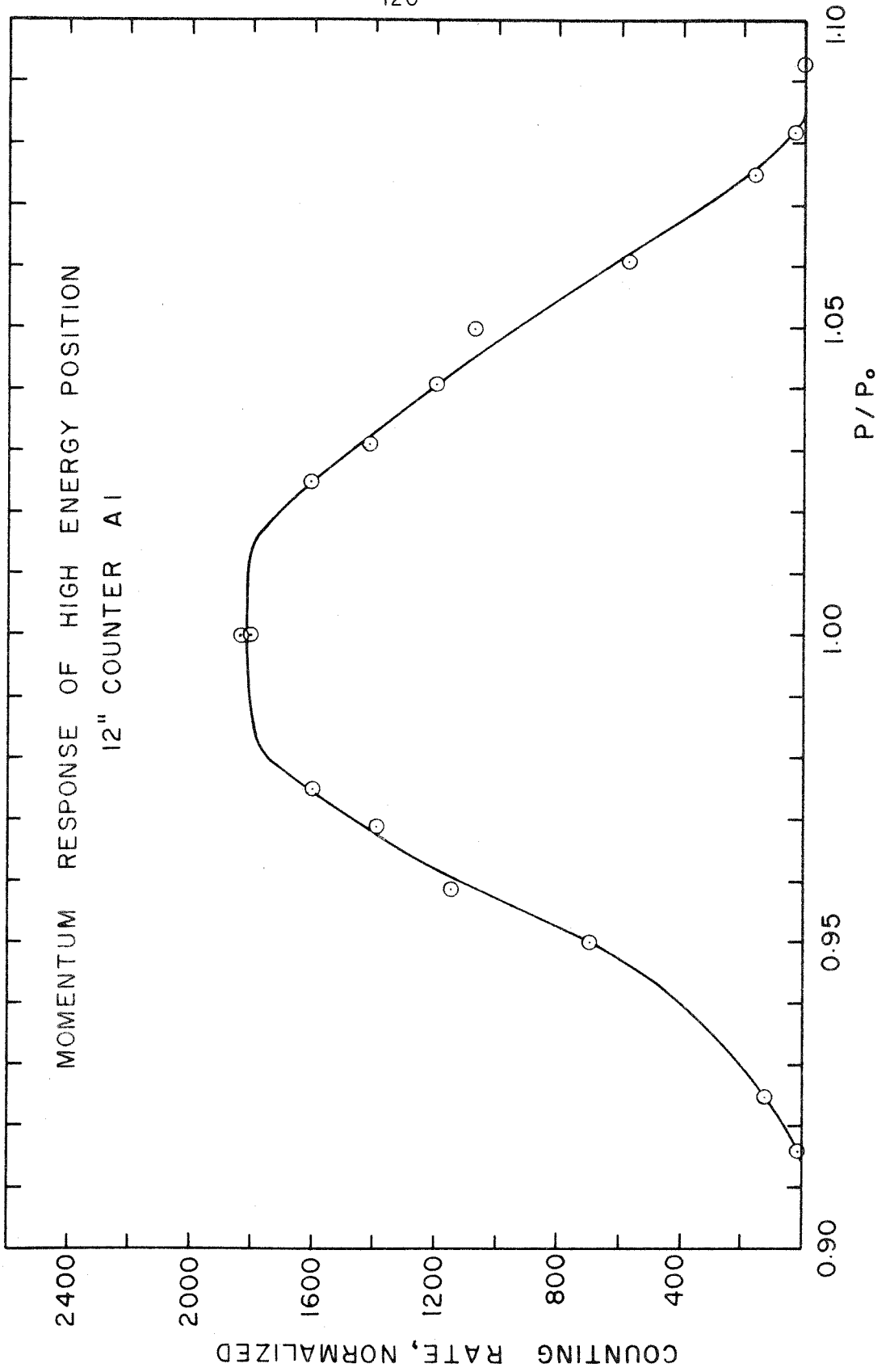


Figure A14. Momentum Response, High Energy Position
with Counter A1

This curve, similar to fig. A10, complements the decay curves of
fig. A13.



APPENDIX IV

ABSORPTION MEASUREMENTS

The nuclear absorption of pions in the material of the counter system was measured and used as a correction to the observed counting rates. The method chosen for measuring the absorption depends on the fact that C3 is not really required in order to define a pion if there are no electrons present. This was determined by measurements at large angles with the Pb absorber removed and C3 not required. Only about 1% of the events that counted as a pion in the other counters did not count in C3.

In order to determine the absorption, the requirement for C3 in the coincidence-anticoincidence circuit was changed from coincidence to veto and a photograph was taken of the pulse heights of every event which counted as a pion in all counters except C3. Therefore, only events which were likely to be absorption events were accepted for further examination. Absorbing material was placed between C2 and C3. The number of absorption events was determined by subtracting absorption-like events which occurred with no absorber, and throwing out a few events which appeared to be accidental. These measurements required considerable running time, even with the relatively poor statistics, because the energy dependence had to be checked, as well as several absorbers. The results are given in Table A2.

This method of measuring the absorption is believed to be superior to that previously used (5), in which an absorption length, L , was measured by adding thick Pb absorbers in front of the counter telescope. The

Table A2

Absorption Measurements

A_π = fraction of pions not absorbed

C_a = counting rate per BIP of absorption type events, counter 3 in veto

C_f = counting rate, counter 3 not required at all

Data

p_o , Mev/c	Absorber	C_a	C_f
700	0" Pb	0.075 ± 0.011	--
700	1/2" Pb	0.154 ± 0.018	--
700	1" Pb	0.256 ± 0.023	--
700	--	--	2.40 ± 0.11
900	0" Pb	0.029 ± 0.008	--
900	1/2" Pb	0.079 ± 0.011	--
900	1" Pb	0.154 ± 0.018	--
900	2" Pb	0.310 ± 0.028	--
900	1/2" Pb + 2-1/2" Lucite	0.143 ± 0.014	--
900	--	--	1.50 ± 0.07

Results

p_o	Absorber	$(1 - A_\pi)$
700	1/2" Pb	0.033 ± 0.009
700	1" Pb	0.075 ± 0.009
900	1/2" Pb	0.033 ± 0.009
900	1" Pb	0.083 ± 0.013
900	2" Pb	0.187 ± 0.019
900	2-1/2" Lucite	0.043 ± 0.021
(with 1/2" Pb to absorb secondaries)		

correction was then taken to be a simple exponential law, $e^{-T/L}$. However, some absorption events produce secondaries with energy sufficient to escape from a thin absorber but not a thick one. Therefore the absorption of a thin piece of material will effectively be smaller than would be calculated on the basis of an absorption length measured with a thick piece, due to counting the secondaries which emerge. This effect can be seen in the results of the absorption measurements. Since there is no energy dependence of the absorption, within the statistics of the measurements, the same value was used at all energies. There will be some error, believed to be small, due to the difference in scattering loss for the absorber placement during the absorption measurement and the actual placement during the experiment.

In the previous experiment (5) the absorption correction was satisfactory, except for geometrical effects due to scattering because all events giving large pulses in C3, using a $1/2''$ Pb convertor, were subtracted, on the assumption that they were due to absorption events and not electrons. At the angles used this was quite valid.

The effective absorption length, L , obtained from the measured values of $(1 - A_{\pi})$ are plotted in fig. A15, together with the calculated geometrical asymptote. The measurements of Dixon and Walker were consistent with this calculated value.

Figure A15. Effective Absorption Length vs. Thickness of Pb

The measured values of the pion absorption have been used to calculate an effective absorption length from the relation $A_{\pi} = e^{-T/L}$. This is compared with the geometrical value of L calculated from

$$L_g = \frac{M}{N_o \pi R_o^2 A^{2/3} \rho}$$

where

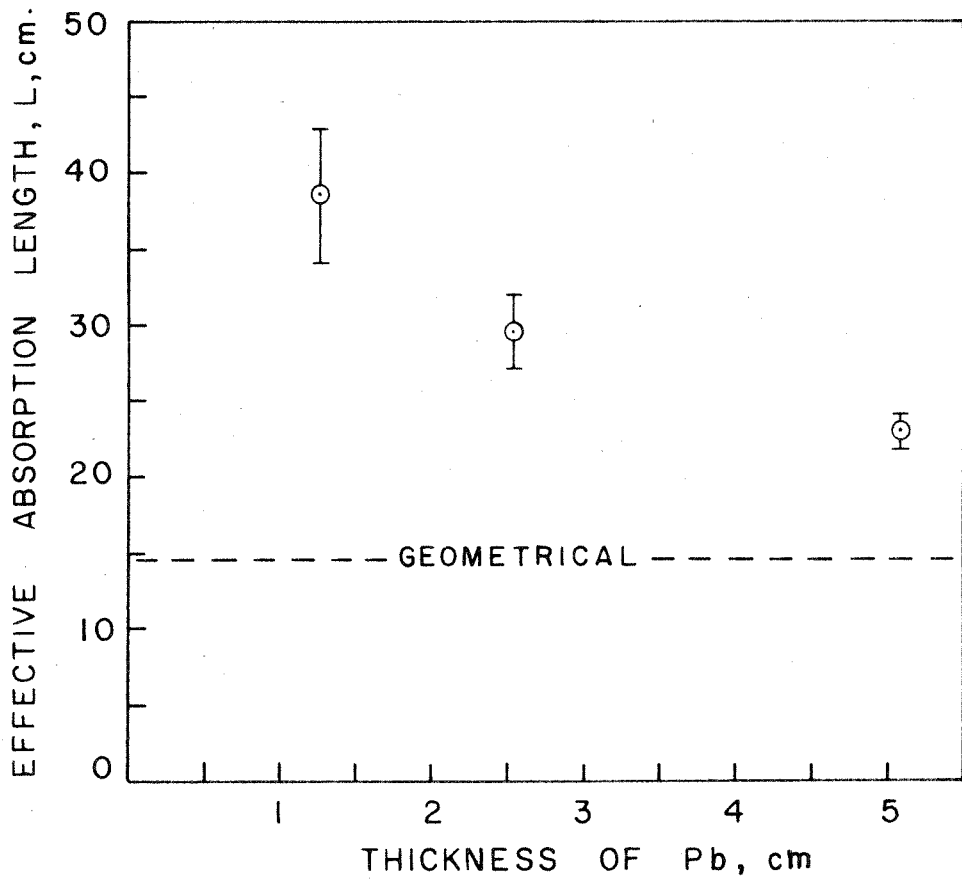
M = atomic weight

N_o = Avogadro's number

R_o = effective nucleon radius = 1.37×10^{-13} cm.

A = mass number

ρ = density



APPENDIX V

ELECTRON COUNTING RATES

It may be of some interest to give the observed counting rates for electrons (positrons) as calculated from the expressions in Section IV C.

$$C_e = \frac{1}{\eta_{Ce}} \frac{1}{\eta_{Ee} \left(1 - \frac{\eta_{E\pi}}{\eta_{Ee}}\right)} [E - C\eta_{E\pi} + \eta_{Cp}(\eta_{E\pi} - \eta_{Ep})C_p]$$

The number of positive electron counts per BIP is given in Table A3. The counting rate from the hydrogen (background subtracted) is shown in fig. A16.

Some data were taken at small angles for reverse field, i. e. counting negative electrons. The following results were obtained, after subtracting backgrounds:

At 3° , with smaller scintillator on A2

$$C_{e+} = 0.225 \pm 0.038 \quad \text{counts/BIP}$$

$$C_{e-} = 0.380 \pm 0.049$$

$$\therefore C_{e-} - C_{e+} = 0.155 \pm 0.062$$

It appears that the predominance of negatives may be statistically significant. The only source of purely negatives must be Compton scattering in the hydrogen target. A calculation of the counting rate to be expected from Compton scattering alone gives too small a contribution due to the strong forward peaking of the high energy electrons. Multiple or plural scattering would have to account for the number seen. This

Table A3

Electron Counting Rate

Point: Photon energy in Mev and laboratory angle.

C_{ef} : Foreground (full H_2 target) counting rate of positive electrons, normalized to unit solid angle and unit momentum dispersion.

C_{eb} : Background (target with H_2 gas only) counting rate

C_{ed} : $C_{ef} - C_{eb}$

Table A3

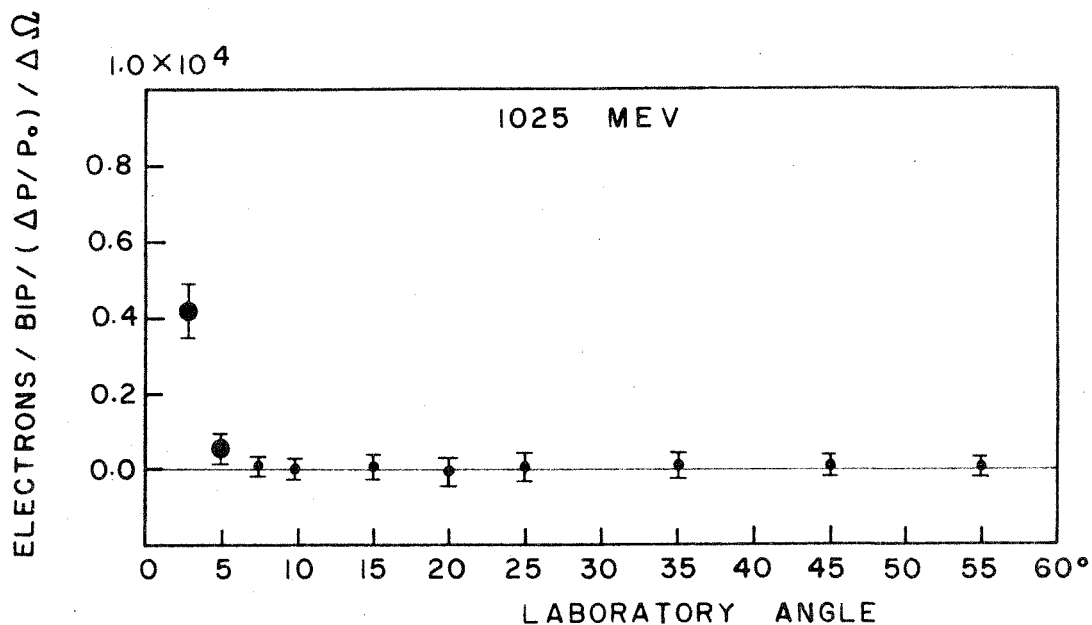
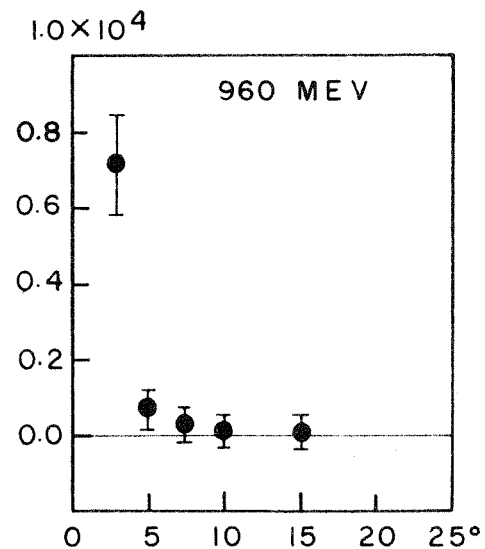
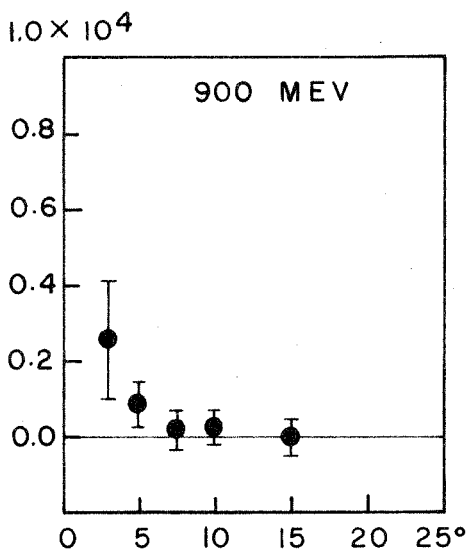
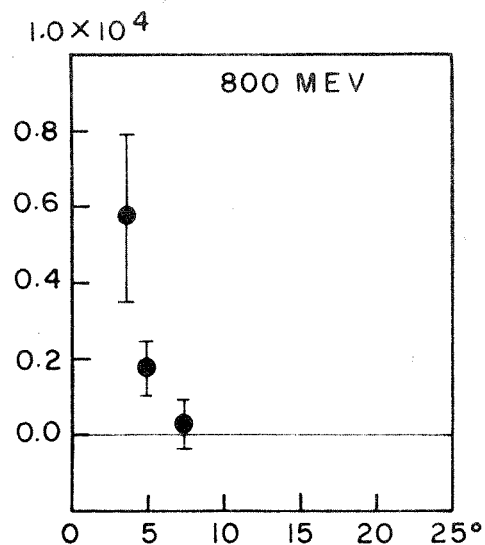
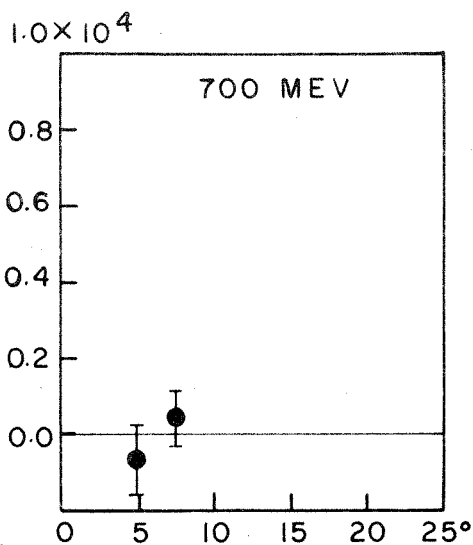
Point	$C_{ef} \times 10^{-4}$	$C_{eb} \times 10^{-4}$	$C_{ed} \times 10^{-4}$
700-5	0.806 ± 0.073	0.870 ± 0.056	-0.070 ± 0.092
700-7.5	0.106 ± 0.067	0.068 ± 0.033	0.037 ± 0.075
800-3.2	4.531 ± 0.161	3.965 ± 0.156	0.567 ± 0.224
800-5	0.422 ± 0.056	0.255 ± 0.039	0.168 ± 0.068
800-7.5	0.051 ± 0.050	0.028 ± 0.038	0.023 ± 0.062
900-3	2.702 ± 0.113	2.442 ± 0.111	0.257 ± 0.157
900-5	0.182 ± 0.048	0.097 ± 0.031	0.084 ± 0.057
900-7.5	0.029 ± 0.045	0.010 ± 0.023	0.018 ± 0.051
900-10	0.020 ± 0.024	-0.004 ± 0.014	0.024 ± 0.028
900-15	0.001 ± 0.041	0.006 ± 0.016	-0.006 ± 0.044
960-3	2.420 ± 0.100	1.707 ± 0.085	0.713 ± 0.130
960-5	0.127 ± 0.042	0.062 ± 0.028	0.065 ± 0.050
960-7.5	0.034 ± 0.035	0.009 ± 0.015	0.025 ± 0.039
960-10	0.010 ± 0.034	0.000 ± 0.009	0.010 ± 0.035
960-15	0.012 ± 0.036	0.006 ± 0.015	0.006 ± 0.040
1025-3	1.248 ± 0.056	0.831 ± 0.044	0.417 ± 0.070
1025-5	0.087 ± 0.024	0.042 ± 0.014	0.045 ± 0.028
1025-7.5	0.039 ± 0.020	0.026 ± 0.011	0.013 ± 0.023
1025-10	0.003 ± 0.022	0.007 ± 0.011	-0.005 ± 0.025
1025-15	0.009 ± 0.025	0.002 ± 0.009	0.007 ± 0.027
1025-20	0.000 ± 0.033	0.006 ± 0.012	-0.007 ± 0.035
1025-25	0.006 ± 0.034	0.002 ± 0.013	0.004 ± 0.037
1025-35	0.013 ± 0.028	-0.001 ± 0.008	0.014 ± 0.029
1025-45	0.002 ± 0.013	-0.002 ± 0.010	0.004 ± 0.017
1025-55	0.003 ± 0.014	0.006 ± 0.009	-0.004 ± 0.017

effect has not been calculated.

Since the measurement of $\eta_{\pi e}$ depends on electrons being absent at large angles one must be sure that such is the case. The argument for a small number of electrons is based on the constancy with angle of the measured $\eta_{E\pi}$ for angles greater than some value, e.g. 15° in the laboratory. However if the electron background should for some reason become constant with angle for large angles there would be no way of determining this from the data. Electrons produced by photons from π^0 decay could conceivably produce a flat angular distribution, but not at such a high energy.

Figure A16. Counting Rates of Positive Electrons
from Hydrogen

The counting rates for e^+ , after subtracting the empty target backgrounds, are shown for each energy, normalized to unit solid angle and unit momentum dispersion.



REFERENCES

1. H. Yukawa, Proc. Phys. -Math. Soc. Japan 17, 48 (1935).
2. Lattes, Occhialini and Powell, Nature 160, 453 (1947).
3. Chew, Low, Goldberger and Nambu, Phys. Rev. 106, 1337, 1345 (1957).
4. M. Heinberg, W. M. McClelland, F. Turkot, W. M. Woodward, R. R. Wilson and D. M. Zipoy, Phys. Rev. 110, 1211 (1958).
5. F. P. Dixon, Ph.D. Thesis, California Institute of Technology (1960).
F. P. Dixon and R. L. Walker, Phys. Rev. Letters 1, 458 (1958).
6. P. L. Donoho, "A Magnetic Spectrometer for Analysis of Particles of Momentum up to 1200 Mev/c." (Nov. 1957), Unpublished.
7. R. L. Walker, High Energy Physics course notes (1959-60), Unpublished.
8. M. J. Moravcsik, Phys. Rev. 104, 1451 (1956).
9. P. Cziffra and M. J. Moravcsik, University of California, Lawrence Radiation Laboratory, report UCRL-8523 Rev. (1959).
10. J. G. Taylor, M. J. Moravcsik and J. L. Uretsky, Phys. Rev. 113, 689 (1959).
11. J. Kilner, California Institute of Technology, experiment in progress.
12. R. R. Wilson, Nuclear Instruments 1, 101 (1957).
13. H. A. Bethe and L. C. Maximon, Phys. Rev. 93, 768 (1954).